A STUDY OF MIXING, MORPHOLOGY, AND RHEOLOGY FOR MELT MIXING OF AB/A POLYMER BLENDS

By

Kevin Louis Nichols

A DISSERTATION

Submitted to
Michigan State University
in partial fulfillment of the requirements
for the degree of

DOCTOR OF PHILOSOPHY

Department of Chemical Engineering

1988

ABSTRACT

A STUDY OF MIXING, MORPHOLOGY, AND RHEOLOGY FOR MELT MIXING OF AB/A POLYMER BLENDS

By

Kevin Louis Nichols

The factors determining degree of fill for the mixing zones of a starved co-rotating twin screw extruder have been studied experimentally. Next, the micelle structure and rheological properties, at equilibrium and due to nonequilibrium melt mixing, of melt blends of a tapered styrene-butadiene diblock (M_w = 136,000, 70% styrene) in an excess of high molecular weight polystyrene (M_w = 235,000) have been determined.

The axial flow characteristics of the twin screw extruder were determined with a novel tracer technique in which radioactive chips of the extruded polymer (PVC, a thermoplastic; or CPE, an elastomer) were used as tracer. The relationship between degree of fill and ratio of throughput to rpm (Q/N) was found to be sensitive to polymer properties in both mixing zones. At comparable operating conditions, less CPE was held up than PVC, and most axial dispersion occurred in the region where polymer melted.

The micelle structure and rheology of styrene-butadiene diblock/polystyrene blends containing up to 20 weight percent

diblock have been examined by transmission electron microscopy and dynamic mechanical testing. As the diblock concentration was increased from 1 to 20 weight percent, the shape of the micelle core changed from spherical to cylindrical, the size of the micelle core went through a maximum, and the total number of diblock molecules participating in micelles stayed constant. The size of the micelle core and the degree of micellization decreased during processing. There was a tendency for micelles to cluster at equilibrium that did not occur during processing. The dynamic moduli as well as the average relaxation time went through a minimum with increasing diblock content for the blends with equilibrium structure.

An existing theory for micelle formation in AB/A blends has been modified to account for the effect of unfavorable entropic interactions between the A-block and the A homopolymer, when molecular weight of A homopolymer is greater than the molecular weight of the A-block, and to account for the effect of energy stored during flow. The modified theory can explain the experimental variation in micelle core size and the decrease in degree of micellization with flow.

To my wife, Joanne, for her exceptional patience.

ACKNOWLEDGMENTS

I would like to thank Dr. Krishnamurthy Jayaraman for his outstanding guidance, enthusiasm, and availability during the course of this work. I would also like to acknowledge the other members of my guidance committee, Dr. Lawrence Drzal, Dr. Jack Giacin, Dr. Eric Grulke, and Dr. David Todd, for their assistance during different phases of this work.

I would like to thank the Department of Chemical Engineering at Michigan State University, Amoco Corporation, Dow Chemical Company, and the State of Michigan RE/ED fund under the auspices of the Composite Materials and Structures Center, for financial support during the course of my graduate work at Michigan State University.

I would like to express my deep gratitude to Dr. Mark Lindsay for the use of his computer during the preparation of this dissertation. Finally, I would like to thank all of my friends who have made my years at Michigan State University memorable, especially Michael Treptau, Craig Chmielewski, and Greg Rorrer.

TABLE OF CONTENTS

LIST OF TABLES

LIST OF FIGURES

NOMENCLATURE

a	length of statistical segment
a^e	radius of ellipsoid defined in Figure 5.8
a_N	constant in empirical first normal stress difference relation (see equation 6.12)
a_t	shift factor for time-temperature superposition
A_1	constant in equation for free energy of a micelle (defined in equation 7.9)
A_2	constant in equation for free energy of a micelle (defined in equation 7.9)
A_3	constant in equation for free energy of a micelle (defined in equation 7.9)
a_4	constant in equation for free energy of a micelle (defined in equation 7.9)
b	Kuhn statistical length
b^e	radius of ellipsoid defined in Figure 5.8
b_N	constant in empirical first normal stress difference relation (see equation 6.12)
b_1	constant in perturbation expansion of first normal stress difference (see equation 7.21)
b_2	constant in perturbation expansion of first normal stress difference (see equation 7.21)
c	number density
c_v	volume of a domain
C_i	radiation counts
C_{io}	radiation counts corrected to time $t = 0$
C_1^o	constant for WLF equation (see equation 6.1)

C_2^o	constant for WLF equation (see equation 6.1)
f	free energy of a micelle/number of diblock molecules in micelle
$f(\epsilon,x)$	dimensionless pressure profile
F	free energy of formation for a single micelle
F_d	free energy of deformation
F_j	joint localization energy
F_{mA}	free energy of mixing in corona
$F_{m,bulk}$	free energy of mixing in matrix
F_s	free energy due to stress
$F(t)$	cumulative distribution function
$F(\epsilon)$	integral of dimensionless pressure profile (see equation 2.7)
G_N^o	plateau modulus
G'	storage modulus
G''	loss modulus
G^*	complex modulus
h^c	height of cylinder
H_p	height of paddle
H_s	height of slit
I	intensity of radiation
$\underset{\cong}{I}$	identity tensor
Je^o	steady-state creep compliance
k	Boltzmann constant = 1.38×10^{-16} dynes·cm/^{o}K
$\dot{m}$	mass feedrate
M	molecular weight
M_e	entanglement molecular weight

M_n	number average molecular weight
M_w	weight average molecular weight
n_o	number of monomers
N	screw rotation rate, degree of polymerization, or number of statistical segments
N_A	number of segments in A-block
N_B	number of segments in B-block
N_c	number of cylinders
N_d	number of domains
N_e	number of ellipsoids
N_H	number of segments in matrix homopolymer
N_o	Avagadros number = 6.023×10^{23}
N_1	first normal stress difference
$N_{1,blend}$	blend first normal stress difference
$N_{1,A}$	homopolymer first normal stress difference
$N_{1,PS}$	polystyrene first normal stress difference
p	number of diblock molecules in a micelle
p_i	percentage of isotope
P	pressure
Q	volumetric flow rate
r	root mean end-to-end distance of polymer molecule
$\underline{r}$	end-to-end vector for polymer molecule
r_A	root mean end-to-end distance of A-block
r_B	root mean end-to-end distance of B-block
r^c	radius of cylinder

r_o	equilibrium end-to-end distance for a polymer molecule
R	radius of micelle
R_{actual}	actual radius of a domain
R_A	width of micelle corona
R_B	radius of micelle core
R_G	gas constant
$R_{measured}$	measured radius of domain
R_{SAXS}	radius of domain determined by small-angle X-ray scattering
R_{TEM}	radius of domain determined by transmission electron microscopy
S_m	translational entropy for a sea of micelles
t	time, or average relaxation time
t_c	time from end of irradiation
t_i	time of irradiation
t_m	mean residence time
t_{mod}	tube modification time
t_r	Rouse relaxation time
t_{rep}	reptation time
t_s	sample thickness
t_p	characteristic time for Brownian diffusion
$t_{1/2}$	half-life of isotope
t_1	time when F(t) = .16
t_2	time when F(t) = .84
t_{192}	relaxation time at 192^oC
t_{200}	relaxation time at 200^oC

t_{160}	relaxation time at 160°C
T	temperature
T_0	reference temperature
v_h	volume held up in zone
v_{PB}	specific volume of polybutadiene
v_x	velocity in circumferential direction
v_z	velocity in axial direction
w	weight
W	width
x	circumferential direction
y	direction perpendicular to axis
z	axial direction
z_s	axial extent of orifice plug

Greek Symbols

α	ratio of diblock segments to homopolymer segments (N/N_H)
β	parameter for breadth of relaxation time distribution (defined in Figure 6.9)
γ	interfacial tension
γ_0	strain amplitude
Γ	nuclear cross-section
δ	phase angle
ΔG^s	free energy due to flow
Δt_{16-84}	time for one standard deviation around the mean of material to leave a zone
ϵ	degree of fill

ζ	volume fraction of diblock molecules participating in micelles
η	volume fraction of A-block in corona
η_m	viscosity of matrix
η_0	zero shear viscosity
η^*	complex viscosity
η'	dynamic viscosity
η''	imaginary part of complex viscosity
μ	viscosity
ξ	ratio of micelle volume to total diblock volume in blend
ξ_0	monomeric friction coefficient
π	pi = 3.141593
ρ	density
σ	shear stress
σ_0	stress amplitude
$\sigma(c_v)$	variance of measured domain sizes
$\underset{\cong}{\tau}$	deviatioric stress tensor
ϕ	volume fraction
ϕ_c	critical micelle concentration
ϕ_{core}	volume fraction of micelle cores in blend
$\phi_{diblock}$	volume fraction of diblock molecules in blend
ϕ_{PB}	volume fraction of polybutadiene in blend
ϕ_1	volume fraction of diblock molecules in blend
χ_{AB}	interaction parameter for A polymer and B polymer
χ_{AH}	interaction parameter for A-block and matrix homopolymer

Ψ	neutron flux
ω	frequency
Ω	number of monomers

CHAPTER I

INTRODUCTION

Blending two or more polymers to form a new material, which combines advantageous properties of the polymers being mixed, is a science that has seen rapid development in the last 20 years (see, for example, reviews by Shen & Kawai, 1978; Paul & Newman, 1978; Bywater, 1984; Robeson, 1984; and Walsh, Higgins, & Maconnachie, 1985). Although advances have been made in many polymer blending research areas in recent years, there is still a great need for research on the rheological behavior of polymer blends, description of mixing processes for polymer blends, and prediction of morphology for polymer blends. At present, our ability to predict what rheological and mechanical properties a new blend of polymers will have is limited, and how to generate a specific morphology during preparation of polymer blends and how this morphology determines the rheological and mechanical properties of the blends is still not extremely well understood. This dissertation presents three studies that are a contribution to the above polymer blend research areas. First, a study of the mixing process in a co-rotating twin screw extruder, which is often used for polymer blending, is presented. Second, experimental relationships between blend rheology, blend morphology, and blend preparation method are presented for melt

blends consisting of a styrene-butadiene diblock copolymer dispersed in an excess of high molecular weight polystyrene. Since the structure of the blends studied here was that of styrene-butadiene diblock copolymer micelles in a matrix of styrene homopolymer, a final study presented here is a modification of existing theories for micelle formation in diblock copolymer/homopolymer blends to account for the trends seen in the experimental study.

For clarity, the remainder of this introduction is divided into three sections. In Section 1.1, the role of diblock copolymers in polymer blends is discussed, and the motivation for the research here on AB/A melt blends is presented. In Section 1.2, the importance of a complete understanding of the mixing process during polymer blending is presented, and Section 1.3 contains an outline of this dissertation.

1.1 Role of Diblock Copolymer in Polymer Blends

Often, problems such as high interfacial tension and poor adhesion between phases result in a poor degree of dispersion and poor mechanical properties for polymer blends. In many cases, addition of small amounts of the appropriate diblock copolymer during preparation of a polymer blend alleviates these problems because the diblock copolymer functions as an emulsifier. Also, since the diblock copolymer acts as a surfactant, it provides a chemical link between phases and thus improves mechanical strength of the blend. Examples of this behavior have been given by Molau (1970), Inoue (1970), Riess and Jolivet (1975), Eastmond and

Phillips (1979), and Cohen and Ramos (1979), who have shown the emulsifying action of AB diblock copolymer in solutions or solution cast blends of homopolymer A with homopolymer B. These researchers have all shown that the molecular weight of the blocks of the diblock copolymer must be greater than the molecular weight of the homopolymers to which it is added for the diblock to act as an emulsifier. Noolandi and Hong (1984) have theoretically examined mixtures of two different homopolymers with corresponding diblock copolymer in a nonselective solvent at thermodynamic equilibrium, which provides further guidance in selecting appropriate diblock copolymers to use as emulsifiers in solution cast polymer blends.

Another role of diblock copolymer in polymer blends is to function as an impact modifier. In this application, a small amount of diblock copolymer, where one of the blocks is a rubbery type polymer, is added to a glassy homopolymer to improve the glassy polymer's impact strength. In these impact modified polymers, either the entire diblock copolymer will form a separate phase from the polymer to which it is added (Geblizlioglu et al, 1985), or the rubbery block of the diblock will form the core of a micelle structure, and the other block of the diblock forms cilia which are mixing to some degree with the matrix homopolymer (Selb et al., 1983). The blends studied here were impact modified polystyrene where the styrene-butadiene diblock copolymer formed a micelle structure.

In impact modified homopolymers, often an increase in size of the rubbery phase results in increased impact properties and a

decrease in tensile properties for the homopolymer, so, usually, there is an optimum particle size for achieving desired overall properties. A problem, then, is how to achieve this optimum domain size for a given impact modified homopolymer. For the blends studied here, this translates into being able to control the size of the diblock copolymer micelle. Another feature that may affect the impact properties of the blends containing micelles is the degree of micellization. For a given blend, as the total number of diblock copolymer molecules participating in micelles decreases, it seems likely that the impact strength decreases for the blend. It will be shown here that melt mixing can cause a decrease in both micelle size and degree of micellization which may be undesirable when trying to improve impact strength of a blend.

A compilation of virtually all of the existing literature on blends of AB diblock with A homopolymer was given by Rigby and Roe (1988), who recently published an excellent review of the existing experimental and theoretical literature on the thermodynamics of polymer blends in which at least one of the components is a copolymer. Most literature on AB/A blends has dealt specifically with solution cast blends. It is generally accepted that it is difficult to achieve thermal equilibrium during solution casting due to solvent effects and the decreased polymer motion at the low temperatures used for solvent casting, especially for polymers with high molecular weight. Nevertheless, existing experimental studies of micelle structures in solution cast AB/A blends have used

matrix homopolymer of very low molecular weight, and thermodynamic equilibrium was achieved (Selb et al., 1983; Rigby & Roe, 1986). The AB/A melt blends here contained a matrix homopolymer with a much larger molecular weight than previously used. Therefore, thermodynamic equilibrium structures were obtained by annealing at high temperature, where there is much polymer motion, and then shock cooling the blends. These structures were then observed with transmission electron microscopy.

Although much of the literature to date is on solution cast blends of diblock copolymer with homopolymer(s), in industry it is most common to manufacture polymer blends by melt mixing rather than by solution casting. The few publications on melt blending with diblock copolymers include Fayt (1981, 1982, 1986) and Heikens (1978), who have shown that addition of diblock will reduce the size of the minor phase during melt mixing of two polymers, but it is still not clear that the criteria established for obtaining a desired morphology in solution casting of blends apply to melt mixing of blends. One objective of the research presented here was to gain further insight into the role of diblock copolymer in structure development during melt mixing of polymer blends.

The blends of styrene-butadiene diblock with styrene homopolymer studied here provide an added advantage in that the micelle structure of the blends can be compared to the thermodynamic equilibrium micelle structure predicted by the theory of Whitmore and Noolandi (1986) or Leibler, Orland, and Wheeler (1983). Rigby and Roe (1986) and Mayes and Olvera de la Cruz (1988) have presented

useful modifications of the theory of Leibler et al. The experimental results of the morphology experiments presented here prompted modifications to the theory of Leibler et al. to account for possible interactions between the styrene block of the diblock copolymer and the styrene homopolymer and the effect of stress imposed in processing on micelle structure. The static equilibrium micelle structures and the micelle structures after processing in the twin screw extruder are then compared to the theoretical predictions.

During melt blending, one would expect that the complex thermo-rheological properties of a diblock copolymer would affect the final morphological and rheological properties of the blend. An example of the complex relationship that can exist between morphology and rheology for pure block copolymers is shown in the analysis of Widmaier and Meyer (1980), where as the temperature was raised, the triblock copolymer they studied changed from having a microheterogeneous structure to having a homogeneous structure which was reflected by the rheology. The published work describing the effect of addition of diblock copolymer on melt rheology for polymer blends is very scant. Another objective of the work here was to establish the relationship between morphology and rheology for the AB copolymer-A homopolymer blends that were prepared here.

1.2 Mixing of Polymer Blends

The dramatic effect that different methods of mixing can have on the properties of polymer blends is illustrated in Figures 1.1

and 1.2, which were taken from Ahuja, Chang, and Schreiber (1982). Figures 1.1 and 1.2 show that the rheological properties and mechanical properties for the same polymer blend prepared by different methods can be drastically different. Ahuja et al. did not give reasons for the differences seen in Figures 1.1 and 1.2, but it seems likely that these differences are due to different morphology or different amounts of degradation.

The development of phase morphology for polymer blends during mixing has been studied by Van Oene (1972), Min, White, and Fellers (1984), and Elmendorp and Ven Der Vegt (1986). In all of these studies, a single screw extruder was employed; Van Oene and Min et al. also used a static mixer attached to their extruder. There is still some controversy as to the effect of elastic properties of the blend components on morphology formation when making the blends. Van Oene found elasticity of the blend components to be very important, while Min et al. stated that elasticity is not very important. Wu (1987) has studied the formation of the dispersed phase in blends of incompatible polymers formed with a co-rotating twin screw extruder and has found that the size of the domains can be directly related to the interfacial tension and the viscosity ratios of the blend components. Plochocki (1986) has presented a computer package for estimating morphology of polymer blends. Plochocki's development was limited by the lack of knowledge there is in some polymer blending areas as discussed earlier. Nevertheless, Plochocki has shown the great potential

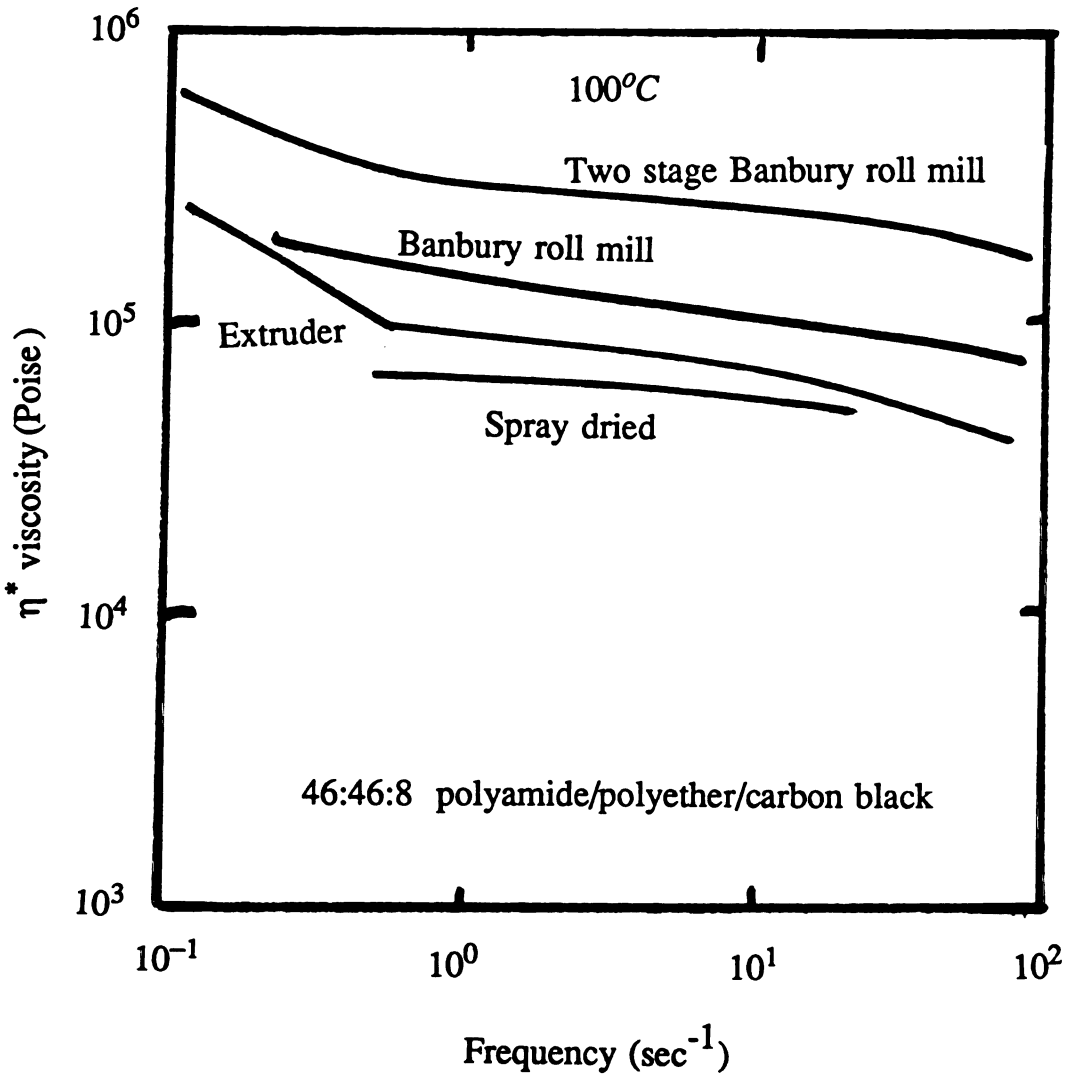

Figure 1.1 The effect of different methods of processing on rheology (Ahuja et al., 1982)

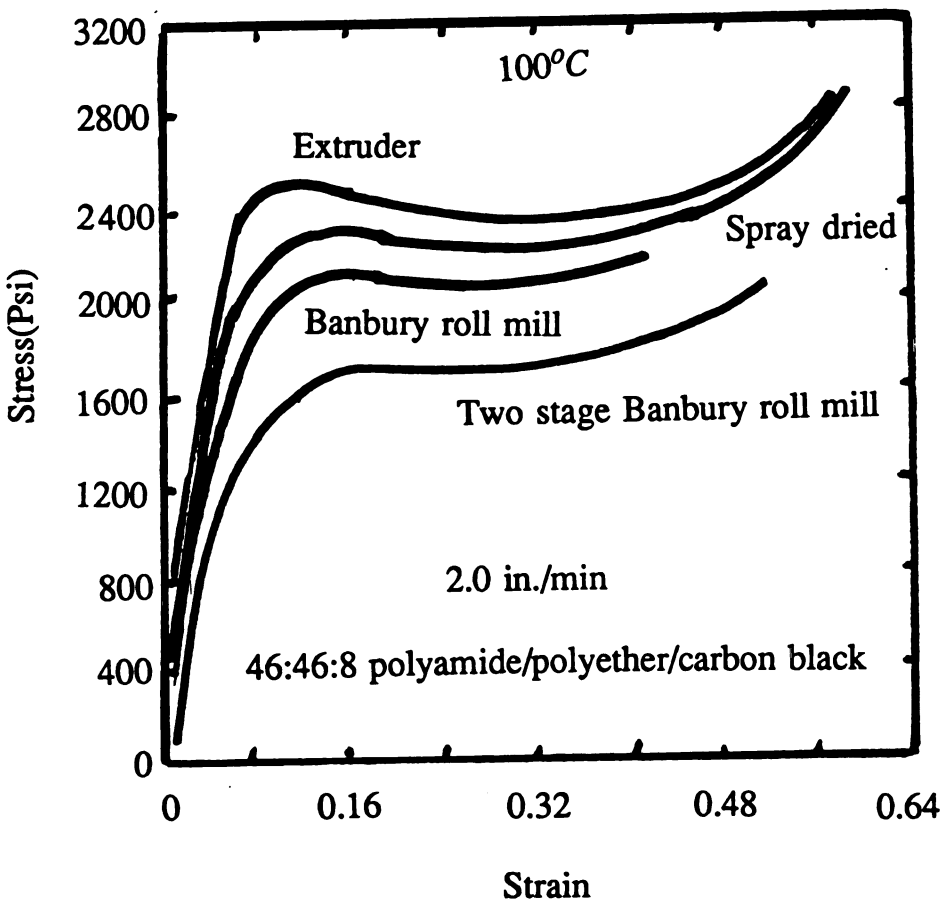

Figure 1.2 The effect of different methods of processing on tensile properties (Ahuja et al., 1982)

there is for computer-aided design of new materials once the mixing mechanisms for polymer blends, and so on, are better understood.

As a first step in understanding the mixing mechanism in the twin screw extruder employed in this work, the effect of operating conditions and polymer properties on residence time distributions was explored. It is important to identify the residence time distributions in different regions of the extruder because the amount of time a polymer blend spends in a certain flow field can have an effect on its morphology. For instance, Rumscheidt and Mason (1961) have shown that if the viscosity ratio between two blend components is greater than four, then shear is ineffective in breaking up different phases beyond a certain size; however, an extensional flow can with enough time result in further break up. Wu (1987) recently has further verified this in his work. Also, Favis and Chalifoux (1988) have shown significant particle break up can happen over two minutes in an internal mixer. As will be seen here, the total residence time of polymer in mixing regions of the twin screw extruder used here is often much less than two minutes, which implies, according to the results of Favis and Chalifoux, the minimum phase size is not achieved. One would then expect that the length of time a polymer blend spends in the mixing zones will govern the amount of phase breakup there is for the blend and hence dictate the morphology of the extrudate.

Another aspect of polymer blending where knowledge of residence times is important is reactive processing. Recently, the twin screw extruder used in this study has been employed to extrude blends of

nylon and propylene with a maleic anhydride copolymer. During extrusion the maleic anhydride reacts with the nylon to form a graft copolymer. Clearly, the thermal history of this polymer system is going to dictate how much graft copolymer is made and hence directly affect the final properties of the blend. In another application of the extruder for reactive processing, a reacting dry ink polymer was extruded, and precise control of the mean residence time of the polymer in the extruder was much more important than maximizing throughput.

Finally, residence time in any polymer processing equipment is an important consideration when one is concerned with polymer degradation. Grassie and Scott (1985) and Owen (1984) have shown that polymer degradation is often an auto-catalytic process. Significant degradation can take some time to occur, but once it starts, it happens very quickly. Many times stabilizers are used to prevent degradation. It seems intuitive that processing time and amount of stabilizer required will be related.

1.3 Dissertation Outline

Because there are two topics studied here which are different in nature, the analysis of residence time distributions in the twin screw extruder is covered in its entirety in Chapter II, and the rest of the chapters contain the analysis of the styrene-butadiene diblock copolymer-styrene homopolymer blends. Chapter III gives a summary of the literature that pertains to the research on AB/A blends performed here, including the effect of stress on polymer

blends and solutions, equilibrium morphology for AB/A blends, and rheology/morphology relations for AB/A blends. Chapter IV gives the experimental details of the structural and rheological analysis performed on the blends. Chapter V is a presentation of the morphology results with discussion, and Chapter VI contains the results and discussion of the rheology experiments. In Chapter VII, the theory for static thermal equilibrium morphology of AB/A blends is presented with the modifications mentioned earlier, and a comparison of the theory to the experimental results is made. The conclusions with recommendations for the morphological, rheological, and theoretical studies of the styrene-butadiene diblock/styrene homopolymer blends detailed in this work are given in Chapter VIII.

CHAPTER II

DEGREE OF FILL AND RESIDENCE TIME DISTRIBUTIONS FOR THE MIXING ZONES OF A CO-ROTATING TWIN SCREW EXTRUDER

2.1 Introduction

Twin screw extrusion is finding increased utility in the polymer processing industry for polymer blending, compounding, and reactive processing. In these applications, the ability to have controlled adjustment of the thermal and flow history of the extruded polymer system is essential for obtaining the optimal product. The effect of changes in screw rotation rate, feedrate, screw geometry, barrel geometry, and polymer properties on the hold up, mean residence time, and axial dispersion in different regions of a twin screw extruder must be understood for effective operation of the extruder.

The published experimental work from which the effect of change in operating variables on hold up, mean residence time, and axial dispersion for twin screw extruders can be deduced is limited. Todd (1969, 1975) did some of the pioneering work in this area by obtaining residence time distributions in twin screw extruders at room temperature with model liquids. Janssen et al. (1978) seem to have been the first to do residence time experiments in a twin screw extruder which took into account the entire extrusion process--solid

feed, melting, and so on. The work presented here is novel in that it appears to be the first published study of the effect of polymer properties on mean residence time, hold up, and axial dispersion in a twin screw extruder taking into account the entire extrusion process. In our research, residence time distributions for polyvinyl chloride (PVC), a thermoplastic whose extrusion behavior has been described by Karian (1985), are compared to those for chlorinated polyethylene, which is an elastomer.

Twin screw extruders which are used for blending, compounding, or reactive processing generally operate in a starved state, and orifice plug restrictions or screw elements which reverse flow are mounted at several axial positions along the shafts to create regions of hold up. To better understand operation of these starved twin screw extruders, one needs to know how hold up or degree of fill in the various hold up regions of the extruder depends on the operating conditions. Eise et al. (1983) have conducted experiments that give some insight into how hold up in co-rotating intermeshing extruders with kneading blocks depends on throughput rate and screw rotation rate. Eise fed his extruder with LDPE melt and studied degree of fill for the entire extruder. In this work, by improving the experimental technique of Wolf et al. (1986), who illustrated that radioactive tracers could be used to determine residence time distributions at various axial locations along a twin screw extruder, we were able to extend the work of Eise et al. and study mean residence times, hold ups, and axial dispersion of different hold up zones in our extruder. With our experimental technique, we

were able to analyze zones in which melting occurred as well as zones that consisted entirely of melt. Another novel aspect of our work is that we were able to study the effect of change in kneading paddle configuration on axial flow in these different axial hold up regions. Recently, barrel valves have been introduced (Todd, 1979) as another means of controlling polymer flow through a twin screw extruder, and a unique aspect of the work presented here was to explore the effect of barrel valve position on axial flow. The results of the experimental work presented here should help in understanding the operation of any type of twin screw extruder which has several flow restrictions and thus different hold up zones.

2.2 Background

A variety of methods have been used to determine residence time distributions in twin screw extruders. Todd and Irving (1969) extruded glucose solutions and used potassium nitrate or sodium nitrate as a tracer to study residence times in a co-rotating intermeshing twin screw extruder. The concentration of tracer at the discharge was determined by conductivity measurements. Eise et al. (1983) also used conductivity measurements to monitor the concentration of iron oxide tracer during the extrusion of LDPE melt in a co-rotating intermeshing twin screw extruder. Todd (1975) extruded polybutene in a co-rotating intermeshing twin screw extruder and monitored the concentration of soluble p-napthol benzein tracer or insoluble methylene blue powder tracer with colorimetric measurements. Sakai et al. (1987) extruded silicone

and used colorimetric analysis of dyes to study residence times in both co-rotating and counter-rotating intermeshing twin screw extruders. Janssen et al. (1978) extruded polypropylene and Wolf et al. (1986) extruded PVC, and both used radioactive manganese dioxide powder as the tracer to study residence times in counter-rotating intermeshing twin screw extruders. The manganese dioxide was master-batched with the extruded polymer, the master-batch tracer was then neutron activated, and the concentration of this radioactive tracer was monitored with radiation detectors. It appears that Wolf et al. (1986) would have activated the chlorine in PVC while activating manganese dioxide during their tracer preparation, although no mention of this is given in their paper.

The objective in selection of a tracer for residence time experiments is to choose a tracer that will flow through the equipment in the same way as the material to which it is introduced does. As can be seen from the above, to date, residence time experiments have been conducted with soluble or insoluble tracers, where the tracer is different from the extruded material. In each of these cases, it is questionable that the tracer is flowing through the extruder in exactly the same way as the extruded material, especially the insoluble tracers. For example, Janssen et al. (1978) found larger agglomerates of manganese dioxide in the extruded samples than were in the original manganese dioxide powder. In the experiments presented here, we have avoided such problems with tracers by employing tracers that are chemically identical to

the extruded polymer. We have extruded PVC or CPE and used radioactive chips of PVC or CPE as the tracer material (the chlorine in the PVC or CPE was neutron activated). These tracers should flow through the extruder in the same way as the extruded polymer.

The residence time experiments described above have yielded useful information about extrusion with twin screw extruders. Todd (1969, 1975) determined that axial dispersion for high viscosity liquids in his twin screw extruder was independent of screw rotation rate, feedrate, and viscosity, but very dependent on the screw configuration. Janssen et al. (1978) found that total volume held up in their extruder did not change much with change in operating conditions, and that an increase in die pressure decreased the tail of the residence time distribution. For a commercial extruder, Wolf et al. (1986) found the flow through the extruder was remarkably close to plug flow. The radiation from the tracer may have been attenuated by the extruder wall in Wolf et al.'s experiment, and thus the tail of the residence time distribution was not detected; i.e., the flow might not have been as close to plug flow as Wolf et al. suggested. Eise et al. (1983) found that throughput was not a linear function of degree of fill, axial mixing was not affected by degree of fill at low screw rotation rates, and axial mixing was enhanced by high screw rotation rates at low degrees of fill for screws containing kneading blocks.

Theoretical understanding of the operation of intermeshing twin screw extruders has been slow in developing. Most theoretical studies on intermeshing twin screw extruders (Maheshri & Wyman,

1980; Kim, Skatsckow, & Jewmenow, 1973; Booy, 1980) have considered extruders with "screw type" geometries. Szydlowski et al. (1987) recently reported a simulation of flow profiles in a twin screw extruder with kneading disks. Virtually all of the existing theories on flow in a twin screw extruder assume that the extruder is full, and reasonable estimates of the volumetric flowrate Q as a function of operating conditions can be obtained from these theories. Hence, the mean residence time t_m of polymer in the extruder can be calculated from the simple expression

$$t_m = v_h/Q \qquad 2.1$$

where v_h is the volume of polymer held up in the extruder, which is presumably known.

For many applications, twin screw extruders operate starved, and for a starved twin screw extruder use of equation 2.1 is more complex, especially if the extruder has multiple hold up regions, because the dependence of v_h on operating conditions must be known. With the exception of Booy's theory (1980), it appears that no theories exist from which one can make predictions of hold up, and hence mean residence time, in any type of starved twin screw extruder, and Booy's theory is for the specific case of a very starved twin screw extruder with "screw type" geometry and no hold up zones. The basis of Booy's theory is that there is a very small bank of polymer at the leading edge of the screw which is pushed down the extruder by the screw, and Booy found that $Q/N \sim \varepsilon$ where N

is the screw rotation rate and ϵ is the degree of fill. Eise et al. (1983) pointed out that in regions of the extruder that contain kneading paddles, downstream flow is a result of staggered pressure profiles generated by the motion of the paddles. In this work, by using the results of Eise et al. we show that an expression relating Q/N to ϵ similar to that of Booy can be derived for mixing zones where a mixing zone is a series of kneading paddles followed by an orifice plug (mixing zones are discussed in detail in the Experimental section). It should be remarked here that there appears to be a common misconception that when there is a restriction to downstream flow in a twin screw extruder, the screw section immediately upstream of the restriction must be full to generate the necessary pressure to forward material past the restriction (see, for example, Rauwendaal, 1986, p. 470). The results of our experiments and the expressions developed in the next section show that this assumption is not correct.

2.3 Relationship Between Operating Conditions and Degree of Fill for a Mixing Zone

On a local scale, the motion of a kneading paddle causes a drag flow in a direction perpendicular to the extruder shaft; however, as the paddle turns, a pressure is generated at the paddle tip which causes polymer to flow upstream and downstream along the extruder into pressureless regions in the mixing zone regions. For example, for a mixing zone (see Figure 2.1b), it is the pressure generated by the paddle in the vicinity of the barrel wall that pushes material past the orifice plug. Eise et al. have presented pressure profiles

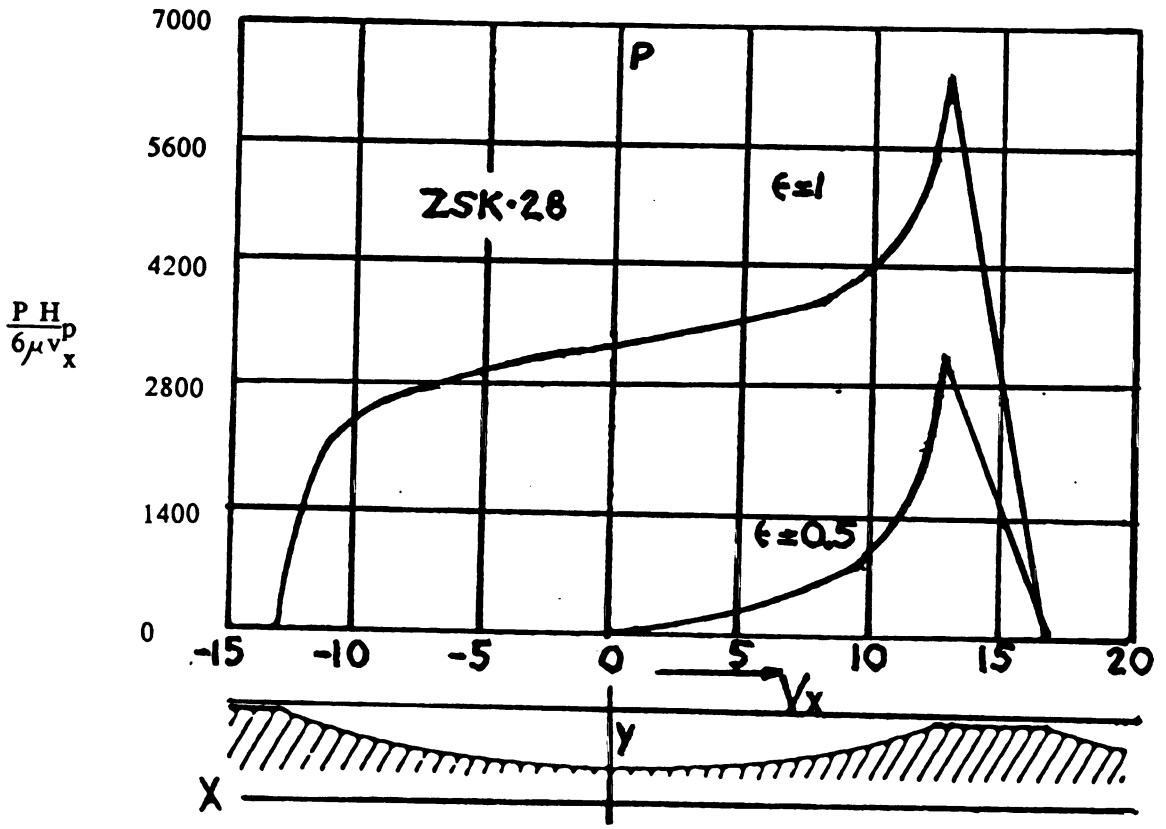

$\frac{P\,H}{6\mu v_x^p}$

Figure 2.1a Circumferential pressure profiles for a kneading paddle. (from Eise et al. (1983)).

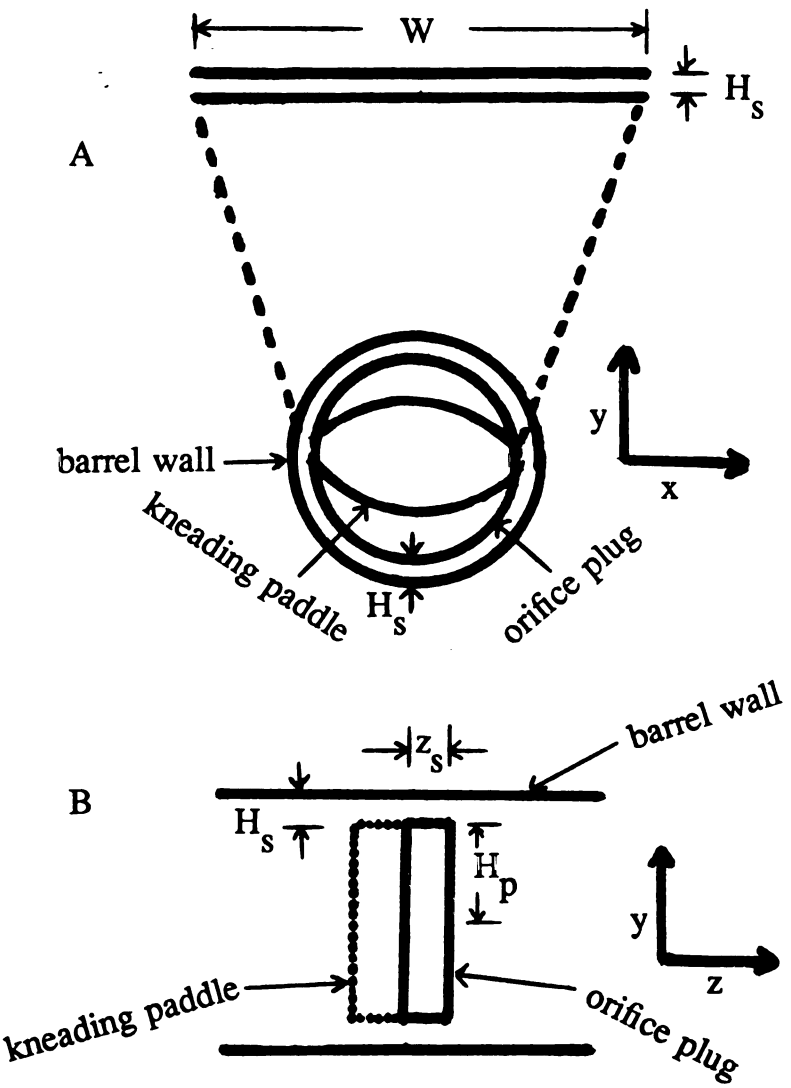

Figure 2.1b Schematic of a mixing zone with one kneading paddle.
(A) cross-section perpendicular to extruder axis.
(B) cross-section parralel to extruder axis.

at the barrel wall for a kneading paddle (Figure 2.1a) which were determined from lubrication theory. Using these pressure profiles, a simple development of a relationship between Q/N and ε for a mixing zone consisting of a single paddle followed by an orifice plug (see Figure 2.1a) is presented below.

As can be seen in Figure 2.1a, Eise et al. (1983) have shown that the circumferential variation of pressure at the barrel wall for a paddle may be expressed for a viscous Newtonian fluid as

$$P(\varepsilon,x) = 6\mu\, v_x\, f(\varepsilon,x)/H_p = 12\pi\,\mu N\, f(\varepsilon,x) \qquad 2.2$$

where x is a circumferential distance along the barrel wall (Figure 2.1b), $v_x = 2\pi H_p N$ is the velocity of the paddle tip, H_p is the distance from the screw axis to the paddle tip, μ is viscosity, and $f(\varepsilon,x)$ is a dimensionless pressure profile. Polymer flows through the gap between the orifice plug and barrel wall into an empty chamber, so for a kneading paddle followed by an orifice plug, the axial pressure gradient over the orifice plug at a circumferential location x may be written as

$$\partial P/\partial z\ (\varepsilon,x) = -12\pi\,\mu N\, f(\varepsilon,x)/z_s \qquad 2.3$$

where z_s is the axial extent of the orifice plug. Equation 2.3 may be used to determine an expression for the volumetric flowrate past the orifice plug in terms of the degree of fill as follows. If one assumes that the gap between the orifice plug and the barrel wall from paddle tip to paddle tip is a slit with height H_s and width $W = \pi H_p$ (see Figure 2.1b), then the axial velocity profile at a

circumferential location x is given by (Bird, Stewart, & Lightfoot, 1960)

$$v_z = -\frac{H_s^2}{8\mu}\frac{\partial P}{\partial z}(\varepsilon,x)\left[1 - 4\left(\frac{y}{H_s}\right)^2\right] \qquad 2.4$$

where y is the direction perpendicular to the extruder axis. The volumetric flowrate past the orifice plug is then given by

$$Q = 2\int_0^w\int_0^{H_s/2} v_z\,dydx = \frac{-H_s^2}{4\mu}\int_0^w\int_0^{Hs/2}\frac{\partial P}{\partial z}(\varepsilon,x)\left[1-4\left(\frac{y}{H_s}\right)^2\right]dydx \qquad 2.5$$

which with equation 2.3 yields

$$Q = \frac{3H_s^2}{z_s}\pi N\int_0^w\int_0^{H_s/2} f(\varepsilon,x)\left[1-4\left(\frac{y}{H_s}\right)^2\right]dydx = \frac{H_s^3\pi N}{z_s}\int_0^w f(\varepsilon,x)\,dx \qquad 2.6$$

or

$$Q/N = \frac{\pi H_s^3}{z_s}F(\varepsilon) \qquad 2.7$$

where $F(\varepsilon) = \int_0^w f(\varepsilon,x)\,dx$

This result reveals that for Newtonian liquids Q/N is proportional to the area under the dimensionless pressure profile, which in turn is a function of the degree of fill, for a mixing zone

consisting of one kneading paddle followed by an orifice plug. The above development shows that the region directly upstream of the orifice plug does not have to be full to generate adequate pressure for flow past the orifice plug. $f(\varepsilon,x)$ is independent of viscosity, so equation 2.7 also predicts that the relationship between Q/N and ε is independent of viscosity. This is similar to the prediction of Booy (1980), who has shown for very starved twin screw extruders with "screw type" segments the relationship between Q/N and ε depends only on the geometry of the screws. Unlike the results of Booy (1980), application of equation 2.7 is not restricted to very small degree of fill. The experimental results for Q/N versus degree of fill are analyzed in terms of the predictions of equation 2.7 in Section 2.6.2.

Theories that extend Booy's theory and the development given above to include viscoelastic liquids and the effect of melting need to be developed for starved twin screw extruders. These theories would be used to predict a priori how hold ups in a starved twin screw extruder depend on changes in operating conditions and would be a basis for understanding how the thermal and flow history of polymer in starved twin screw extruders change with changes in operating conditions. Ultimately, greater control of these extruders could be obtained. One objective of the experimental work here was to provide data against which future theories for flow in starved twin screw extruders may be tested.

2.4 Experimental

2.4.1 Operating Variables

The twin screw extruder used in this study was a Baker Perkins 30 mm co-rotating intermeshing twin screw extruder with a length-to-diameter ratio of 13:1. A schematic of the extruder is given in Figure 2.2, which shows the four temperature zones. The extruder could be "dead stopped" (screw rotation stopped and the melt cooled quickly) and the barrel halves opened in a clamshell manner to obtain a qualitative picture of material distribution inside the extruder at a given set of operating conditions.

The extruder shafts were composed of slip-on screw, kneading paddle, and orifice plug segments. In all of our experiments, a two mixing zone screw configuration was employed as depicted in Figure 2.3, where each mixing zone consists of six kneading paddles followed by an orifice plug. As Figure 2.4a indicates, transversely neighboring kneading paddles are at 90 degrees to each other, while axially neighboring paddles (Figure 2.4b) can take a number of orientations depending on the amount of forwarding action desired in each mixing zone. In this work, the first mixing zone always had the same arrangement of paddles as the second mixing zone. For some experiments, the arrangement of paddles was altered to change the forwarding abilities of the zones. A code such as 4(60F) 2(90) is used to denote the relative paddle orientations. This code means that proceeding downstream the first four paddles in both mixing zones had the 60^{o}F orientation of Figure 2.3, and the last two paddles had a 90^{o} orientation.

1. Feed Ports
2. Barrel Valves
3. Vacuum Port
4. Die Attachment
5. Barrel Thermocouples
6. Melt Thermocouples
7. Die Melt Thermocouple and Pressure Transducer

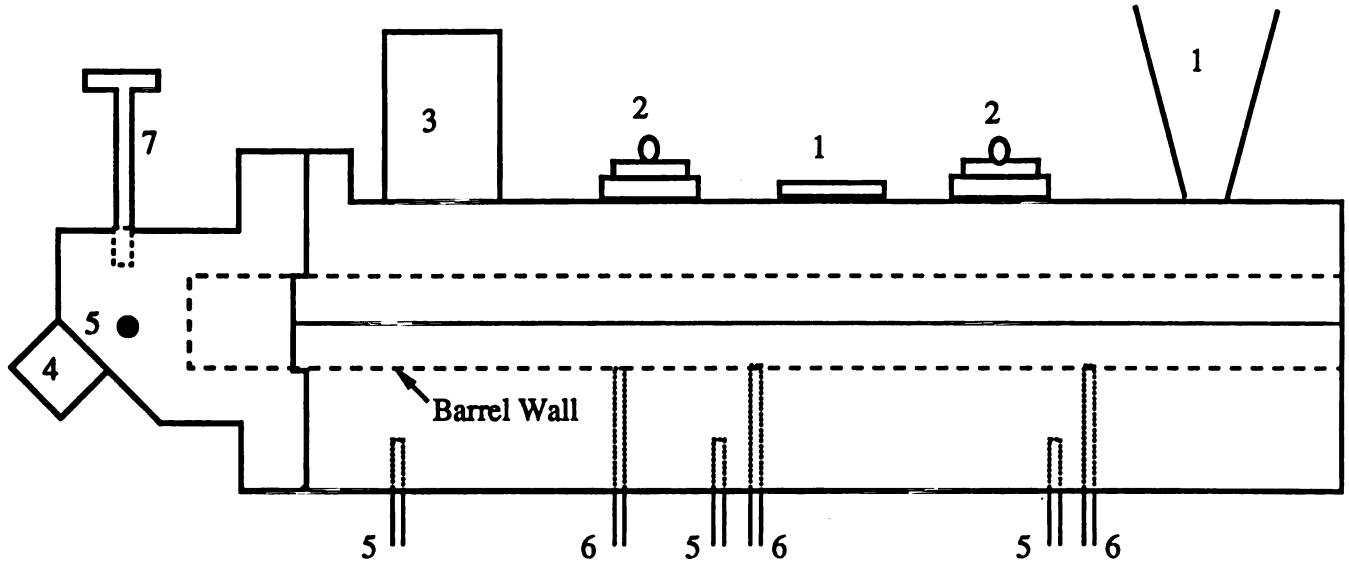

Figure 2.2 Schematic of Twin Screw Extruder

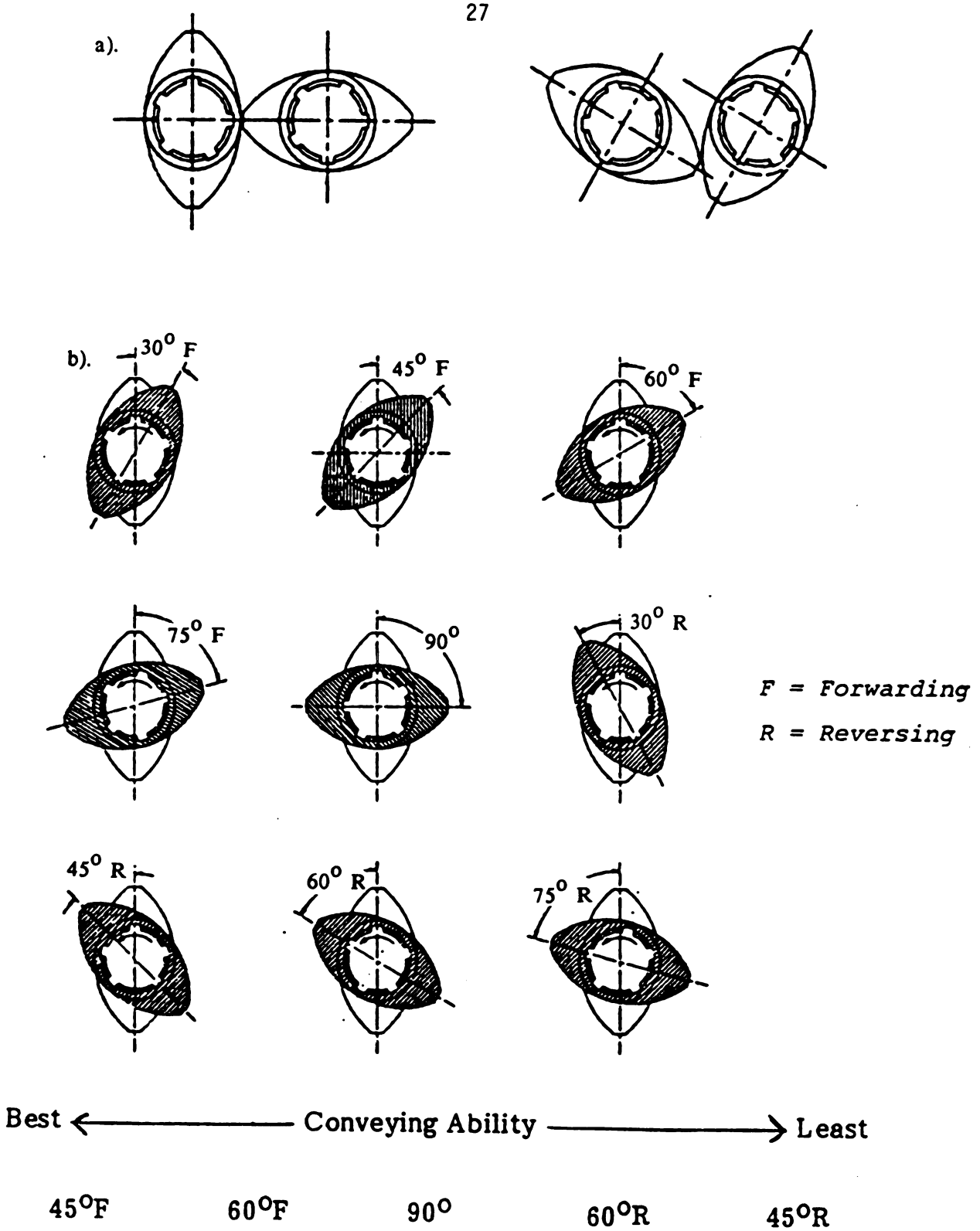

Figure 2.3 a). Transversely neighboring and b). axially neighboring kneading paddle configurations (Baker Perkins 30 mm Mp-cv manual)

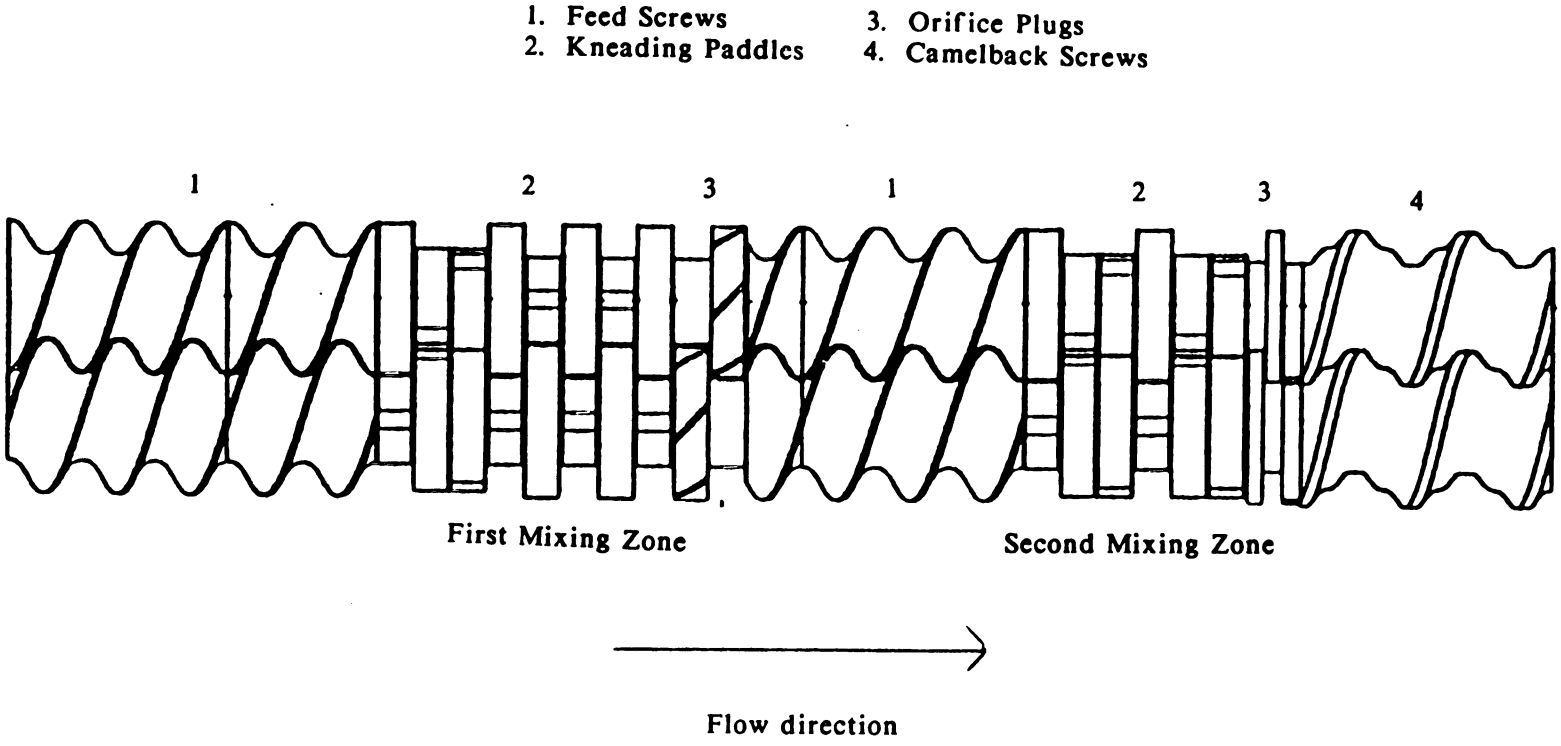

Figure 2.4 Typical two stage shaft configuration.

Barrel valves are used in conjunction with orifice plugs to control the amount of cross-sectional area available for axial flow. The orifice plugs are disks of diameter close to that of the barrel, and the barrel valve is a triangular-shaped vane positioned directly over the orifice plugs. As the barrel valve was turned from fully closed to fully open, the cross-sectional area available for axial flow around the orifice plugs increased. Equation 2.7 shows that by varying the diameter and width of the orifice plugs, the resistance to axial flow can be altered. For instance, increasing the orifice plug diameter or width increases the resistance to axial flow at the orifice plug. Orifice plug dimensions were not a variable in our experiments, and in all of the experiments orifice plugs with diameter 29.62 mm were used after the first mixing zone, and orifice plugs with diameter 29.44 mm were used after the second mixing zone. The width of the orifice plugs at the barrel wall was 3.75 mm.

The various operating conditions used in the residence time experiments here are shown in Table 2.1.

The polymers used in these experiments, PVC and CPE, are prone to degrade at processing temperatures. Appropriate stabilizers were used, and the screw rotation rate and barrel temperature selected to avoid thermal and shear degradation over the widest range of operating conditions. When degradation occurred, experimental results were discarded.

Table 2.1.--Operating conditions for twin screw extrusion residence time experiments.

Operating Variable	Possible Values
Screw rotation rate	100, 250, and 500 rpm
Feedrate	10-40 g/min
Barrel valve position	Fully open, fully closed
Polymers	PVC,[a] CPE[b]
Paddle orientation	6(45F) most forwarding[c] 4(60F) 2(90) moderate forwarding 6(90) least forwarding
Temperature (all zones)	PVC (180°C, CPE (150°C)

[a]Goodrich rigid pipe compound.

[b]Dow Tyrin 2552 with 3 ppm Ba/Cd stabilizer.

[c]These are mixing zone configurations as explained in text.

To study the effect of feedrate, screw rotation rate, and polymer properties, a screw configuration of 4(60F) 2(90) with barrel valve closed was used. This base configuration was then altered to examine the effect of change in barrel valve position and geometry.

2.4.2 Activation and Detection of Tracer

The tracer samples for determining residence time distributions were formed by cutting a 6.8 mg chip from some previously extruded PVC pipe compound, or by cutting a 15 mg chip from a chunk of pure CPE without stabilizer. The chunk of pure CPE was formed by melting

the CPE powder in a laboratory beaker while avoiding thermal degradation. The chips were then irradiated in the nuclear reactor at Michigan State University at a neutron flux of 10^{12} neutrons/(cm^2 sec) for 3 minutes, resulting in an activity of 10 microcuries. During irradiation both PVC and CPE can degrade and/or cross-link. However, Chapiro (1962) presented an analysis which revealed that less than 1% of the tracer degraded or cross-linked in our experiments.

In some experiments, the radiation was detected outside the extruder wall, as described in more detail later, and other experiments, the radiation intensity for the extrudate, without attenuation from the wall, was monitored. These experiments revealed that 10 microcuries of activity was adequate to detect a majority (85% or greater) of the tracer through the extruder wall. The tail of the residence time distributions was not detected very well through the extruder wall.

The intensity of radiation, I, for the radioactive tracer chip at any time was given by

$$I = N_0 \Gamma \Psi w p_i (1-\exp(-.693\ t_i/t_{1/2})\ \exp(-.693\ t_c/t_{1/2})/3.7x10^7 M \qquad 2.8$$

where N_0 is Avagadros number, Γ is the nuclear cross-section (.43b for Cl), Ψ is the neutron flux, w is weight of chlorine in sample (.0038 g), p_i is percentage of isotope found in nature, M is molecular weight of chlorine (35.45), t_i is time of irradiation, t_c

is time from end of irradiation, and $t_{1/2}$ is the half life of the isotope (37.3 min for Cl^{37}).

Each tracer experiment was conducted by allowing the twin screw extruder to come to steady state (this took approximately 10 minutes) at the desired operating conditions. Steady state was assumed when temperature readings, torque readings, and the appearance of the extrudate did not change for five minutes. The radioactive chip was then dropped into the feed funnel while simultaneously starting the radiation detection equipment. Radiation intensity versus time was then detected after the first or second mixing zone or at the end of the shafts, and three sets of measurements were made at each detector location. Radiation intensity was detected on the outside of the extruder with a Harshaw sodium-iodide 1-1/4" scintillation crystal. This detector was centered behind a 1-1/2" by 3/4" rectangular hole in a 2" wide lead brick. The radiation counts were accumulated over every other 5 or 10 seconds with a scaler, and a printout of radiation counts versus time was obtained. Some tests were repeated with both 5 and 10 second accumulation periods with no effect on the results. The experiment was stopped when the radiation intensity was equal to background radiation levels for five consecutive measurements.

The duration of each experiment varied from 3 to 10 minutes. Because of the short half-life of the Cl^{37} isotope (37.3 min), it is clear from equation 2.8 that the effect of radiation decay with time had to be taken into account in all of our experiments. The

radiation counts C_{i0} corrected for decay to a reference time t = 0 were calculated from

$$C_i/C_{i0} = \exp(-.693\ t/t_{1/2}) \qquad 2.9$$

where C_i was the radiation counts measured at time t. Background counts were first subtracted from the measured counts before using equation 2.9. Equation 2.9 can be used to show that the intensity of radiation for the chlorine is essentially equivalent to background radiation after four hours, which is convenient in terms of waste disposal.

Figures 2A and 2B in the appendix give examples of the radiation counts versus time obtained after the first mixing zone, the second mixing zone, and the end of the screws for PVC and CPE, respectively. Background radiation counts have been subtracted from the radiation counts in Figures 2A and 2B, and the counts have been corrected for decay by equation 2.9.

2.5 Data Analysis

The residence time experiments performed here consisted of a pulse input of radioactive tracer to the extruder. Radiation counts, which were proportional to the concentration of tracer, were then measured at various axial locations. From the radiation counts, the mean residence time for the tracer was calculated using:

$$t_m = \int_0^\infty t_i\ C_i\ dt / \int_0^\infty C_i\ dt \qquad 2.10$$

where C_i is the radiation counts obtained over the time interval dt at time t_i.

In our experiments, the twin screw extruder had two hold up zones called the first and second mixing zones, where the first mixing zone was upstream of the second mixing zone. The value of mean residence time calculated from the experimental data for the second mixing zone using equation 2.10 included the time that the tracer spent in the first mixing zone. To calculate the mean residence time of material in exclusively the second mixing zone, the average value of mean residence time for the first mixing zone was subtracted from the average value of mean residence time that was obtained after the second mixing zone.

If a reasonable estimate can be made for the density, ρ, of a polymer system in a given region of the twin screw extruder, then the volumetric flowrate of material through that region is given by $Q = \dot{m}/\rho$, where m is the mass feedrate. From the experimentally determined mean residence time t_i for region i, the hold up v_i of polymer in region i can be calculated from equations 2.1 and 2.10 as

$$v_i = t_i \dot{m}/\rho \qquad 2.11$$

For meltable polymers, the hold up in regions where melting takes place cannot be analyzed with equation 2.11 because the sharp change in density in these regions is difficult to describe analytically. To calculate hold ups in regions that consisted totally of PVC melt or CPE melt for our experiments, the densities of PVC and CPE at the melt temperature were calculated from the measured densities of PVC

and CPE at room temperature (1.41 g/cm^3 and 1.08 g/cm^3, respectively), by using thermal volume expansion coefficients. Heydeman and Guicking (L959) reported values of the thermal volume expansion coefficient for a PVC formulation similar to that used in this study of approximately 2 x $10^{-4}/^oC$ for temperatures between the glass transition temperature and the crystalline melt temperature, and 5.5 x $10^{-4}/^oC$ for temperatures above the crystalline melt temperature. Published data on CPE are scant, so the PVC thermal volume expansion coefficients were used for CPE. Since the calculated density change from room temperature to the melt temperature for CPE is only on the order of 5% and the thermal volume expansion coefficients used are close to those published for other polymers (Modern Plastics Encyclopedia, 1982), the error in the calculated density for CPE melt is small. The glass transition temperatures for PVC and CPE are below room temperature, and the crystalline melt temperature was assumed to be 80^oC for PVC (Modern Plastics Encyclopedia, 1982) and 125^oC for CPE (Tyrin 2552 Technical Data Sheet, Dow Chemical Company, 1987) during the above density calculations.

It is informative when studying v_i for a region of the extruder to know the total volume available for polymer in that region. The volume of a region was calculated by determining the free cross-sectional area perpendicular to the screw, for a particular region of the screw, with an image analyzer and then multiplying this cross-sectional area by the length of the region.

It is important to obtain a good estimate of axial dispersion in reactive processing with a twin screw extruder where a very narrow residence time distribution results in a uniform product. On the other hand, great amounts of axial dispersion may be beneficial when the extruder is used for mixing operations. To compare the spread in residence time distributions at different axial locations, we found it most informative to use a quantitative measure of axial dispersion. To quantify axial dispersion, the cumulative distribution function, F(t), which is defined as:

$$F(t) = \int_0^t C_i \, dt / \int_0^\infty C_i \, dt \qquad 2.12$$

was employed. F(t) gives the fraction of tracer that has left a zone during times less than or equal to t. The expression used to quantify the axial dispersion was then

$$\Delta t_{16\text{-}84} = t_2 - t_1 : F(t_2) = .84, \; F(t_1) = .16 \qquad 2.13$$

Assuming a Gaussian distribution in residence times, $\Delta t_{16\text{-}84}$ is just the dimensional time for one standard deviation around the mean of material to leave a zone.

2.6 Results and Discussion

2.6.1 Visual Examination of Mixing Zones

In each case when the extruder was "dead stopped," as described earlier, visual inspection of the inside of the extruder revealed that the mixing zones always contained much more polymer than the

screw type segments, and the mixing zones were never completely full for the operating conditions tested here. This difference between screw segments and mixing zones is illustrated in the photographs of Figures 2.5 and 2.6, where it can be seen that the screw segments contain only small chunks of PVC or CPE that had torn off from around the orifice plugs and were being forwarded quickly by the screw elements. The shapes of these chunks in the screw regions during different runs reflect the more rubbery behavior of CPE. As the photographs of Figures 2.5 and 2.6 show, PVC appears to be flowing through the screw sections, whereas pieces of CPE in the screw sections show evidence of being rolled, sliced, and shredded. The photographs of Figures 2.5 and 2.6 also demonstrate that the degree of fill in the mixing zones was affected by changes in operating conditions, and since mean residence time depends on degree of fill, the thermal and flow history of polymer in our extruder depends on the relationship between operating conditions and degree of fill for the mixing zones. The following sections seek to establish this relationship.

Figures 2.5 and 2.6 show that the cross-sectional degree of fill on the upstream side of the orifice plug can be considerably less than unity, and yet polymer is being pushed past the orifice plug. Also, visual examination revealed that there was a tendency for polymer to be pushed past the orifice plug in the vicinity of the leading edge of the paddle tip. Both of these results support the development leading to equation 2.7. Other specific aspects of

First Mixing Zone

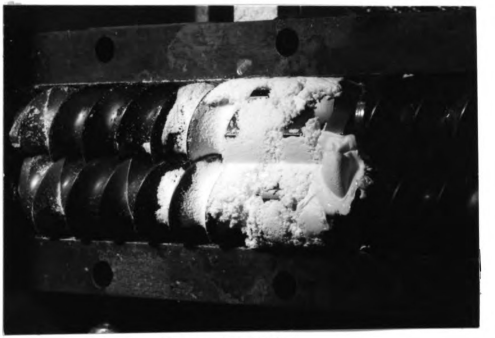

Feed = 11 g/min

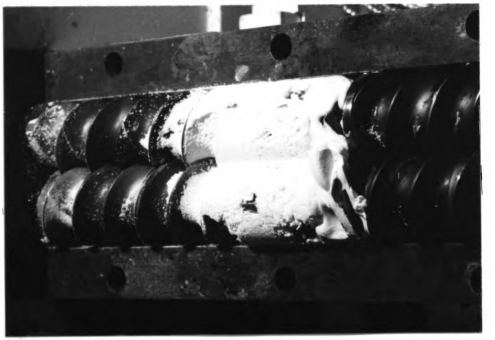

Feed = 38 g/min

Figure 2.5 Photographs showing effect of feedrate on hold-up of PVC in first and second mixing zones at 250 rpm, with 4(60F) 2(90) configuration and barrel valves closed.

Second Mixing Zone

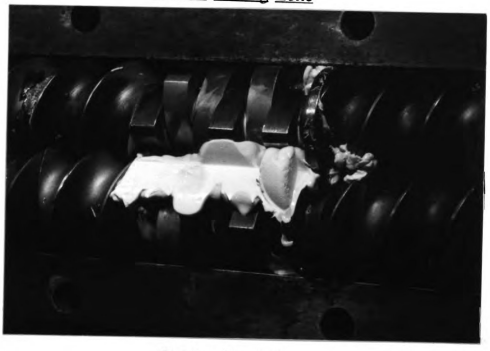

Feed = 11 g/min

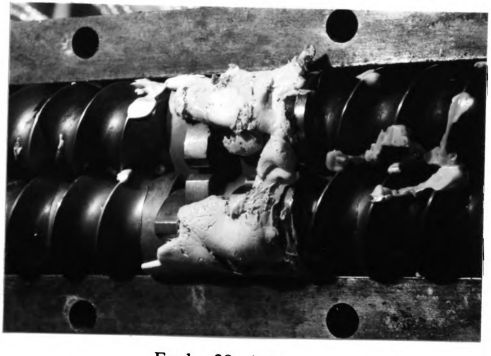

Feed = 38 g/min

Figure 2.5 Continued.

First Mixing Zone

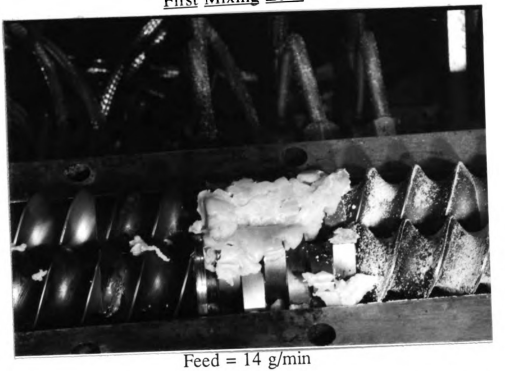

Feed = 14 g/min

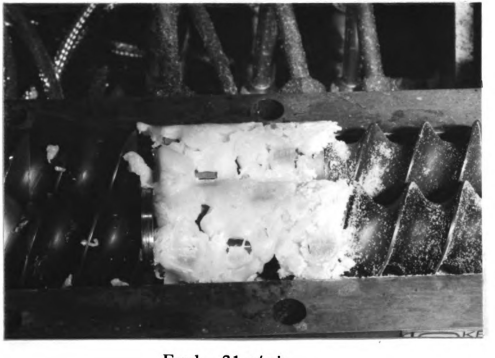

Feed = 31 g/min

Figure 2.6 Photographs showing effect of feedrate on hold-up of CPE in first and second mixing zones at 250 rpm, with 4(60F) 2(90) configuration and barrel valves closed.

Second Mixing Zone

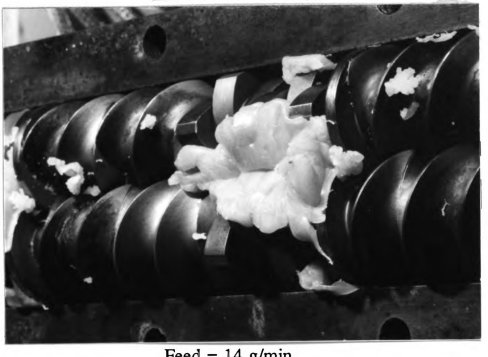

Feed = 14 g/min

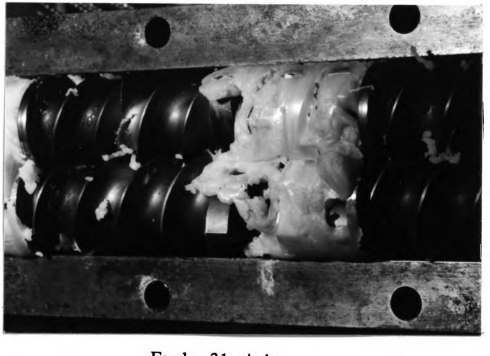

Feed = 31 g/min

Figure 2.6 Continued.

Figures 2.5 and 2.6 will be discussed in later sections when they are pertinent.

2.6.2 Effect of Operating Conditions on Mean Residence Times and Hold Up in the Mixing Zones

Effect of screw rotation rate and feedrate of volumetric flowrate. The effects of volumetric flowrate and screw rotation rate on mean residence time and degree of fill for PVC and CPE in the second mixing zone are displayed in Figures 2.7 and 2.8. As the photographs of Figures 2.5 and 2.6 illustrate, for each run in which the shafts were visually examined, the second mixing zone appeared to contain polymer melt. Therefore, by use of the methods outlined in the Data Analysis section, a melt density of 1.33 g/cm^3 was calculated for PVC, a melt density of 1.03 g/cm^3 was calculated for CPE, the total volume available for melt in the second mixing zone was determined by image analysis to be 28.2 cm^3, and these values were then used to compute the degree of fill and volumetric flowrate results of Figure 2.8. Each data point in Figures 2.7 and 2.8 is the average of three experimental values, and the error bars are given to illustrate typical spreads in the experimental measurements. Figure 2.7 demonstrates that both screw rotation rate and feedrate can be used to vary the mean residence time (or history) of PVC in the second mixing zone, where an increase in feedrate or screw rotation rate decreases the mean residence time. On the other hand, a variation in screw rotation rate or feedrate did not have much of an effect on mean residence time of CPE in the

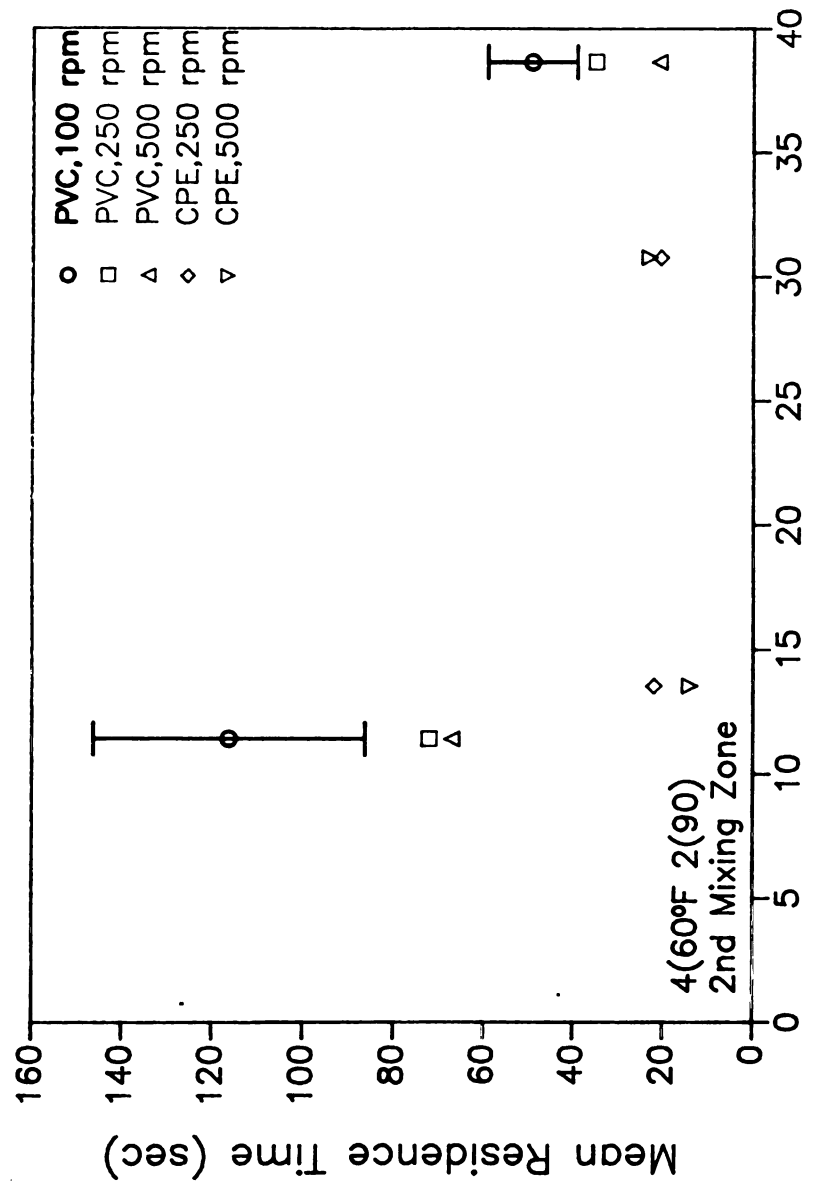

Figure 2.7 Mean residence times for second mixing zone.

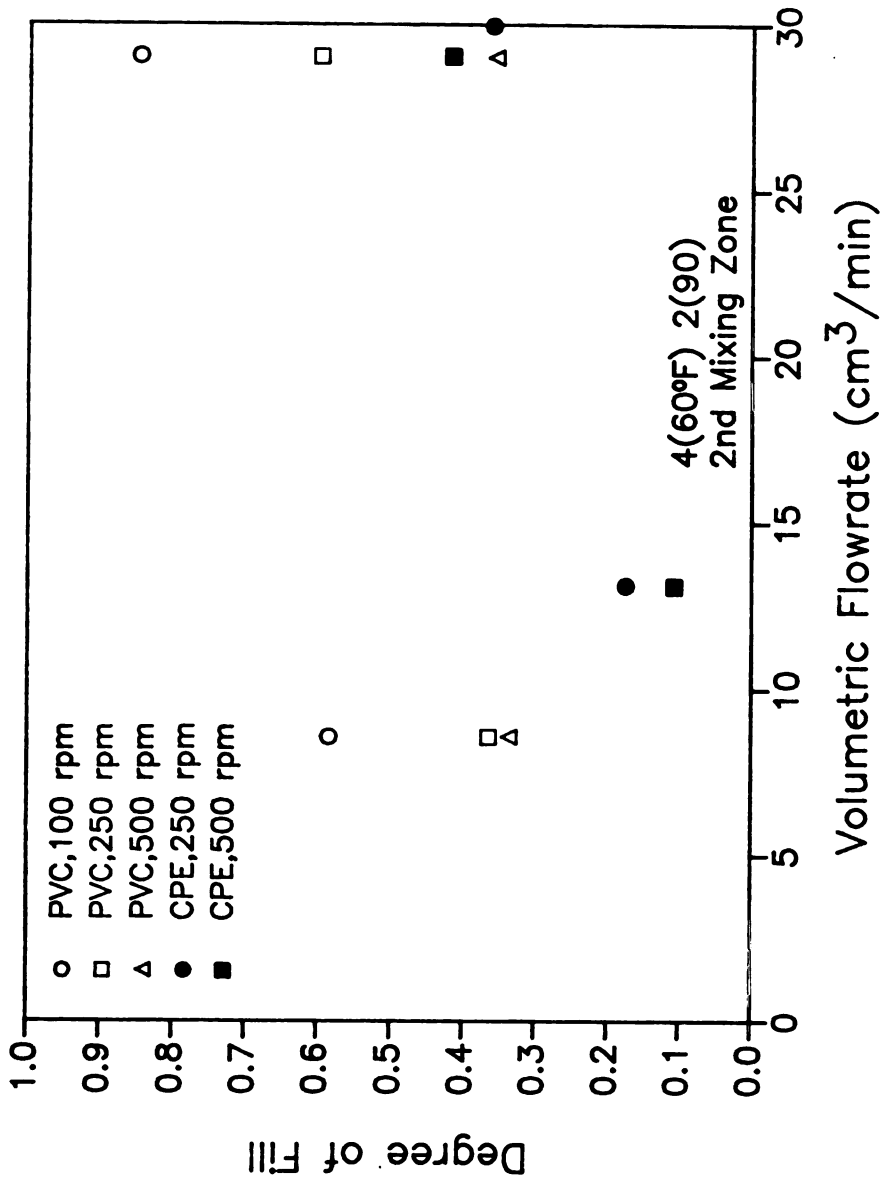

Figure 2.8 Degree of fill for second mixing zone.

second mixing zone. It should be noted here that decreasing the screw rotation rate to 100 rpm caused extensive thermal degradation in the CPE extrudate, which indicates that the mean residence time of CPE in the extruder and hence the mixing zones may have increased significantly at this screw rotation rate.

Figure 2.8 shows that for both PVC and CPE the hold up in the second mixing zone increases with increase in volumetric flowrate, but only the hold up of PVC decreases with increase in screw rotation rate. The photographs of Figures 2.5 and 2.6 show in a qualitative fashion that there is an increase in hold up with increase in feedrate for the second mixing zone as the results of Figure 2.8 indicate. It is interesting to examine the distribution of hold up in Figures 2.5 and 2.6 over several cross-sections in the second mixing zone as feedrate changes for PVC and CPE. For PVC, the cross-sectional degree of fill in the second mixing zone is uniform along the total length of the mixing zone at low feedrates, but at high feedrates, the cross-sectional degree of fill is quite high at the orifice plugs and then tapers off upstream from the orifice plugs. In contrast, the cross-sectional degree of fill for CPE in the second mixing zone is small at low feedrates and larger at high feedrates, and is fairly uniform throughout most of the first mixing zone with a slight reduction at the entrance to the mixing zone for both feedrates.

To gain an understanding of the controlling factors for degree of fill, and hence mean residence time, that generate the results

seen in Figures 2.7 and 2.8, experiments were conducted in which the orifice plugs were removed or the kneading paddles were replaced with continuous screws in the second mixing zone and the extruder was "dead stopped." In each of these experiments, a visual examination of the screws revealed that the amount of polymer held up in the second mixing zone without orifice plugs or without paddles was very small compared to a mixing zone composed of both kneading paddles and orifice plugs. These results imply that the relationship between the forwarding ability of the screw elements upstream of the orifice plugs and the resistance at the orifice plugs is a controlling factor for degree of fill in the second mixing zone.

The data in Figure 2.8 have been replotted as Q/N versus degree of fill in Figure 2.9 to examine the range of applicability of equation 2.7. Figure 2.9 shows that Q/N is linearly related to the degree of fill at low degree of fill for the mixing zones, where this linear relation is different for PVC than CPE. This result is contrary to the results of Eise et al. (1983), who obtained a nonlinear relationship between Q/N and degree of fill for a co-rotating twin screw extruder with kneading block screws. Eise et al.'s extruder did not contain orifice plugs, which may explain the above difference, because it has already been established that orifice plugs play a major role in determining the hold up in the mixing zones studied here. From the development leading to equation 2.7, a linear relationship between Q/N and ε suggests that $F(\varepsilon)$, the area under the dimensionless pressure profile curves, increases

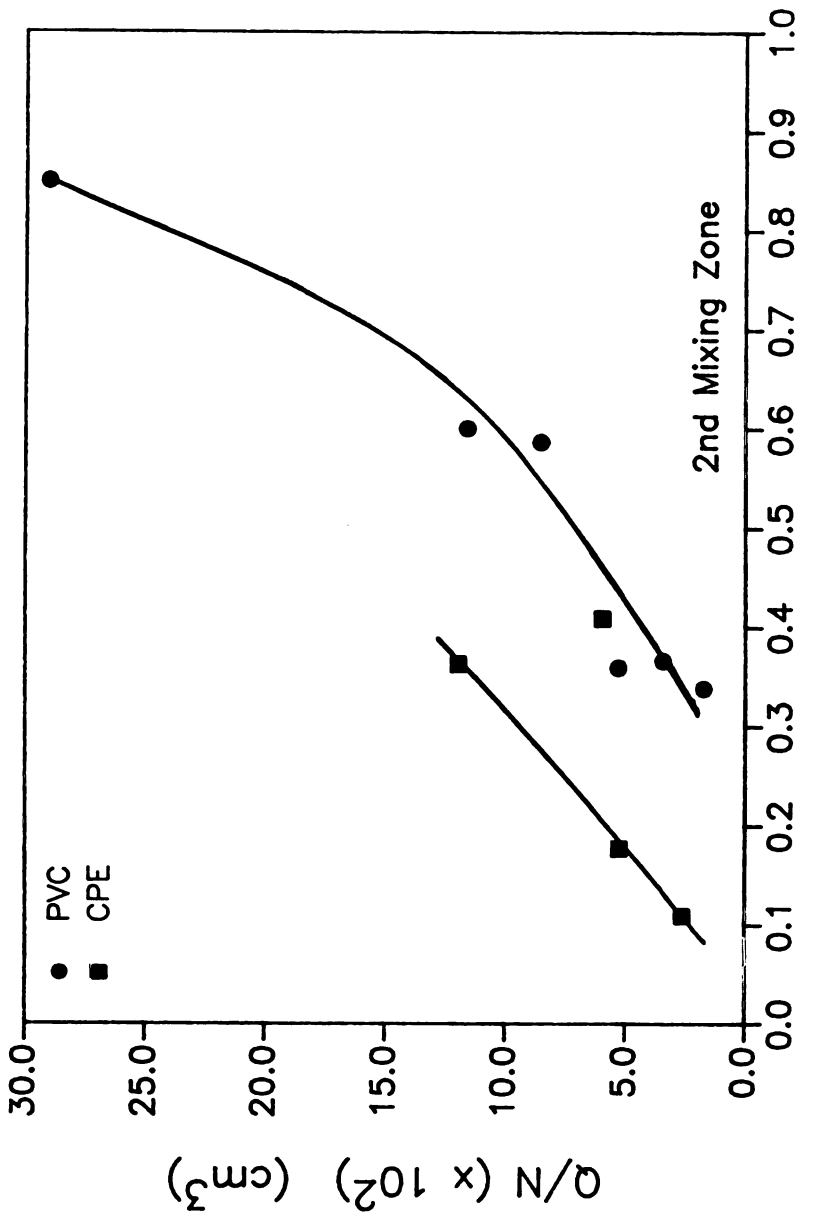

Figure 2.9 Relationship between Q/N and degree of fill for second mixing zone.

proportionally with Q/N at low degree of fill. Also, at comparable operating conditions, $F(\varepsilon)$ is smaller for CPE than PVC.

The linear relation between Q/N and ε at low degree of fill in Figure 2.9 is identical to the prediction of Booy's (1980) theory for extruder sections with "screw type" geometry. In Booy's theory, the slope of the Q/N versus ε relationship comes solely from geometric considerations. Since the slopes of the lines are similar for PVC and CPE at low degree of fill, these slopes might also be determined by geometric considerations. Booy related the value of degree of fill at Q/N equals zero to the material that was wiped out in stagnant layers in his screw geometry. For mixing zones, the paddles are self-wiping, and thus there are no stagnant layers in the mixing zones, as can be seen in Figures 2.5 and 2.6. Therefore, the x intercept in Figure 2.9 represents the amount of material that cannot be forwarded past the orifice plug when the feed is stopped. It is interesting to note that there is more of this material when PVC is extruded than when CPE is extruded.

As can be seen from Figure 2.9, at high degrees of fill a linear relationship between Q/N and degree of fill no longer exists. Szydlowski et al. (1987) modeled the flow in a full intermeshing kneading disc region of a co-rotating twin screw extruder and found that Q/N is equal to a geometric constant. The results of Figure 2.9 show that this prediction no longer holds when $\varepsilon < 1$. The nonlinear relationship between Q/N at high degree of fill can probably be attributed to the complex relationship that exists between axial flow, degree of fill, and the staggered pressure

profiles in the kneading paddle region (examples of these pressure profiles were given by Szydlowski et al., 1987).

In all cases, when the extruder was dead stopped, visual examination revealed that the transition from powder to melt occurs in the first mixing zone. An analysis of degree of fill in the first mixing zone was not attempted here because of the complex change in density that occurs as the polymer melts. Nevertheless, exploration of the effect of operating variables on mean residence time for the first mixing zone was revealing. Figure 2.10 shows the variation of mean residence time with feedrate at various screw rotation rates for CPE and PVC in the first mixing zone. It is remarkable that although the powder to melt transition occurs in the first mixing zone, the trends and magnitude for mean residence times shown in Figure 2.10 are very similar to those for the second mixing zone shown in Figure 2.7. It follows that the apparent changes in hold up for the first mixing zone must be similar to those calculated for the second mixing zone, and the same factors govern hold up in the two mixing zones.

Effect of polymer properties. The differences between the results for PVC and the results for CPE in Figures 2.7 and 2.8 are quite striking, especially at comparable low volumetric flowrates where the mean residence time and degree of fill for CPE were much lower than that of PVC. It seems intuitive, then, that there are polymer properties that play a key role in how much hold up there is in the mixing zones, although it is not clear what these

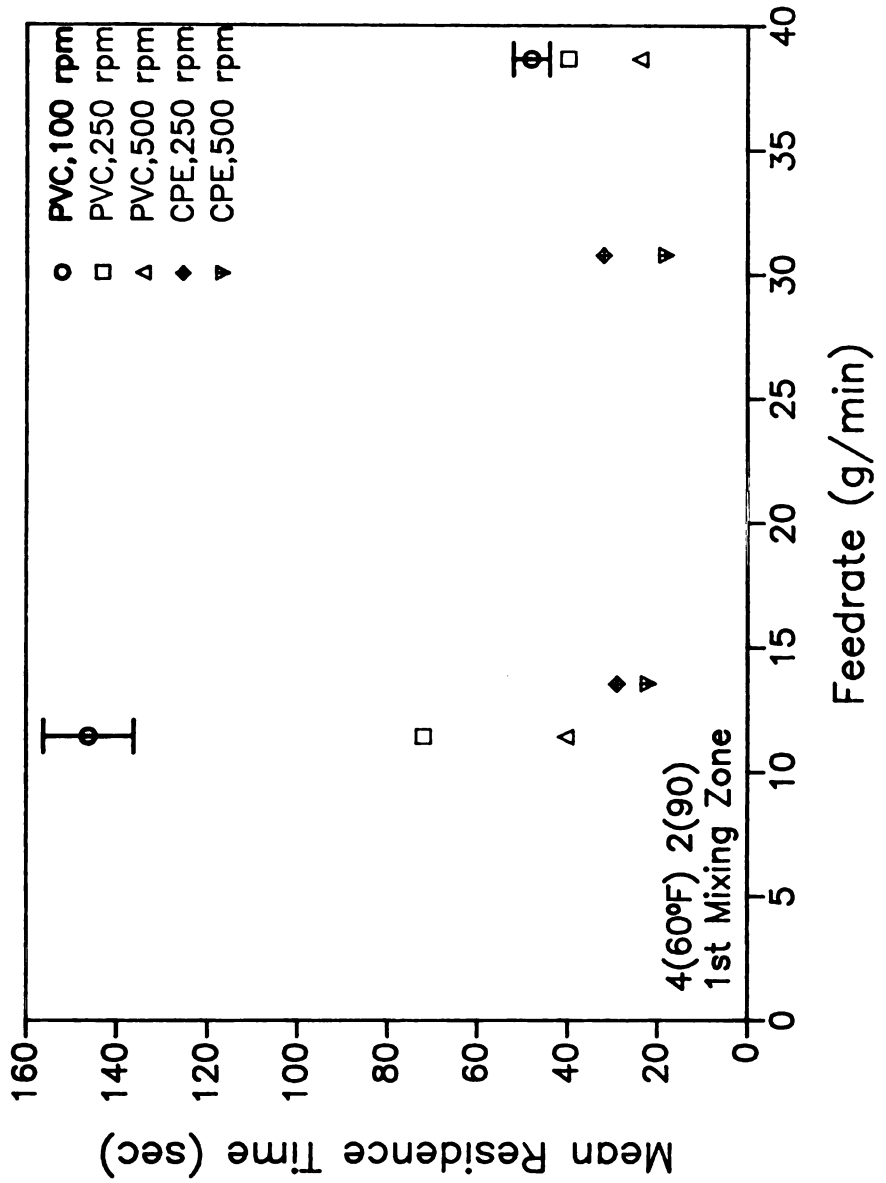

Figure 2.10 Mean residence times for first mixing zone.

properties are. Here we present some of the differences in properties between PVC and CPE and discuss the possible effects of these differences on hold up in the mixing zones.

Equation 2.7 states that the degree of fill is not dependent on polymer viscosity. Since equation 2.7 was developed for a Newtonian fluid and in general polymers are non-Newtonian, the validity of equation 2.7 was examined by trying to correlate shear viscosity to the hold up in the mixing zones. Figure 2.11 shows a plot of steady shear viscosity versus shear rate for PVC and CPE obtained with an Instron capillary rheometer. One can see from Figure 2.11 that both PVC and CPE are quite shear thinning. From the clearance between the tip of the paddle and the extruder, and the linear velocity of the paddle tip, a maximum shear rate of 913, 809, and 1,618 sec^{-1} was calculated for screw rotation rates of 100, 250, and 500 rpm, respectively. From Figure 2.11, it can be seen that the viscosity of PVC at the maximum shear rate decreased by about a factor of 8 as screw rotation rate was increased from 100 to 500 rpm, but the degree of fill for PVC seen in Figure 2.8 only decreased by a factor of 2 as screw rotation rate was increased from 100 rpm to 500 rpm. The viscosities at maximum shear rate also show that there was much more of a decrease in viscosity between 250 and 500 rpm than between 100 and 250 rpm, which was not evident in the degree of fill data for either polymer. Also the decrease in viscosity between 250 rpm and 500 rpm should be greater for CPE than PVC according to Figure 2.11, but screw rotation rate had little

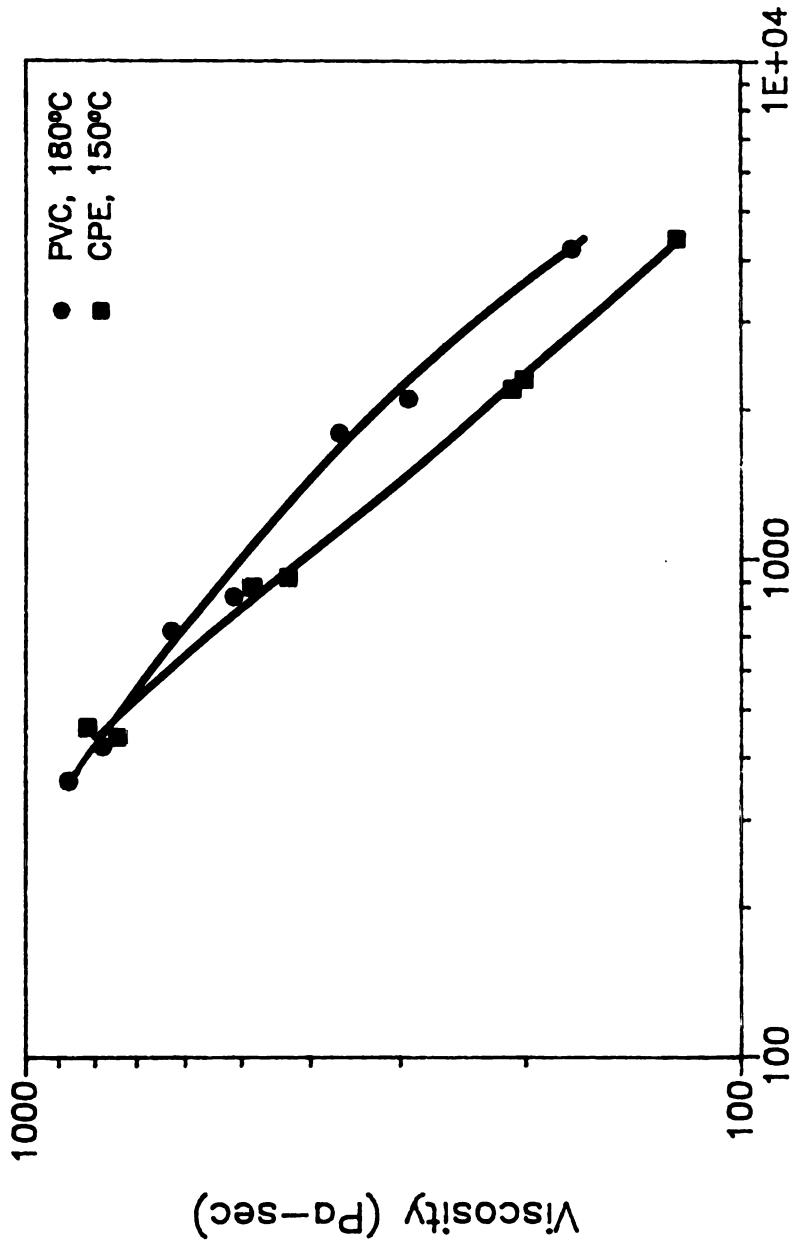

Figure 2.11 Viscosity of PVC and CPE.

effect on hold up of CPE as seen in Figure 2.8. At most, the viscosities of PVC and CPE differ by a factor of 1.5, but as Figure 2.8 shows, at low volumetric flowrate, there was a factor of 2.5 to 4.0 difference in the degree of fill. At high volumetric flowrates, there was a factor of .95 to 2 difference between the degree of fill of PVC and CPE. All of these results suggest that the degree of fill behavior for CPE and PVC was not directly linked to shear thinning effects in any straightforward fashion.

The photographs of Figures 2.5 and 2.6 show that the melting profiles for PVC and CPE are quite different, and this may have an effect on how polymer is held up in the mixing zones, although how is not very clear. Figure 2.5 demonstrates that PVC fuses at the end of the first mixing, while Figure 2.6 shows that CPE appears to melt very quickly, almost before it enters the first mixing zone. This suggests that it takes much more energy to fuse PVC than it does to fuse CPE, and these results are in line with the published heat of fusion for PVC (10.5 cal/g) (Smith, 1964) and CPE (7 cal/g) (Tyrin 2552 Data Sheet, Dow Chemical Company, 1987). Figure 2.5 also shows that the melting region for PVC gets shifted upstream from the orifice plugs at the end of the first mixing zone with increase in feedrate. This result is in line with the results of Karian (1985), who showed that the melting profile for PVC gets shifted upstream or downstream depending on the operating conditions. In fact, Karian showed that for many operating conditions PVC is not completely fused after the first six paddles in the first mixing zone, which means that in many of the runs with

PVC here, the fusion of PVC must be completed in the second mixing zone. The difference in mean residence time between PVC and CPE for the first mixing zone might be explained by the fact that PVC is mostly powder in the first mixing zone, while CPE is a melt throughout the first mixing zone. One would expect a powder to be forwarded in a different manner than melt. What this fails to explain is why the mean residence times for PVC in the first mixing zone where PVC is mostly powder is similar to the mean residence time of PVC in the second mixing zone where PVC is mostly melt. The possibility mentioned above that fusion of PVC may have to be completed in the second mixing zone might explain the trends seen with PVC as compared to CPE. During the compaction-densification-fusion-elongation melting mechanism for PVC detailed by Karian (1985), there is a large change in density of the PVC. Also, during melting, the PVC changes from a powder to a suspension to a liquid where each state of the PVC can be expected to have different flow properties. Since these transitions for PVC are happening in both the first and second mixing zone, they might explain the similarity in residence times for the two zones, and also the differences seen between PVC and CPE.

Blends containing 50 weight percent PVC and 50 weight percent CPE were extruded, and the extruder was "dead stopped" to observe the melting profiles for the blend. It appeared that the CPE melted very quickly, and the unmelted PVC and CPE formed a suspension. The PVC then melted much further down the extruder axis. It was not in

the scope of this work to study this system in detail, but analysis of this system might be quite revealing in how melting profiles affect hold up in these extruders. Also, a thorough study of the PVC/CPE system might give insight into how polymer blends are formed in a twin screw extruder.

Although the axial temperature profile for polymers in extruders is very difficult to measure, it is likely that the normalized axial temperature profiles for PVC at various operating conditions are quite different from those of CPE. This conclusion follows from the difference in the location of melting for the two polymers, which has already been discussed, and also the analysis of Rawendaal (1986), who showed that for polymer melts with different power law indexes, viscous dissipation and conduction from the barrel walls causes different axial temperature profiles. The axial temperature profiles will have a large effect on the viscosity of the polymer at various axial locations. However, the result of equation 2.7, which has been supported above, states that degree of fill is independent of viscosity, which implies that the axial temperature profile is not a determining factor for hold up in the mixing zones.

It is interesting to note that there was not much die swell for CPE, while there was some die swell for PVC, which suggests PVC melt is more elastic than CPE melt. The effect of melt elasticity on flow through the mixing zones and past the orifice plugs is not clear. It is probable that the circumferential pressure profiles shown in Figure 2.1 will be altered for elastic fluids, and also the

velocity profiles for flow past the orifice plug will be affected by fluid elasticity. It seems likely, then, that fluid elasticity plays a key role in how material flows through and is held up in mixing zones; therefore, future work that shows the effect of elasticity on these flows would be very useful.

Effect of barrel valve position. Table 2.2 shows the effect of altering barrel valve position or paddle configuration on degree of fill and mean residence time of PVC and CPE in the second mixing zone. The results presented in Table 2.2 demonstrate that with all other operating conditions held constant, opening the barrel valve caused the degree of fill and mean residence time of PVC in the second mixing zone to increase. This is counter-intuitive because opening the barrel valve increases the cross-sectional area available for downstream flow at the orifice plug; i.e., the resistance at the orifice plug is decreased. In fact, Karian (1985) showed that for a screw configuration similar to the 4(60F) 2(90) screw configuration employed by us (Karian used a 6(60F) 2(90) configuration), there is an order of magnitude decrease in pressure throughout the entire mixing zone when the barrel valve is moved from completely closed to completely open. Following the logic used to develop equation 2.7, the hold up should decrease due to the decreased resistance when the barrel valve is opened. Dead stopping the extruder showed that when the barrel valve was closed polymer got squeezed out around the orifice plugs. With the barrel valve open, most of the polymer flowed through the opening created by

Table 2.2.--Effect of barrel valve position and paddle configuration on mean residence time and degree of fill for PVC and CPE.

Polymer	Paddle Configuration	Screw Rotation Rate (rpm)	Feedrate (g/min)	Barrel Valve Position	Second Mixing Zone		First Mixing Zone Mean Residence Time (sec)
					Degree of Fill	Mean Res. Time (sec)	
CPE	4(60F) 2(90)	250	13.5	closed	.176	22	29
		250	13.5	open	.207	25	23
		250	30.8	closed	.397	21	32
		250	30.8	open	.397	21	19
PVC	4(60F) 2(90)	100	38.6	closed	.848	49	48
		100	38.6	open	1.887	110	35
		100	28.0	closed	.408	33	93
		100	28.0	open	.773	62	160
		250	28.0	closed	.596	48	51
		250	28.0	open	.784	63	43
		250	9.7	closed	.227	53	62
		250	9.7	open	.418	97	97
PVC	4(60F) 2(90)	100	11.4	closed	.585	116	146
		100	38.6[a]	closed	.840	49	48
	6(90)	100	9.7	closed	.826	192	96
		100	18.9[a]	closed	.989	118	64
	6(45F)	100	9.7	closed	.305	71	59
		100	28.0[a]	closed	.571	46	40

[a]These were maximum possible feedrates at given screw configuration.

moving the barrel valve vane. In other words, a change in barrel valve position from fully closed to fully open results in a complete change in axial flow mechanism in the vicinity of the orifice plugs. This change in axial flow mechanism may be the cause of the observed increase in hold up when the barrel valve was opened. A plot of Q/N versus ε for PVC with barrel valve open revealed that Q/N does not appear to be a function of ε. This implies that the change in axial flow mechanism past the orifice plug when the barrel valve is open renders equation 2.7 invalid, and an alternative expression to equation 2.7 must be developed for when the barrel valve position is altered. As Table 2.2 demonstrates, barrel valve position did not have much of an effect on the degree of fill and mean residence time for CPE in the second mixing zone.

Table 2.2 shows the effect of variation of barrel valve position on mean residence time for the first mixing zone. For PVC, at a constant screw rotation rate and low feedrates, opening the barrel valve causes the mean residence time in the first mixing zone to increase. However, at high feedrates, opening the barrel valve caused the mean residence time to decrease. Karian demonstrated that opening the barrel valve shifts the fusion process for PVC closer to the orifice plugs at the end of the first mixing zone, which may be an indication that the location of the melting profile helps determine the hold up in the mixing zones. For CPE, opening the barrel valve caused a slight decrease in mean residence time for the first mixing zone.

Effect of mixing zone configuration. Table 2.2 shows the effect of kneading paddle configuration on degree of fill and mean residence time for the second mixing zone. At comparable operating conditions, the least forwarding 6(90) paddle arrangement had the highest degree of fill and largest mean residence times, the most forwarding 6(45F) configuration resulted in lowest degree of fill and smallest mean residence times, and the results for the moderate forwarding 4(60F) 2(90) were somewhere in between. Table 2.2 can be used to show that it is possible to get quite different values of degree of fill at the same Q/N for the different mixing zone paddle configurations. Recall that equation 2.7 was developed for the case of a mixing zone with a single pair of kneading paddles, and although we have shown that equation 2.7 appears to hold for a mixing zone made up of many pairs of kneading paddles, the present results show that the degree of fill for these mixing zones is also a function of kneading paddle configuration. Eise et al. (1983) showed that axial flow in kneading paddle sections results from the staggered pressure profiles generated by the motion of the paddles, as mentioned earlier. A change in kneading paddle configuration will result in a different staggered pressure profile, which in turn appears to affect the amount of polymer held up in the mixing zone, as reflected by the above results. Further work needs to be done to establish the exact relationship between kneading paddle configuration and hold up for the mixing zones.

The effect of mixing zone geometry on mean residence time for the first mixing zone is not straightforward as shown in Table 2.2. The mean residence time for the least forwarding geometry 6(90) is between those for the most forwarding geometry 6(45F) and the medium forwarding geometry 4(60F) 2(90). Korian had results that showed that as the forwarding ability of the paddle arrangement behind the orifice plugs is decreased, the fusion profile for PVC is shifted upstream from the orifice plugs, so possibly the results seen here are related in some way to an axial shift in the melting profile.

2.6.3 Axial Dispersion as a Function of Operating Conditions

Figure 2.12 shows the spread in residence times at three axial positions for various operating conditions with PVC. Figure 2.12 shows the interesting results that in a majority of cases practically all of this spread occurs in the first mixing zone. In many cases, the fact that $\Delta t_{16\text{-}84}$ does not change much after the first mixing zone means that axial dispersion occurs only in the first mixing zone, and then there is essentially plug flow the rest of the way down the extruder. Since in all cases the powder/melt transition occurs in the first mixing zone, the above results suggest that this transition plays a major factor in axial dispersion. In turn, this implies that if one could control the dispersion during melting, one could control dispersion for the whole extruder in most cases, which is desired during reactive processing with a twin screw extruder.

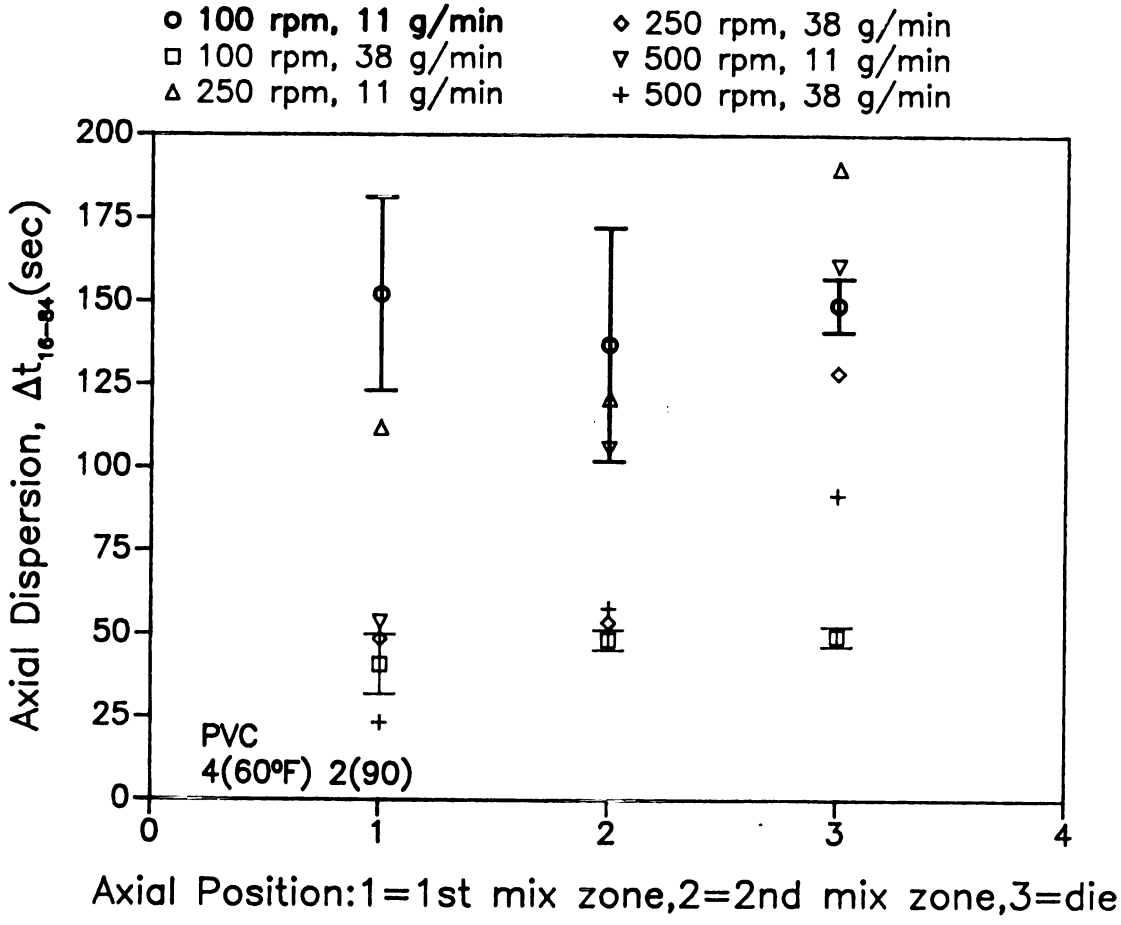

Figure 2.12 Spread in residence time distributions for PVC.

The error bars are given for two sets of data in Figure 2.12 because they demonstrate that typically the variance in experimental values for axial dispersion was much greater at low feedrates or more starved conditions than they were at high feedrates for a given screw rotation rate.

A comparison of PVC and CPE revealed that the spread in the residence time distribution relative to the mean residence time each polymer spent in an extruder region (this comparison was made by calculating Δt_{16-84} divided by the mean residence time) was about the same for both polymers. Also, comparison of Δt_{16-84} divided by mean residence time for the different paddle configurations revealed that the axial dispersion was about the same for the different configurations.

2.7 Conclusions

A novel tracer technique, where the tracer was a radioactive chip of the extruded polymer (PVC or CPE), was found to be very successful for determining residence time distributions in a co-rotating twin screw extruder with multiple mixing zones. The residence time experiments and visual observations revealed that the degree of fill in the mixing zones was greater for PVC as compared to CPE at comparable operating conditions. A development of a relationship for Q/N versus degree of fill for a mixing zone consisting of a single paddle revealed that the Q/N was linearly related to the area under the circumferential pressure profile curve

at the extruder wall for a kneading disc, which in turn is related to degree of fill. The above relationship predicts that Q/N versus ε should be independent of viscosity, and the experimental results illustrated no correlation between shear thinning effects and hold up in the mixing zones. It is hypothesized that the difference between PVC and CPE may be due to the fact that the melting region for CPE is located significantly upstream of the melting region for PVC, or the effect of elasticity on the flow behavior for the two polymers. Decreasing the restriction to axial flow by opening the barrel valve at the end of the second mixing zone resulted in an increase in hold up for this zone, which is counter-intuitive and is related to the change in axial flow mechanism that was seen with change in barrel valve position. In the majority of experiments, most axial dispersion occurred in the region where melting occurred.

The work presented in this chapter serves to illustrate the effect of operating conditions and polymer properties on degree of fill for a starved twin screw extruder with multiple hold up regions. Future research might explore further the difference seen between the two polymers used here. For instance, determination of the dimensionless circumferential pressure profile for a kneading paddle with an elastic fluid might be very revealing. How different degrees of fill affect the flow profiles in the entire mixing zones is another question that needs to be answered when considering the twin screw extruder as a mixing device. Finally, as mentioned earlier, analysis of the formation of blends of PVC with CPE may

give interesting insight into the formation of blends in a twin screw extruder.

CHAPTER III

BACKGROUND FOR STRUCTURAL ANALYSIS AND RHEOLOGY OF AB/A POLYMER BLENDS

In this chapter, information from the literature that is pertinent to the research performed here on AB diblock copolymer in excess A homopolymer blends is presented and discussed. This chapter is divided into the three topic areas that the research detailed in the rest of this dissertation covers, namely, equilibrium morphology of AB/A blends, effect of shear stress on polymer blends and polymer solutions, and morphology-rheology relationship for AB/A blends.

3.1 Equilibrium Morphology of AB/A Blends

Before discussing the morphology of AB/A diblock copolymer/homopolymer blends, it is informative to discuss the morphology of AB diblock copolymer by itself. If the A-block is incompatible with the B-block, which is the case studied here, the microstructure of the diblock will consist of spheres, cylinders, or lamellae, depending on the relative proportions of the two blocks, as shown in Figure 3.1. If the block lengths are quite short, the diblock forms a homogeneous unstructured mixture. Many times the diblock is synthesized by anionic polymerization, in which case the

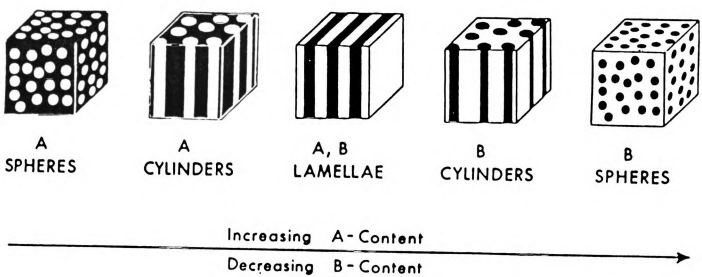

Figure 3.1 Possible morphologies for a pure AB diblock copolymer (from Molau, 1970).

polydispersity of block lengths is quite minimal, and hence the shape and size of the microdomains of the diblock are very uniform (Rigby & Roe, 1980). Roe, Fishkis, and Chang (1981) and Widmaier and Meyer (1980) have shown by small-angle X-ray scattering and rheological measurements, respectively, that a change in temperature can induce a transition from an ordered microdomain structure to a disordered homogeneous structure for pure block copolymers.

Now let us consider the phase behavior for homopolymer A mixed with AB diblock copolymer. The complex nature that a phase diagram for AB/A blends can have is shown in Figure 3.2, which is a phase diagram for a styrene/butadiene diblock in very low molecular weight polystyrene (Roe & Zin, 1984). Depending on the relative block lengths of the AB diblock and the length of the A homopolymer, and the degree of incompatibility between polymers A and B, the phase behavior for the AB/A blend can be quite different from that shown in Figure 3.2.

For AB/A blends where there is an excess of A homopolymer, as is the case for the AB/A blends studied here, often the AB diblock forms a micelle structure, as depicted in Figure 3.3. Due to incompatibility with the A homopolymer, the B-blocks of the diblock copolymer associate to form the core of a micelle structure (Region 1 of Figure 3.3), and the A-blocks form cilia that mix to some degree with the A homopolymer to create a corona (Region 2 of Figure 3.3). The matrix phase (Region 3 of Figure 3.3) consists of A homopolymer with small amounts of dissolved AB diblock.

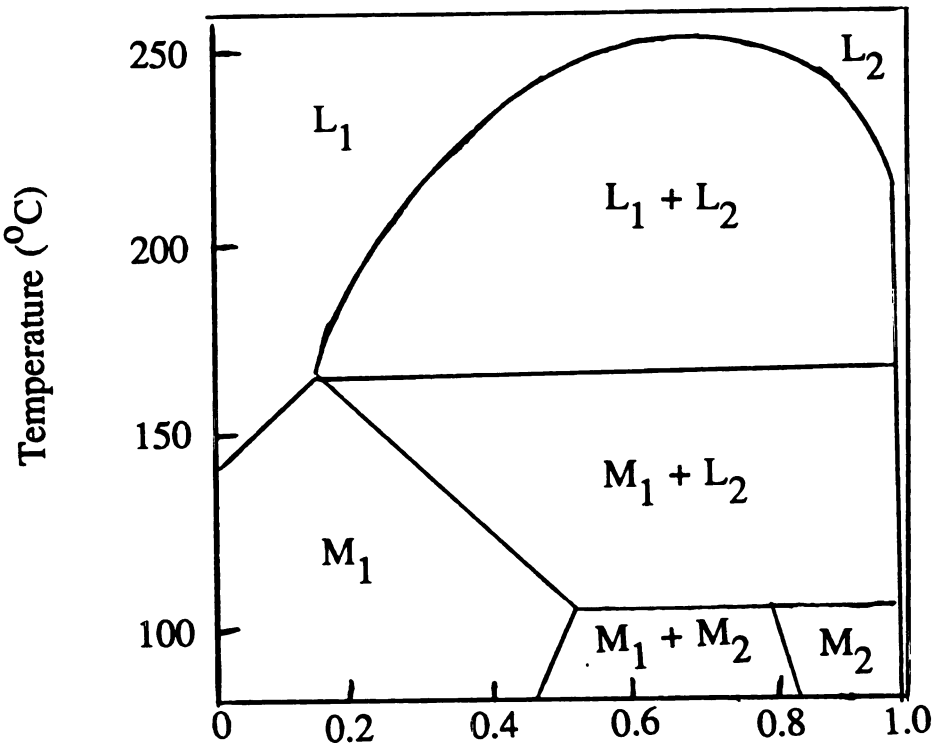

Figure 3.2 Phase diagram for a styrene-butadiene diblock (27% styrene, M_w=28,000) in low molecular weight polystyrene (M_w=24000). L corresponds to a homogeneous mixture of homopolymer and diblock, and M corresponds to a mesophase consisting of ordered microdomains of diblock.

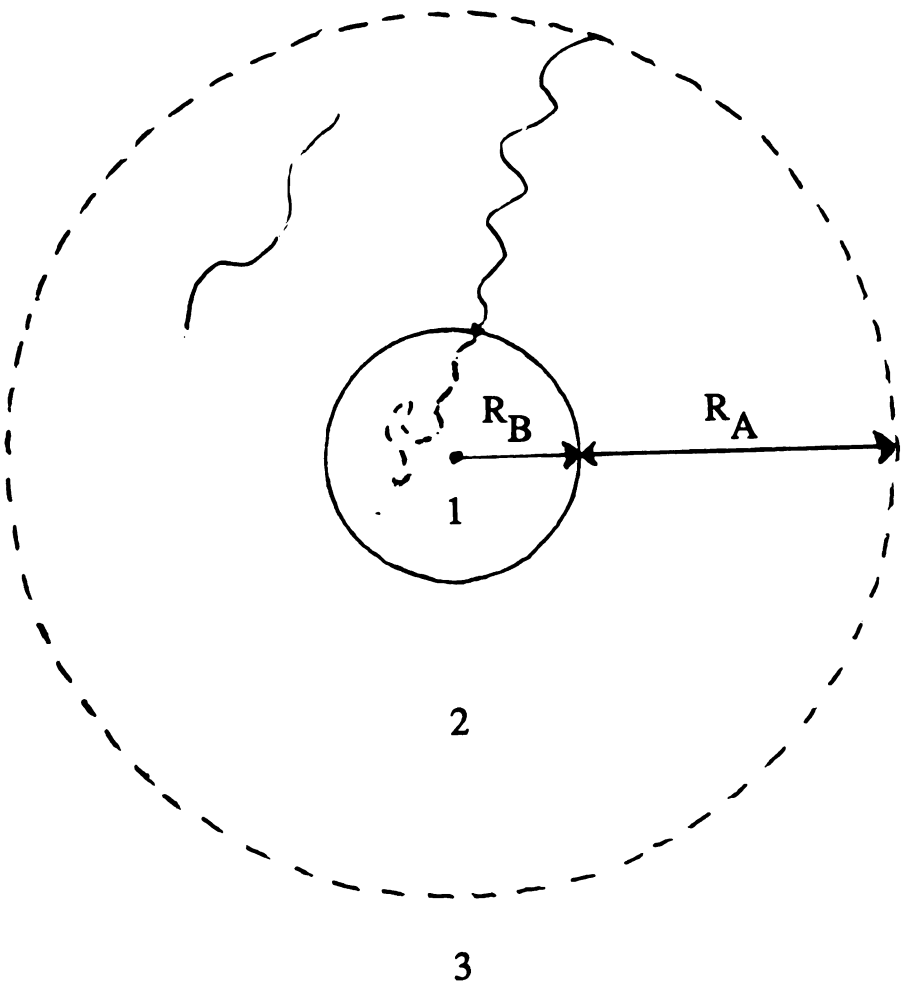

Figure 3.3 Schematic of a spherical micelle in an AB diblock/A homopolymer blend. Region 1 is the core and contains B-blocks. Region 2 is the corona and is composed of A-block mixed with A homopolymer. Region 3 is the matrix and consists of A homopolymer mixed with AB diblock copolymer.

Rigby and Roe (1986) and Selb et al. (1983) appear to be the only published experimental work that looks specifically at the formation of micelles in AB/A blends. Selb et al. used small-angle neutron scattering to observe the sizes of micelles of styrene-butadiene diblock in a matrix of very low molecular weight polybutadiene as a function of molecular characteristics of copolymer and matrix, and concentration of copolymer, and made the following four observations: for a given diblock copolymer, as the molecular weight of the matrix increased, the size of the micelles increased; with increasing diblock copolymer concentration, the size of the micelles decreased; for copolymers with the same PB block, the higher the molecular weight of the PB block, the lower the radius of the micelles; and for diblock copolymers with a fixed ratio of block lengths, the size of the micelles increased with increasing total molecular weight of the copolymer. In a more detailed study with styrene-butadiene diblock/low molecular weight polybutadiene mixtures, similar to those used by Selb et al., Rigby and Roe used small-angle X-ray scattering to explore the effect of temperature, molecular characteristics of the diblock, and diblock concentration on the size of the micelles. They found the critical micelle concentration (the concentration at which no micelles exist in the solution) decreased as the proportion of styrene in the copolymer increased. The variation of critical micelle concentration with temperature can be seen in Figure 3.4, taken from Rigby and Roe, where for temperatures and concentrations to the left

and above the curves in Figure 3.4 the styrene-butadiene diblock/polybutadiene homopolymer blends existed as a homogeneous mixture; otherwise, the blends contained micelles. Contrary to Selb et al., Rigby and Roe found the size of the micelles was independent of micelle concentration. The most striking result found by Rigby and Roe was micelle cores became increasingly swelled, as temperature was raised, immediately before the final dissolution temperature.

Leibler, Orland, and Wheeler (1983) were the first to develop a theory for AB/A blends containing micelles. They developed an expression for the total free energy of a system containing the micelles structures shown in Figure 3.3, and by minimizing this free energy determined the number of diblock molecules in a micelle, the volume fraction of A-block in the corona, and the volume fraction of diblock in the matrix at equilibrium. Leibler et al. only considered the case where the degree of polymerization of both blocks in the diblock was equal to one-half the degree of polymerization of the homopolymer, and no homopolymer could be dissolved in the core. Roe (1986) modified Leibler et al.'s theory to allow for the blocks of the diblock and the homopolymer to have arbitrary lengths and to allow for dissolution of homopolymer in the core. In other modifications to Leibler et al.'s theory, Mayes and Olvera de la Cruz (1988) considered the probability of forming micelles with cylindrical geometry rather than spherical geometry, and ten Brinke and Hadziioannou (1987) treated the formation of micelles in blends containing ABA triblock copolymers. Whitmore and

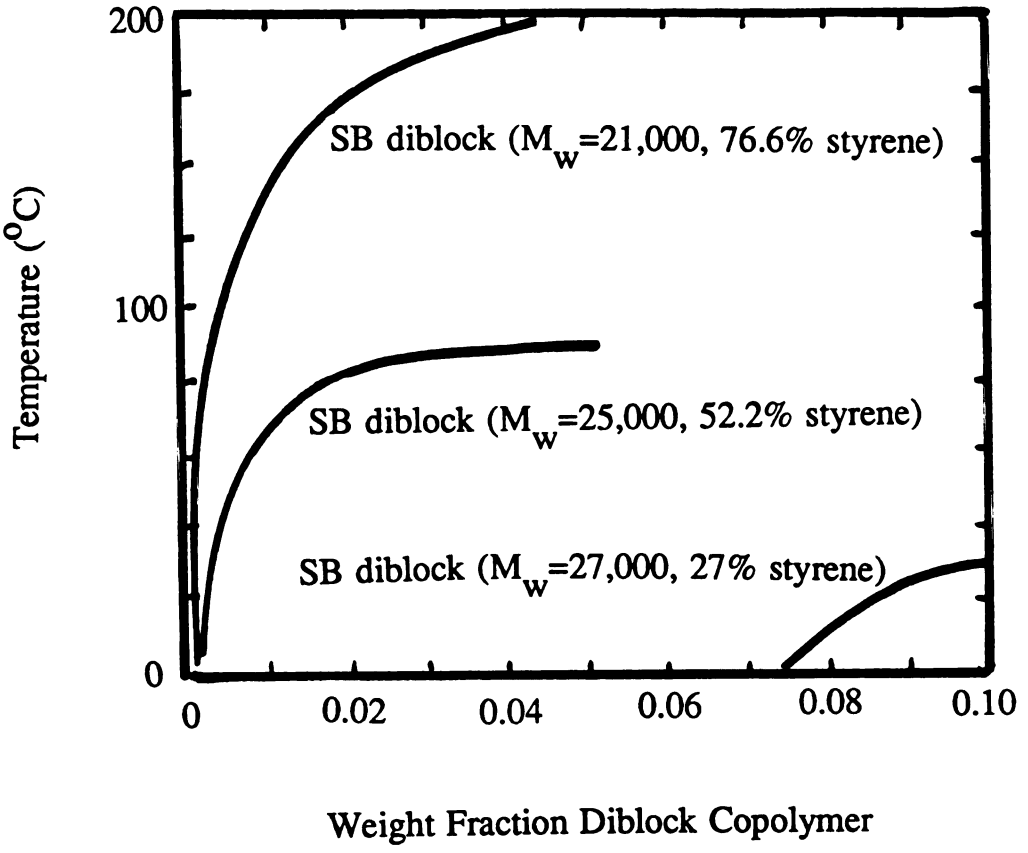

Figure 3.4 Critical micelle concentration as a function of temperature for three different blends of SB diblock copolymer in a low molecular weight polybutadiene (M_w=2350) (from Rigby and Roe, 1986).

Noolandi (1985) presented a theoretical development very similar to that of Leibler et al. based on a Kuhn statistical length, which also allows for polymers of different lengths and allows homopolymer to swell the core.

Roe (1986) found good agreement between the predictions of his modified theory and his experimental results for micelle dimensions; however, quantitative agreement between the theory and experiment were not so good for the critical micelle concentration (CMC), although the predicted theoretical trends for CMC were observed experimentally. Whitmore and Noolandi (1985) found good agreement between their theoretical predictions and the experimental results of Selb et al. (1983) for the relative magnitude of the core radius and the effect of diblock copolymer architecture on core radius. Other experimental features mentioned earlier that the present micelle formation theories fail to predict are the swelling of micelle cores with temperature seen by Rigby and Roe (1983) and the decrease in core radius with increase in copolymer concentration seen by Selb et al. (1983).

There is some controversy as to what the long-range order is in AB/A blends containing micelles. According to Leibler and Pincus (1984), the interaction of cilia of different micelles is unfavorable due to entropic considerations, which causes the micelles to tend to stay separated. This effect would then cause a macrolattice of micelles to form at a critical concentration of micelles in the blend. While interpreting the results of their experiments, Rigby and Roe (1986) deduced that the strong repulsion

between micelles predicted by Leibler and Pincus probably develops only after some degree of overlap between the two coronae has been realized. If this is true, it seems likely that there will be large agglomerations of micelles in the blend because as micelles travel about and interact with other micelles, it will take a large amount of time for the cilia of interacting micelles to become untangled so that the micelles can separate. It should be noted that the tendency to agglomerate is contrary to the idea of the micelles forming a regular macrolattice predicted by Leibler and Pincus.

In a completely different view to that of Leibler and Pincus, Watanabe et al. (1982) suggested that micelles of AB diblock copolymer in a selective solvent (in these mixtures a solvent that dissolves one of the blocks and precipitates the other block is used, and therefore micelles are formed) form a macrolattice because a concentration gradient of A-block would exist if they did not. In other words, if the micelles were to agglomerate in these solutions, there would be areas of the solution rich in A-block and other areas of the solution without A-block; hence, a concentration gradient of A monomers would exist in the solution. Since formation of this concentration gradient is energetically unfavorable, the micelles stay separated. For blends with AB diblock micelles in A homopolymer, agglomeration of micelles does not result in a concentration gradient of A monomers, so the micelles are much freer to interact. Finally, this suggests that a macrolattice will not form in an AB/A blend containing micelles. Watanabe et al. (1982)

and Watanabe and Kotaka (1983) presented evidence based on the rheology of blends containing styrene-butadiene diblock micelles in a very low molecular weight polybutadiene that a macrolattice does not exist in these blends. Furthermore, these workers found the rheology of these blends reflected a slow relaxation mechanism attributable to formation and dissociation of aggregates of micelles.

One question that arises in the research here is what the composition of the corona is for the micelles seen here. Inoue et al. (1970) reported extensive observations on the phase morphology of toulene cast films of styrene/isoprene diblock copolymer with and without the addition of polystyrene homopolymer and/or polysisoprene homopolymer and found that if the molecular weight of the homopolymer was equal to or less than the molecular weight of the corresponding block in the diblock, then the homopolymer was solubilized into that domain. It should be briefly noted that Inoue et al. found that morphology of their blends depended on the solvent used to cast the blends. In other work with solvent cast blends, Eastmond and Phillips (1979) and Berney et al. (1988) reached the conclusion that, in general, at equilibrium, polymers that are tethered to an interface are not miscible with chemically identical chains of comparable or greater molecular weight. In fact, both groups have much empirical evidence that the molecular weight of the A homopolymer must be an order of magnitude less than that of the A-block in the diblock before it will be solubilized in this block. Eastmond and Phillips suggested that the incompatibility of

chemically identical blocks and homopolymers arises from an unfavorable entropy of mixing as a result of the blocks in the vicinity of the microphase interfaces adopting different sets of conformations than the randomly coiled chains in the bulk polymer. In the research here, the styrene homopolymer had a molecular weight about three times greater than the molecular weight of the styrene-block in the copolymer, which, according to the results of Inoue et al., Eastmond and Phillips, and Berney et al., suggests the diblock copolymer and homopolymer may form completely separate phases for the blends considered here. In other words, the styrene homopolymer might not mix with the styrene-block, and therefore the corona might not contain much homopolymer. The conclusions drawn by Inoue et al., Eastmond and Phillips, and Berney et al. must be considered in the light that, as Kinning and Thomas (1984) pointed out, it is generally accepted that the morphology of solution cast blends of copolymers with homopolymers, particularly those with spherical morphology, is a nonequilibrium morphology characteristic of the temperature/solvent conditions used to make the blends. These nonequilibrium morphologies caused by decreased molecular mobility at solution casting temperatures are especially evident for large molecular weight samples with a glassy polymer matrix. It should be mentioned that these nonequilibrium effects result in much smaller domain sizes than those predicted by theory (see, e.g., Bates, Berney, & Cohen, 1983). An oddity seen by Eastmond and Phillips (1979) and Gebizlioglu, Argon, and Cohen (1985), and seen here for

solution cast styrene-butadiene diblock/styrene homopolymer blends, where the styrene homopolymer has larger molecular weight than the styrene-block, is that when the styrene-block is incompatible with the styrene homopolymer, the morphology formed is that of shells of butadiene-block alternating with shells of styrene-block or large droplets of butadiene containing small droplets of polystyrene. In the work presented here, for melt blends of the same polymers, the morphology was that of a shell of styrene-block of butadiene-block. The blends formed here were studied at high temperature where there was much molecular mobility, and hence, as will be supported further in Chapter V, an equilibrium structure existed. At equilibrium, one would expect the styrene homopolymer and the styrene-block to start mixing somewhat because the styrene-blocks would have to assume very constricted configurations to totally avoid mixing with the styrene homopolymer, which would be energetically unfavorable. Therefore, it seems likely that the corona of the micelles in the blends here were at least partially swollen with homopolymer.

The theories for micelle formation in AB/A blends described earlier do not include an allowance for incompatibility between the A-block and the A homopolymer when the A homopolymer has equal or greater molecular weight than the A-block. Since, as described above, some incompatibility may exist, the theory of Leibler et al. (1983) is modified to include this aspect for comparison to the experimental results here. The theory is further modified to account for the effect of stress during processing on micelle formation.

3.2 Effect of Stress on Polymer Blends and Polymer Solutions

The stress imposed during processing of polymer blends or polymer solutions can affect the size of the dispersed phase. The average particle size obtained by phase break up and coalescence during processing is usually related to the rheological and interfacial properties of the components of the blend. Recent studies in this area include Wu (1987), Elmendorp and van der Vegt (1986), and Plochocki (1986).

Another effect of stress on polymer blends and polymer solutions is to cause mixing or demixing of the phases. The miscibility of phases in polymer blends and polymer solutions during stress is determined by thermodynamic considerations. Katsoros, Malone, and Winter (1988) recently gave a review of this area.

There appears to be no literature on the effect of stress on AB/A blends. Since the formation of micelles in AB/A blends under static conditions is determined by thermodynamic considerations, the approach taken here is that the effect of stress on micelle formation in these blends can also be represented by thermodynamic considerations. Therefore, the literature on miscibility of polymer blends and polymer solutions is most applicable to the work presented here. A summary of this literature follows.

Most of the published work on the effect of stress on the miscibility of systems containing polymers is concerned with polymer solutions, and there is still controversy as to what the effect is. The original work in this area was done by Silberg and Kuhn (1952),

who studied the miscibility of the ternary system polystyrene and ethyl cellulose in benzene and found that stress induced compatibility. In other words, the upper critical solution temperature (UCST) (the temperature above which the solution contained a single phase) decreased because of stress. Rangel-Nafaile, Metzner, and Wissbrun (1984) had a compilation of the work done on the effect of stress on polymer solutions since the work of Silberg and Kuhn, and they claimed that much of this work demonstrated that stress causes demixing in polymer solutions. Wolf and Kramer (1980), on the other hand, concluded that much of the experimental data that has been used to show stress-induced demixing has been misinterpreted. For instance, most studies on the effect of stress on polymer solutions have used turbidity measurements to establish when a phase transition has occurred, and Wolf and Kramer found that sometimes solutions cloud due to shear darkening, rather than a shear-induced phase transition, which causes some workers to assume a phase transition has occurred when it has not. In fact, Wolf and Kramer found that stress actually decreased UCST for systems that had previously been reported as having a UCST that increased due to stress. Still, there seems to be a fair number of polymer solutions for which stress clearly causes demixing (sometimes irreversibly) (Rangel-Nafaile et al., 1984), and other polymer solutions for which stress clearly causes increased miscibility of the phases (Wolf, 1984).

As one might expect from the experimental results above, the theoretical understanding of the effect of shear on polymer

solutions is not complete. One of the first attempts to explain the effect of stress on polymer solutions was made by Wolf (1980), who used a balance of shear stress, normal stresses, and interfacial tension to determine the equilibrium size of the droplets in a polymer solution. Wolf hypothesized that when the equilibrium size of the droplets is decreased to the radius of gyration of the polymer molecule by shearing, then redissolution of the polymer will occur. In an interesting occurrence, Rangel-Nafaile et al. (1984) and Wolf (1984) simultaneously developed virtually identical theories for the effect of stress on polymer solutions and came to opposite conclusions. Both groups assumed that the Gibbs energy of the sheared system is the sum of the energy of mixing at rest plus the energy stored during flow, and both based their development of the energy stored during flow on the work of Marruci (1972). On the one hand, Rangel-Nafaile et al. found that their theory predicted demixing due to stress, which was in agreement with their experimental work on polystyrene in dioctyl pthalate. On the other hand, Wolf found that his theory predicted shear-induced compatibility, which was in agreement with his experimental work with polystyrene in trans-decalin. It seems safe to say that the effect of stress on polymer solutions is not completely understood yet, and it seems obvious that stress affects each polymer solution differently. Since the only difference in the developments of Rangel-Nafaile et al. and Wolf was the way each related the rheology of their solutions to the energy stored at a constant shear stress,

a fundamental experimental and theoretical study of the rheology of these solutions may help in explaining the different effect of stress seen for different polymer solutions. It is intuitive that the energy due to flow is stored differently in different polymer solutions, and a next step in the theoretical developments should take account of this in some way.

Lyngaae-Jorgensen, Alle, and Marten (1979) appear to be the first researchers to have experimentally determined the effect of stress on the miscibility of two-phase polymer systems that were not solutions. These workers have shown for a pure styrene/butadiene/styrene triblock that above a critical shear stress the diblock became homogeneous; i.e., stress decreased the UCST for the triblock.

All of the literature on the effect of stress on incompatible polymer blends of two polymers seems to have appeared within the last five years. In the initial work in this area, Mazich and Carr (1983) studied the effect of shear stress on blends of polystyrene and poly(vinyl methyl ether) with the novel approach of maintaining a constant first normal stress difference N_1 during testing. The reason for using a constant N_1 was to keep the amount of energy stored during flow constant, as can be seen with the theoretical expression for the energy stored during a constant shear deformation given by Marruci (1972) as

$$\Delta G^S = 1/2 \text{ tr } \underline{\underline{\tau}} = N_1/2 \qquad 3.1$$

for an elastic dumbbell model. Mazich and Carr found stress increased the lower critical solution temperature (LCST) 2 to 7^{o} K for the PS/PVME blends. A conclusion of Mazich and Carr, of use for the researcher presented here, was that N_1 is a good measure of the energy stored during flow. Katsoros, Malone, and Winter (1988) found for PS/PVME blends similar to those of Mazich and Carr that in stagnation flows the LCST can be increased by 10^{o} K. This effect was found to be sensitive to the amount of polystyrene in the blend, and above a blend styrene content of 65%, the effect was greatly diminished. Lyngaae-Jorgensen and Sondergaard (1987b) performed some experiments with a styrene/acrylonitrile-poly(methylmethacrylate) blend that has a LCST and found for samples that were rapidly quenched after shearing there was no detectable structure in transmission electron micrographs. If these same samples were allowed to anneal for 10 minutes, there was a two-phase structure. These results in conjunction with the results of light scattering experiments during flow established that stress increased the LCST. The rapid quenching technique of Lyngaae-Jorgensen and Sondergaard was employed here.

Lyngaae-Jorgensen and Sondergaard (1987a) developed a hypothesis for the transition from a two-phase system to a homogeneous system for a polymer blend in steady shear flow. The basis of the Lyngaae-Jorgensen and Sondergaard development is that as long as change in chemical potential due to stress plus the change in chemical potential due to mixing is less than or equal to zero during a transition from a two-phase system to a single-phase

system, then the transition can occur. Lyngaae-Jorgensen and Sondergaard found for a critical value of shear stress that the transition from a two-phase system to a one-phase system is possible. Although they did not mention it specifically, the hypothesis that Lyngaae-Jorgensen and Sondergaard presented suggests that the UCST will be decreased by stress for a system with an UCST.

A summary of the experimental and theoretical work on the effect of pressure on the miscibility of polymer blends and polymer solutions was given by Rostami and Walsh (1987) and Katsoros et al. (1988). So far, only polymer blends with LCST have been explored, and an increase in pressure has increased the LCST. Rostami and Walsh also found for polymer solutions with UCST that an increase in pressure increased the UCST. It was shown in Chapter II that significant pressures can develop in the mixing regions of twin screw extruders that contain kneading paddles; however, it was not possible to determine what these pressures were for the twin screw extruder used in this study. Therefore, only the effect of the very high shear deformation in the mixing zones was explored.

It appears that all of the work to date on the effect of stress on polymer blends has been done on blends that have a LCST. All of the results so far have indicated stress increases the LCST. As more research is done in this area, it will be interesting to see if the different effects seen with polymer solutions occur with polymer blends. The experimental and theoretical study of the effect of stress on styrene-butadiene diblock/styrene homopolymer blends

presented here is novel because it appears to be the first work that has been done with polymer blends that have an UCST, and this also marks the first attempt to look at the effect of stress on micelle formation in polymer blends. Actually, since the blends contain micelles here, the study of blend miscibility translates to a study of degree of micellization for the blends studied here. As will be seen in Chapter V, the effect of stress is to decrease the degree of micellization, or viewed differently, to increase the miscibility of diblock in the matrix phase for the blends studied here.

3.3 Rheology-Morphology Relationships for AB/A Blends Containing Micelles

Virtually all of the literature on rheology-morphology connections for systems containing micelles of AB diblock copolymer has been done with AB diblock in selective solvents (the formation of micelles in these systems was described in Section 3.1). It has been shown that these systems have a peculiar rheology (such as yield stress and thixotropic behavior) due to their morphology (see Watanabe et al., 1982, for a summary of this work). Watanabe et al. attributed much of this peculiar rheology to the macrolattice that is formed in these solutions as described in Section 3.1. As mentioned earlier, in a later study Watanabe and Kotake (1983) examined the morphology-rheology relation for a blend of styrene/butadiene diblock with low molecular weight polybutadiene and found a second plateau in their G' and G' versus w curve, which they attributed to the disengagement of the cilia of overlapping micelles. In Watanabe and Kotaka's work, the molecular weight of

the matrix polybutadiene was below the entanglement molecular weight. In the research here, the molecular weight of the matrix is much higher than the entanglement molecular weight, so the motion of the matrix molecules is much different from the motion of the matrix molecules in the blends considered by Watanabe. This being the case, the present literature on how rheology is affected by the motion of long polymer molecules is briefly reviewed below.

For long polymer chains that are entangled, De Gennes (1971) proposed that the chains rearrange their conformations by reptation along their contours, as shown in Figure 3.5. Based on the physical picture of Figure 3.5, Doi and Edwards (1978) developed a theory relating the dynamics of reptating chains in a monodisperse polymer to the rheological properties of the polymer. Graessley (1982) modified the reptation model in two ways that seem applicable here. First, Graessley introduced the concept of constraint release, which takes into account the fact that the tube through which a polymer chain is reptating is made up of other polymer chains, and therefore the tube is changing with time. There have been a few studies of the effect of constraint release on the relaxation of polymer chains. Graessley and Struglinski (1986), Roovers (1987), and Monfort, Marin, and Monge (1984) are some of the recent literature in this area. Another concept explored by Graessley was that of a tethered chain. In the work here, the blocks of the diblock can be viewed as being tethered to the micelle interface, so the analysis of Graessley is used here.

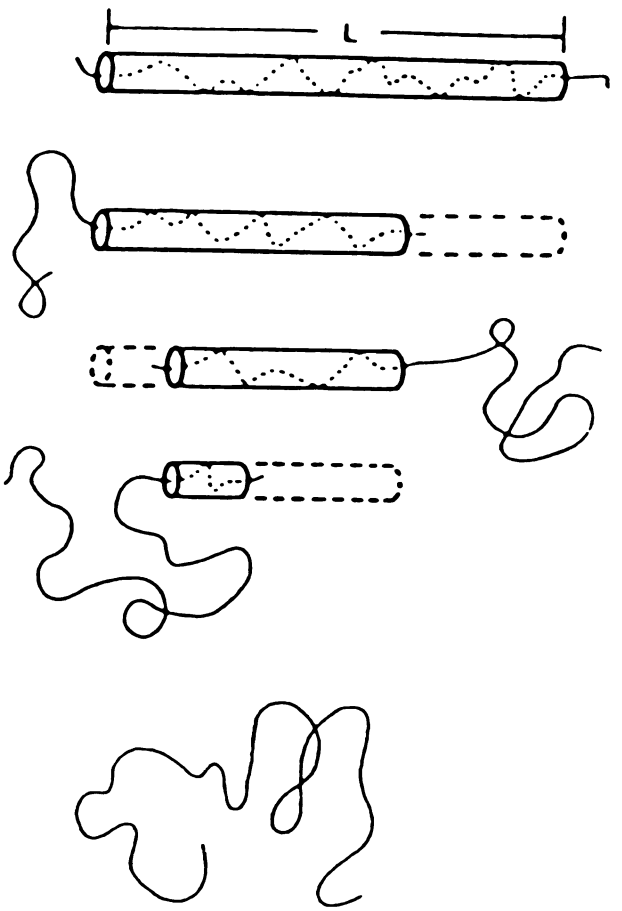

Figure 3.5 Schematic of a polymer molecule reptating out of its initial tube. The tube is made up of strands of other polymer molecules (from Graessley, 1982).

The work of Monfort et al. (1984) is of interest here because they analyzed the relative magnitude of relaxation due to reptation and constraint release in monodisperse polystyrenes. Monfort et al. found that for polystyrenes with a molecular weight on the order of 100,000, the magnitudes of the relaxation times for reptation and constraint release were comparable. As molecular weight increased, reptation was the dominant mechanism for relaxation of the chains.

For the styrene-butadiene diblock/styrene homopolymer blends studied here, the rheology is assumed to be largely due to the motion of the matrix polystyrene, and how micelles affect the relaxation due to reptation and constraint release of the matrix polystyrene is assumed to be reflected in the rheology for the blends. Since the matrix of the blends studied here was polystyrene, the concepts and experimental results of Monfort et al. (1984), as mentioned above, were very useful. This information is introduced as it becomes applicable in Chapter VI.

CHAPTER IV

EXPERIMENTAL PROCEDURES

The objective of the experiments performed here was to prepare well-mixed melt blends of an AB copolymer with A homopolymer in a twin screw extruder and then to determine how processing affects the morphology of the blends as compared to the equilibrium morphology. Also, the relationship between the morphology and rheology of these blends was examined. This chapter details the various experimental procedures that were used.

4.1 Materials

The AB copolymer and A homopolymer used in this study were two commercially available polymers--Finaprene 315 and Dow Styron 666D. Samples of these polymers were kindly donated by Fina Corp. and Dow Chemical U.S.A. Dow Styron 666D is an amorphous polystyrene, and the molecular weight characteristics of the Styron 666D used in this study were determined with a GPC by Frank Burkett of Dow Chemical U.S.A. The results of the GPC run are shown in Figure 4.1 and demonstrate that the polystyrene used here had a weight average molecular weight of 235,000 and polydispersity of 2.5. Finaprene 315 is a tapered styrene/butadiene diblock copolymer that contains 70 weight percent styrene and 30 weight percent butadiene, where 50

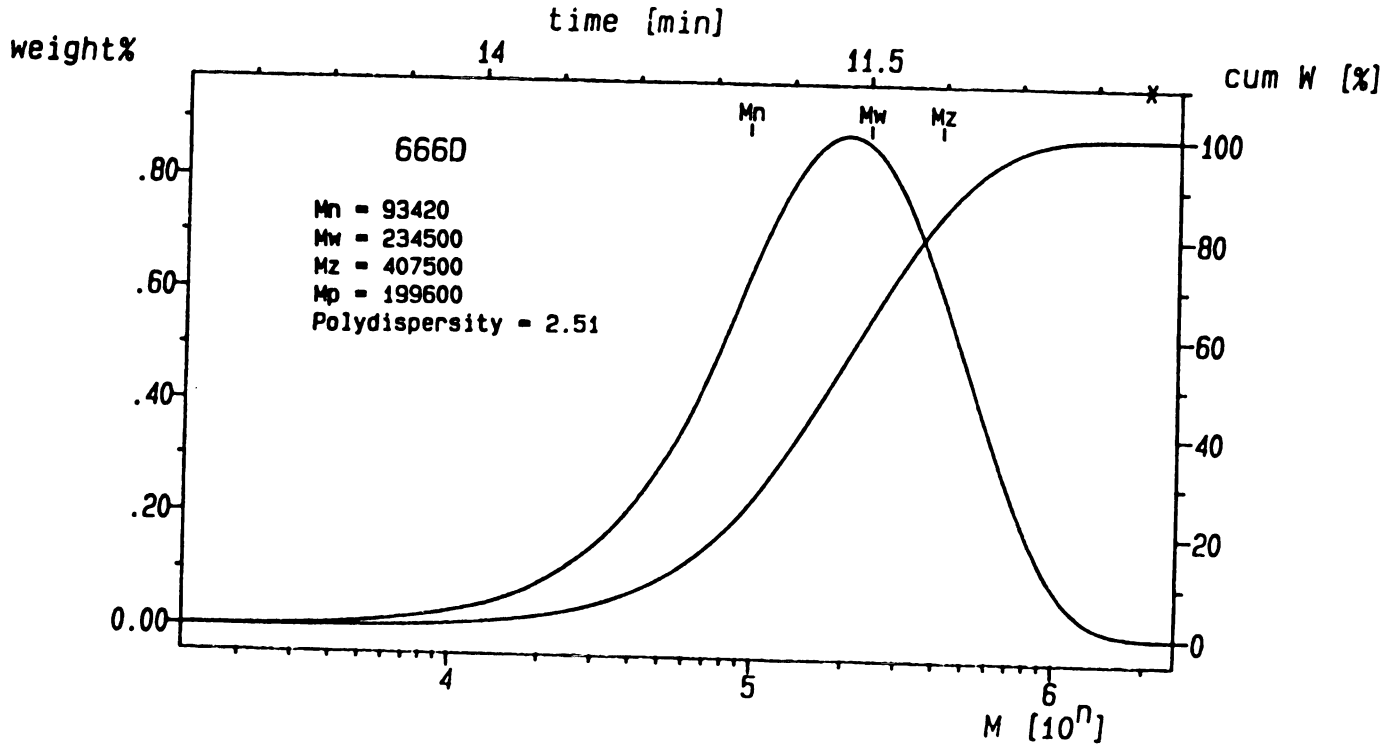

Figure 4.1 Molecular Weight Distribution for Styron 666D.

weight percent of the styrene forms a pure block and the remainder of the styrene tapers off into a butadiene block (communication with Fina technical service personnel). Finaprene 315 has a weight average molecular weight of 136,000 and a polydispersity of 1.1 and contains two anti-oxidants--one weight percent trisnonylphenyl phosphite (TNPP) and .4 weight percent butylated hydroxy toulene (BHT).

4.2 Blend Preparation

Melt blends of 1, 5, 10, and 20 weight percent Finaprene 315 were prepared by first mixing 1500 grams of the correct proportions of the polymer pellets, as supplied by the manufacturer, in a beaker. (Henceforth, the blends will be referred to as 1%, 5%, 10%, and 20% blends, respectively). This mixture was prepared with a Baker-Perkins 30 mm co-rotating twin screw extruder (see Chapter II for an in-depth description of the twin screw extruder) where, for all runs, the extruder was operated at maximum allowable feedrate with all zones set at 170^{o}C, a screw rotation rate of 250 rpm, and a two mixing zone configuration. Each mixing zone had four 60 degree forwarding paddles followed by two 90 degree paddles. The upstream orifice plugs had a diameter of 29.66 mm and the downstream orifice plugs had a diameter of 29.44 mm. Both orifice plugs were 3.5 mm wide. It should be mentioned here that the blends were extruded through a two strand die, and for the two strand die, there did not appear to be a macrophase separation; i.e., a core/sheath structure did not exist. Some preliminary experiments were done with a strand

die with a large diameter, and a visible core/sheath structure existed in the extrudate. To guarantee thorough mixing, the extrudate was pelletized and the pellets were mixed well by hand. The pellets were then extruded again, re-pelletized, and extruded a third time. As will be seen, this method of mixing resulted in a fairly uniform morphology throughout the blends. However, it will also be seen that this repetitive processing of the blends resulted in a very slight degradation of the polymers.

For comparison purposes, pure Styron 666D was stabilized with .05 weight percent TNPP and .02 weight percent BHT and processed in the same manner as the blends were. The amount of stabilizer used for the pure Styron 666D is equivalent to the amount of stabilizer that is in the 5% blend. It will be shown in Chapter VI that this amount of stabilizer resulted in minimal degradation of the polystyrene.

To compare the morphology of solution cast blends with that of melt blends, solution cast blends were prepared as follows. A mixture of 20 g of polymer, with the proper proportions of diblock and homopolymer, was mixed in a beaker with 100 g of toulene. This mixing was done with a magnetic stirring rod and was continued until all polymer was dissolved. The mixtures were then allowed to sit for four days in an oven at 30^{o}C. Next, the samples sat in a vacuum oven for 3 days at 30^{o}C, followed by annealing in the same vacuum oven for 3 days at 70^{o}C. After this, the samples were annealed at 100^{o}C in a vacuum oven for 1 day, and finally, to drive off any remaining solvent, the temperature was increased to 150^{o}C and the

sample was allowed to sit for 1 hour. The oven was then turned off and the samples allowed to cool slowly under vacuum to room temperature. During the 70°C and 100°C annealing periods, the samples were weighed on successive days and the weight did not change. Nevertheless, when the samples were annealed at 200°C as part of the experiment here, the samples foamed, suggesting there was some residual solvent in the samples. The final 150°C annealing period took care of this foaming problem.

4.3 Determination of Blend Morphology

To prepare samples for structural analysis, small pieces of the strands of extrudate were placed on a spare 5 cm diameter Weissenberg Rheogoniometer platen, which in turn was placed on the bottom platen in the Weissenberg Rheogoniometer oven chamber. Each blend sample was annealed under a blanket of nitrogen for 1 hour. For these experiments, annealing temperatures of 130°C and 200°C for each blend sample were chosen to determine the effect of temperature on morphology over the range of temperatures used in the rheological tests. To quickly quench the sample after the annealing period, the Weissenberg Rheogoniometer oven was quickly opened and the platen with the sample on it was knocked into a large beaker of cold water. This whole quenching process took a maximum of 5 seconds, and the hope was that this quick quench "locked in" the internal structure of the blend at the annealing temperature.

The next steps in determination of blend morphology were performed by Dr. John Heckman of the Center for Electron Optics at

Michigan State University, and the method used is derived from that presented by Kato (1966). From the center of the quenched blend samples, billets 2 x 4 x 16 mm were carved at 90 degrees to each other. A trapezoid sectioning face with dimensions 200 x 300 microns was carved into the billet with a razor. These billets were then placed in a Reichert Ultracut ultramicrotome, and 90 nm thick samples were sectioned from them with a diamond knife. As the sections are removed for the billets in the ultramicrotome, they are compressed due to the cutting. Since the sections are floated onto water as they are cut, a wooden dip stick is dipped into xylene and waved over the section as it sits in the water. The xylene vapor causes the sample to relax and the surface tension of the water causes the sample to stretch and become uncompressed. One can tell when the sample is satisfactory because it comes unwrinkled. This whole relaxation process takes about 30 seconds. The sections are then picked up on a 300 mesh copper grid, and a drop of 1% osmium tetroxide solution is placed on them. The osmium tetroxide reacts with the unsaturated double bonds in the butadiene and causes the butadiene phase to appear black in the electron microscope, while the polystyrene phase appears white. After 15 minutes, the osmium tetroxide was drawn off the sample with filter paper, and the samples were rinsed 3 times with distilled water. To dissipate charge in the electron microscope, the sections were coated with a .5 to 1 nm carbon film in a vacuum evaporator. Finally, the sections were observed in a JEOL 1000 CX-II transmission electron

microscope, and micrographs were taken of the blends at magnifications of 10,000x and 58,000x. It should be noted here that initially attempts were made to embed the blend samples in a styrene-based resin before sectioning. The styrene in the blend appeared to affect the curing of the resin because the resin with blend in it would not cure unless it was placed in an oven at 70°C for an extended period of time. The samples that were successfully embedded by this technique showed inclusions of styrene that did not show up when the resin was not used. Therefore, the embedding method of sample preparation used by Kato (1966) was not used here.

4.4 Rheological Measurements

To prepare specimens of the blends and pure polystyrene for rheological testing, two strands of extrudate were placed side by side on release ply on an aluminum plate. Another sheet of release ply and aluminum plate was placed on top of the strands, and the plates were placed in a hydraulic press and heated to 140°C to soften the extrudate. The plates were then pressed until the separation between the plates was 1 to 1.5 mm (this was accomplished by placing a penny between the plates at each plate corner), and the pressure was raised to 10,000 psi. After 15 minutes of compression, the sheets of polymer were removed from the press and allowed to cool to room temperature. From the resultant polymer sheets, bubble-free disks 25 mm in diameter were punched out with a special punch manufactured by Rheometrics, Inc.

A Rheometrics Mechanical Spectrometer RMS-800 was used to perform dynamic mechanical and steady shear tests. For the dynamic mechanical tests, 25 mm diameter parallel plates were used. Initially, dynamic mechanical tests were performed with a 25 mm cone and plate set-up, but it was found that it took on the order of 11 hours at low testing temperatures for the normal stress to relax to zero when loading the sample, and for this long waiting period the morphology of the blends could change substantially. Therefore, parallel plates were used because the sample could be loaded (described below) in this geometry in such a way that the normal stress was zero at the end of a 1 hour annealing period. The dynamic mechanical tests were performed at temperatures of 130^{o}C, 160^{o}C, and 200^{o}C where the sample was annealed for 1 hour at each temperature before testing. A different sample was used at each temperature. At each temperature, the platens were allowed to come to thermal equilibrium and the gap-setting meter was zeroed when the platens just came into contact as determined by the normal force meter. The platens were then separated and the 25 mm polymer sample disk described above was coated onto the bottom platen. Martinez and Williams stressed the need to avoid bubbles when loading samples for rheological testing and stated that they did this by letting their samples droop freely onto the bottom platen at the test temperature. It was found in the tests here that pockets of air were trapped under the sample if the polymer was allowed to droop freely over the bottom platen; hence, the polymer disk was coated onto the bottom platen in the test here, which seemed to minimize

the entrapment of air bubbles. After the polymer was coated onto the bottom platen, the sample was held for about 5 minutes at the testing temperature before setting the gap. At 160°C and 200°C, the top platen was then brought down so that the gap between platens was 1 mm. The normal stress decayed within 5 minutes after setting the gap at 160°C and 200°C. At 130°C, the top platen was brought down until the normal force meter was at about one-half of full scale. This normal stress did not decay away completely in 1 hour, so 50 minutes after loading the sample, the top platen was raised slightly so that the normal stress was zero. At each testing temperature a frequency sweep of .1 to 100 rad/sec was performed where 5 data points were obtained over each frequency decade. Strains of .05, .1, and .2 were used for the 130°C, 160°C, and 200°C tests, respectively. After the frequency sweep, a strain sweep was performed on every sample, which revealed that the strains used at each temperature were in the linear viscoelastic region; i.e., stress was directly proportional to strain. Time-temperature superposition (Ferry, 1980) was used to create master curves from the data taken at the different temperatures.

The steady shear testing was performed at 170°C and 190°C (the probable limits on the range of melt temperatures seen by the polymer in the extruder) with a 25 mm cone and plate assembly (cone angle = 1 radian). The samples were loaded as above with the exception that the gap was set at the 50 microns as required for the cone and plate assembly. Tests were conducted at shear rates of

10^{-2} to .3 sec^{-1} above .3 sec^{-1} the polymer extruded out from the gap between the platens.

It is not possible, at present, to purge our Rheometrics RMS-800 test chamber with nitrogen at the temperatures used in the rheological tests here because this required heating a liquid nitrogen purge stream to 200°C in a short period of time. The temperature fluctuations in the test chamber were not acceptable when this was attempted. This raises the question of whether oxidative degradation is occurring in the samples tested at high temperatures. Some auxiliary experiments were conducted in which the rheological properties of different samples were monitored versus time. It was found that, over times much greater than those used to conduct the rheological tests described above, the rheological properties of the blends did not change. This confirmed the absence of oxidative degradation during the rheological testing.

CHAPTER V

RESULTS AND DISCUSSION OF MORPHOLOGY EXPERIMENTS

5.1 Introduction

In this chapter, the micelle structures of blends of 1, 5, 10, and 20 weight percent of a tapered styrene-butadiene diblock copolymer (Fina 315) in polystyrene homopolymer (Styron 666D) are presented. The motivation for this work was to understand the factors determining the micelle structure of AB diblock/A homopolymer blends, consisting of high molecular weight polymers, under equilibrium and nonequilibrium melt mixing conditions. The results of this chapter will serve to motivate the modified theory for micelle formation developed in this work and presented in Chapter VII.

There appear to be three groups who have looked specifically at the formation of micelles in AB/A blends. Selb et al. (1983) used small-angle neutron scattering to observe the sizes of micelles of styrene-butadiene diblock in a very low molecular weight polybutadiene as a function of molecular characteristics of the copolymer and the matrix, and concentration of the copolymer. These workers made the following four observations: for a given diblock copolymer, as the molecular weight of the matrix increased, the core radius increased; with increasing diblock copolymer concentration,

the core radius of the micelles decreased; for copolymer with the molecular weight of the PS-block kept constant, the higher the molecular weight for the PB-block, the lower the radius of the micelles; and for diblock copolymers with a fixed ratio of block lengths, the core radius of the micelles increased with increasing total molecular weight of the copolymer. In a more detailed study with styrene-butadiene diblock/low molecular weight polybutadiene mixtures similar to those used by Selb et al., Rigby and Roe (1986) used small-angle X-ray scattering to explore the effect of temperature, molecular characteristics for the diblock, and diblock concentration on the size of the micelles. They found that the critical micelle concentration (the concentration at which no micelles exist in the solution) decreased as the proportion of styrene in the copolymer increased. Contrary to Selb et al., Rigby and Roe observed that the size of the micelles was independent of diblock concentration. The most striking result found by Rigby and Roe was that the micelle cores became increasingly swollen as temperature was raised, immediately before the final dissolution temperature. Kinning and Thomas (1988) used small-angle X-ray scattering and transmission electron microscopy to show a change from spherical to cylindrical micelle geometry as the molecular weight of butadiene block or the homo-polystyrene increased. The work presented here extends the previous experimental studies by analyzing micelle formation in a high molecular weight matrix homopolymer with transmission electron microscopy. Also, this

appears to be the first study of the effect of stress during processing on micelle formation in AB/A blends.

Mayes and de la Cruz (1988) recently cited a number of workers who have questioned whether a thermodynamic equilibrium structure can be achieved for AB diblock/A homopolymer blends when the A homopolymer has a greater molecular weight than the A-block of the diblock. This conclusion has arisen from experimental work on solution cast blends where the low temperatures used in solution casting cause decreased mobility of the polymer chains. For high molecular weight polymer, this decreased chain mobility means it will take a very long time for the system to reach an equilibrium state. In the work presented here, the A homopolymer has a much higher molecular weight than the A-block of the diblock, and yet it is believed that equilibrium structures were achieved for the AB/A blends presented here by annealing blend samples at 200^{o}C and then quenching them rapidly. Thermodynamic equilibrium is achieved because polymer mobility is high at 200^{o}C. Monfort, Marin, and Monge (1984) showed experimentally that for monodisperse polystyrene the longest relaxation time, which is a measure of the time it takes for the polymer chain to renew its surroundings, is given by $t = 5.2 \times 10^{-18} M^{3.4}$ at 160^{o}C. Using the appropriate shift factor obtained from rheological testing and the molecular weight of the matrix polystyrene used here (M = 235,000), the longest relaxation time at 200^{o}C is t = .0651 seconds. This implies that the polymer chains may diffuse over great distances during the one hour annealing period at 200^{o}C. Other evidence based on morphology considerations

will be given here which shows an equilibrium structure exists for blends annealed for one hour at 200°C.

Other blend samples were annealed at 130°C because this represents the lower end of the temperature range over which rheological tests were performed on the blends. It turns out that the observed structures for the samples annealed at 130°C correspond to the nonequilibrium structure imposed on the blend during melt mixing in the twin screw extruder. Micrographs of the 5% and 10% blends annealed for one hour at 130°C were compared to micrographs of 5% and 10% blends that had not been annealed, and the morphologies seen in the micrographs for blends with comparable amounts of diblock were identical. This verifies that the structure seen in the micrographs for the blends annealed at 130°C is equivalent to the structure caused by melt mixing. The fact that annealing for one hour at 130°C did not cause much change in the structure is not surprising when one considers the time it takes for a polymer chain to renew its surroundings at this temperature is approximately 23 minutes.

Before discussing the experimental results for micelle formation in AB/A blends, it is helpful to understand some of the parameters that are important for comparison of experiment to theory. Leibler, Orland, and Wheeler (1983) were the first to develop a theory for AB/A blends containing micelles. They developed an expression for the total free energy of a system containing the spherical micelle structures shown in Figure 5.1a,

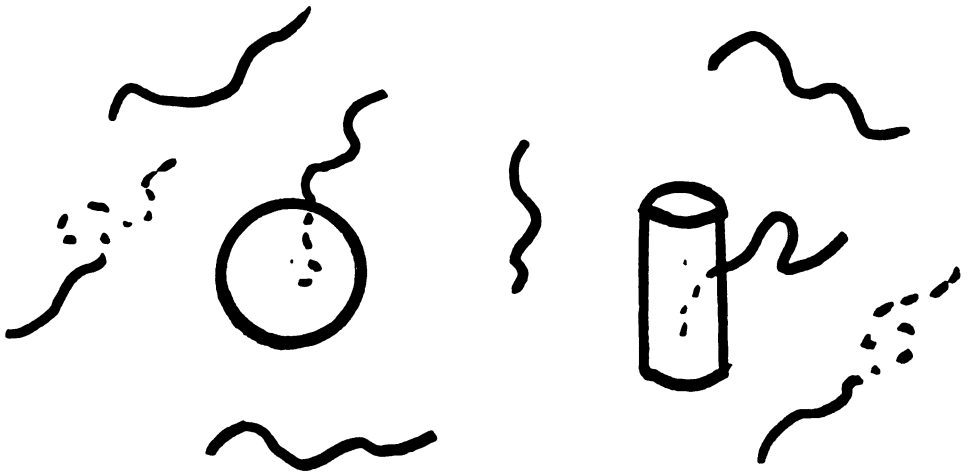

Figure 5.1 Schematic of micelle shapes for AB diblock/A homopolymer blends which have been studied theoretically. Leibler, Orland, and Wheeler (1983) have studied (A) spherical micelles, and Mayes and de la Cruz (1988) have extended Leibler et al.'s theory to analyze (B) cylindrical micelles.

and by minimizing this free energy, determined the number of diblock molecules participating in a single micelle p, the volume fraction of A-block in the corona η, and the total fraction of diblock in the system participating in micelles ζ (ζ is called the degree of micellization). From the parameters p, η, and ζ, other quantities of interest such as core size, corona size, and amount of diblock dissolved in the matrix can be determined. Mayes and de la Cruz (1988) modified the theory of Leibler et al. to include the possibility of cylindrical micelle formation (Figure 5.1b). Mayes and de la Cruz's work, which was motivated by the experimental work of Kinning and Thomas (1988), mentioned earlier, shows that the reason cylindrical micelles are favored in some cases is because there is less stretching of the core blocks for cylindrical micelles than for spherical micelles. It will be shown here that a similar tendency to form cylinders occurred for the blends studied here as the amount of diblock in the blend increased.

With the exception of Whitmore and Noolandi (1985), the theoretical work on micelle formation in diblock copolymer-homopolymer blends has not considered the case of the homopolymer molecular weight being greater than the A-block molecular weight because, as mentioned above, most workers have assumed thermodynamic equilibrium cannot be achieved readily for this case. Whitmore and Noolandi predicted for the case of the homopolymer molecular weight larger than the A-block molecular weight that the A-block in the micelle corona is stretched very little during micelle formation,

which leads to the result that the corona contains a high percentage of homopolymer. In this work, the hypothesis is introduced that the A-block is actually compressed during micelle formation due to unfavorable interactions between the A-block molecules and the matrix homopolymer molecules. It will be shown here that there are two trends seen for the morphology of the blends studied here that fail to be predicted by the theory of Whitmore and Noolandi, or for that matter any other existing theory for formation of micelles in AB/A blends, namely, the size of the micelles decreased and the degree of micellization for the blends decreased with increase in diblock content for the blends. Finally, it will be shown here that the shapes of the micelles and the degree of polymerization for the blends change when the blends are stressed during processing.

The remainder of this chapter is organized as follows. In Section 5.2, representative micrographs of the blends are presented and the shapes of the micelles are discussed. A description of how micelle core sizes were determined and a summary of the trends seen with micelle core sizes are given in Section 5.3. A discussion of the tendency for micelles to cluster is given in Section 5.4, and Section 5.5 contains arguments based on the morphology seen for solution cast and melt mixed blends that the morphology seen at 200^{o}C is an equilibrium morphology. The degree of micellization seen for the blends is described in Section 5.6, and Section 5.7 contains a hypothesis about the composition of the micelle corona. Finally, Section 5.8 contains a summary of the morphology results presented in this chapter.

5.2 Micelle Shapes

The micelle structures for the blends studied in this work arose from mixtures of a tapered styrene-butadiene diblock, containing the lamellar structure shown in Figure 5.2, with an excess of an amorphous polystyrene. Recall that in all micrographs presented here, the dark region corresponds to a phase that contains a majority of butadiene and the white region corresponds to a phase that contains mostly styrene. One interesting aspect of the pure Fina 315 morphology is the lamellar structure persists over a much longer range for samples annealed for one hour at 200^{o}C (Figure 5.2a) than for other samples annealed for one hour at 130^{o}C (Figure 5.2b). Although not shown here, these differences in structure are very evident in lower magnification micrographs. It is believed here that the lamellar structure seen at 130^{o}C is a nonequilibrium morphology imposed on the Fina 315 during manufacturing. The average lamellae of butadiene seems to be thinner for the 130^{o}C, Fina 315 samples than the 200^{o}C samples, which suggests that during processing there is more mixing of butadiene block into the styrene phase than would exist at equilibrium.

The shapes of the micelles for samples of the 1%, 5%, 10%, and 20% blends annealed at 130^{o}C or 200^{o}C are shown in Figures 5.3 through 5.6. To ascertain the true shape of domains, orthogonal sections of the blend of interest must be observed. For instance, Figures 5.4b, 5.4c, and 5.4d show the three orthogonal sections of a 5%, 130^{o}C blend sample and illustrate that the domains are disks for

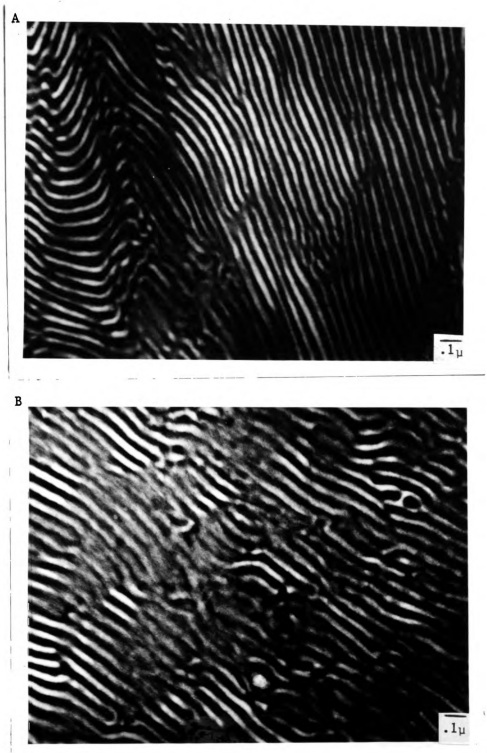

Figure 5.2 Transmission electron micrographs of pure Fina 315 tapered styrene-butadiene diblock annealed for one hour at (A) 200^{o}C or (B) 130^{o}C. For both samples,the resin as received from the manufacturer was annealed.

these conditions. For the other blends created here, just one representative orthogonal section is presented, but observation of the other orthogonal sections revealed the following micelle shapes. The 1%, 130°C (Figure 5.3b) and the 1%, 200°C (Figure 5.3a) samples both contained micelles that were nearly spherical. The 5%, 200°C (Figure 5.3a) and the 10%, 200°C (Figure 5.4a) blend samples contained micelles that were ellipsoidal, and the 10%, 130°C blend (Figure 5.5b) samples contained disks with an occasional cylinder. The 20%, 130°C (Figure 5.6b) and 20%, 200°C (Figure 5.6a) samples contained both ellipsoids and cylinders.

The electron micrographs in Figures 5.3 through 5.6 show that a transition from nearly spherical micelles to cylindrical-shaped micelles occurs as the concentration of diblock in the blend increases. This transition appears to occur much less gradually for the blends that still have their structure due to processing (130°C blends) than for the blends that have their equilibrium structure (200°C blends). This conclusion arises because for the 130°C blends, between a diblock composition of 1% and 5% a transition from spheres to disks occurs and disks are really very short cylinders. As described earlier, Kinning and Thomas (1988) saw a transition from spherical to cylindrical micelles for AB/A blends when the molecular weight of the B-block or the A homopolymer increases. Although the transition from spheres to cylinders is caused by diblock concentration rather than molecular weight considerations here, it is likely that transition is due to B-blocks in the micelle

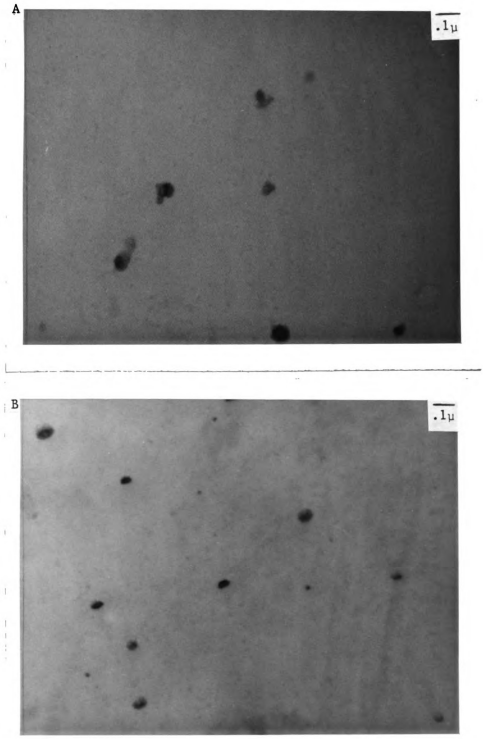

Figure 5.3 Transmission electron micrographs for blend of 1 weight % Fina 315 tapered styrene-butadiene diblock (M_w=136,000, 70% styrene) in Styron 666D polystyrene homopolymer (M_w=235,000). Sample (A) was annealed for 1 hour at 130°C, and sample (B) was annealed for 1 hour at 200°C. Samples annealed at 200°C contain equilibrium structures, and samples annealed at 130°C contain stuctures due to melt mixing in a twin screw extruder.

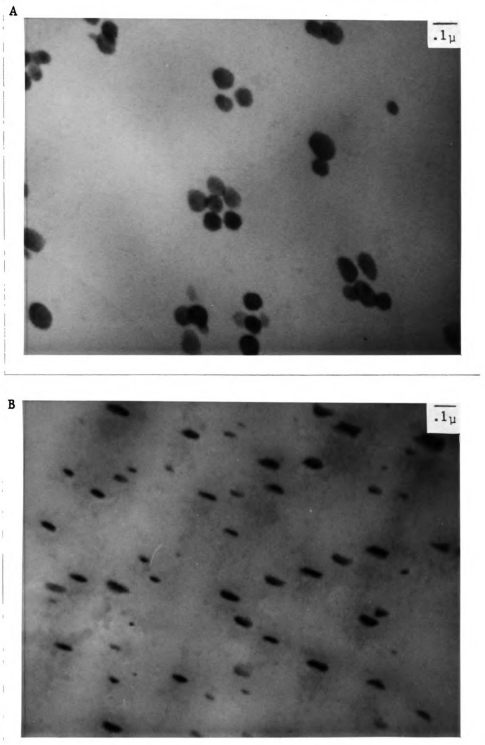

Figure 5.4 Transmission electron micrographs of 5 weight % Fina 315 in Styron 666D annealed for 1 hour at (A) 200°C or (B), (C), and (D) at 130°C. Micrographs (B), (C), and (D) illustrate that processing has resulted in domains with a disk shape.

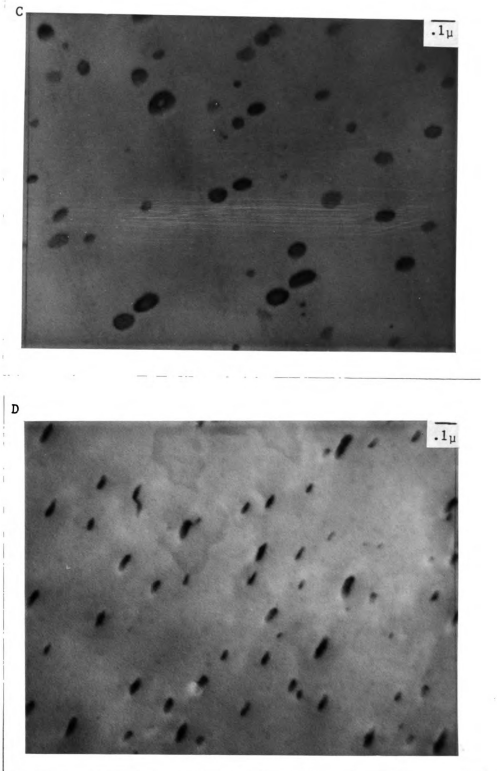

Figure 5.4 (continued)

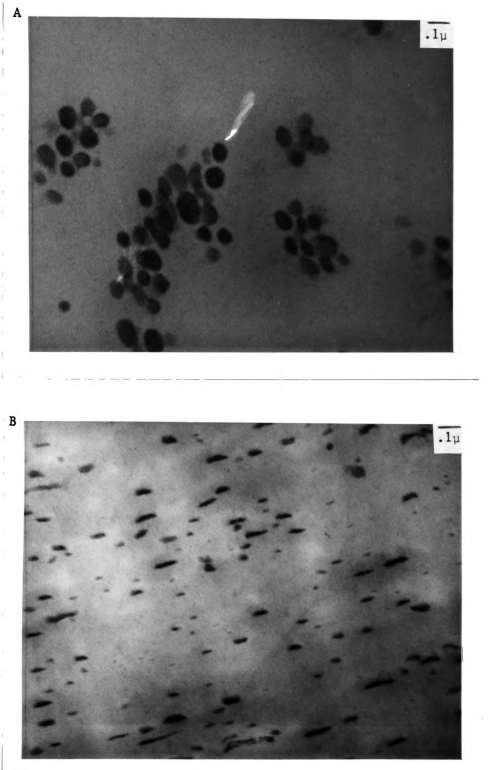

Figure 5.5 Transmission electron micrographs for 10 weight Fina 315 in Styron 666D annealed for 1 hour at (A) 200°C or (B) 130°C.

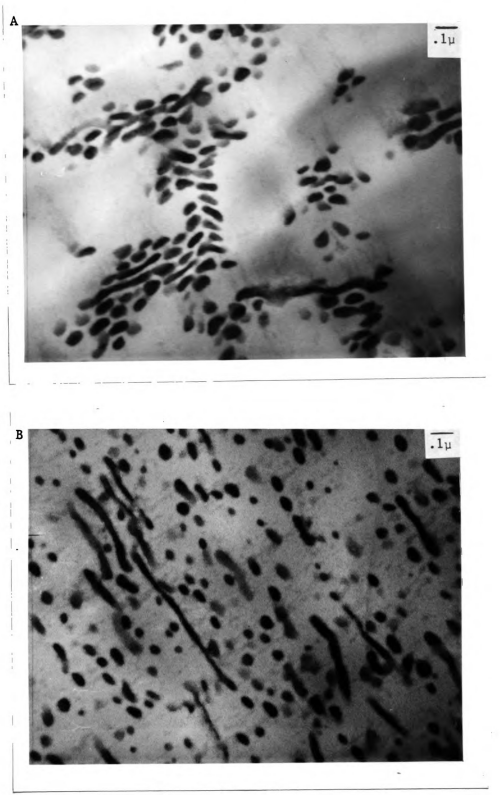

Figure 5.6 Transmission electron micrographs of 20 weight % Fina 315 in Styron 666D annealed for 1 hour at (A) 200°C or (B) 130°C.

core being deformed much less for cylinders than spheres, as suggested by Mayes and de la Cruz (1988), for both cases.

Mayes and de la Cruz (1988) suggested that equilibrium morphologies other than spheres and cylinders may be possible for Ab/A blends as the molecular characteristics of the blend are altered. To verify that this is true, the equilibrium (200^{o}C) morphology obtained for a melt blend of 1% Kraton D1000I, which is a styrene/butadiene diblock with M_w = 130,000 and 9 weight percent styrene, is shown in Figure 5.7. The domains for the 1% Kraton D1000I are much larger than those for the 1% Fina 315 blend and have a much different structure (compare Figures 5.3 and 5.7). It appears that the diblock and the homo-polystyrene form completely separate phases in the 1% Kraton D1000I blend because the pure Kraton D1000I diblock has the same structure as the domain shown in Figure 5.7, i.e., spherical domains of polystyrene in a matrix of polybutadiene. Other micrographs suggest that the structure after processing was the same as that shown in Figure 5.7, although more research needs to be done to establish this conclusively.

5.3 Micelle Core Sizes

Before details are given on the method and results of determination of micelle core sizes from the electron micrographs, the width of the lamellae for the pure Fina 315 will be discussed briefly. In the theories for micelle formation in AB/A blends mentioned earlier, a term is introduced to describe the deformation of the A-block and B-block, away from their equilibrium end-to-end

Figure 5.7 Transmission electron micrograph of melt blend of 1 weight % Kraton D-1000I styrene-butadiene diblock copolymer (M_w=130,000, 9% styrene) in Styron 666D. Sample was annealed for 1 hour at 200^{o}C.

distance in the pure diblock state, during the process of forming a micelle. Therefore, it is of interest to determine if the theoretical expressions used to evaluate the end-to-end distance in these theories are accurate. Although the widths of the lamellae in Figure 5.1a vary throughout the micrographs, rough estimates of the butadiene and styrene domain thickness were obtained by measuring domain thickness at a number of points. The width of the styrene domain was determined to be 20 nm and the width of the butadiene domain was 12 nm. Roe (1986) assumed the root mean square radii r of the butadiene and styrene blocks for pure block copolymers are given by $r = .9(M_w)^{.5}$ Å and $r = .7(M_w)^{.5}$ Å, respectively, during his check of the theory of Leibler et al. (1983) for micelle formation against experimental results. Applying these expressions to Fina 315 yields r = 18.1 nm for the butadiene block and r = 21.5 nm for the polystyrene block. Whitmore and Noolandi (1985) used $r = N^{1/2}b$, where N is the degree of polymerization and b is a Kuhn statistical length (b = .68 nm for polystyrene and b = .71 nm), when comparing their theory for micelle formation in AB/A blends to the experimental results of Selb et al. (1983). For Fina 315, where N for the polystyrene block equals 915 and N for the polybutadiene block equals 785, Whitmore and Noolandi's expression yields r = 20.5 and r = 19.8 nm for the styrene block and butadiene block, respectively. It can be seen that both the expression used by Roe and the expression used by Whitmore and Noolandi for predicting the length of the styrene block in the pure diblock are satisfactory,

but the expressions used for the butadiene block over-predict the actual length of this block.

A characteristic radius for the core of the ellipsoidal and cylindrical micelles for each blend composition and for both annealing temperatures used here was calculated by determining the average volume of the micelle cores and then setting this volume equal to the volume of a sphere. This sphere radius was then considered to be the characteristic radius of the micelle core for a given blend. During the determination of an average volume for the micelle cores, the volume of each micelle core was calculated based on its shape, and the resultant expression for the characteristic radius is

$$r_{characteristic} = \left(\sum_{i=1}^{N_e} a_i^e \, (b_i^e)^2 + \sum_{j=1}^{N_c} \frac{3}{4} \, h_i^c \, (r_i^c)^2 \right)^{1/3} \qquad 5.1$$

where N_e is the number of ellipsoidal domains, N_c is the number of cylindrical domains (recall that a disk is a short cylinder), $N_d = N_e + N_c$ is the total number of domains, and the dimensions a^e, b^e, h^c, and r^c are defined in Figure 5.8. For ellipsoids that have been sliced in the direction of Figure 5.8c, the calculation of the domain volume will be slightly in error because one cannot determine the value for a^e. The micrographs show that usually ellipsoids were sliced in the direction shown in Figures 5.8a and b, and therefore the error is minimal. For the 20% blends, a domain was considered to be a cylinder when the large dimension was four times greater

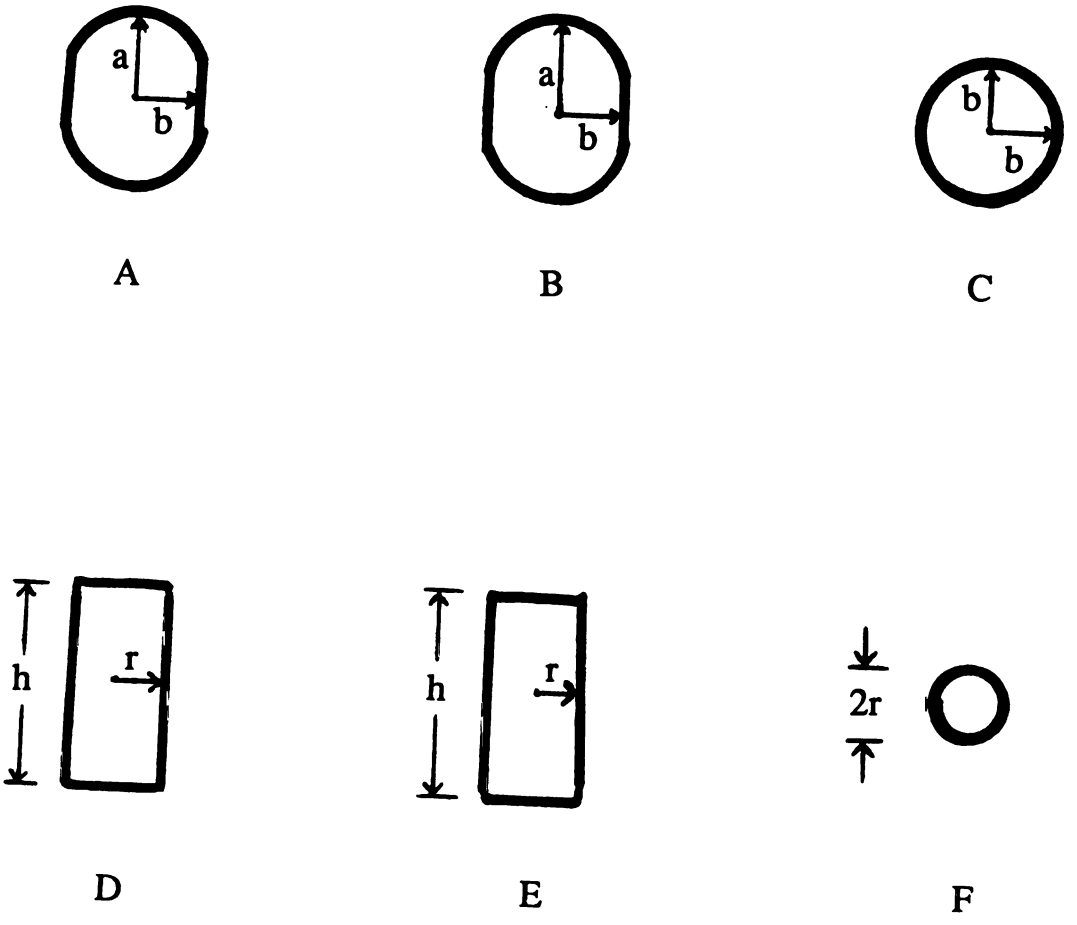

Figure 5.8 (A), (B), and (C) are domain shapes that can be obtained when sectioning ellipsoids. (D), (E), and (F) are domain shapes that can be obtained when sectioning cylinders. Note that ellipsoids and cylinders can be sectioned in other directions that will result in slightly different shapes.

than the small dimension. This criterion was arbitrary and was based on visual inspection. Using this criterion, 10% of the domains at both annealing temperatures for the 20% blends were cylinders. One cannot calculate the volume of a disk that has been sectioned in the direction shown in Figure 5.8f (see Figure 5.4c) because the height of the disk cannot be determined. Micrographs that contained disks sectioned in this way were not used.

The domain dimensions used in equation 5.1 were determined by measuring domains on characteristic micrographs of each blend with a digital caliper that allowed readings to the 1/100th of a millimeter. The domains' longest dimension and shortest dimension were determined for the calculations. The actual domain dimensions were calculated by scaling the measurements based on the magnification of the domain. In most cases, the domains were magnified by 58,000x (the 1% blends were magnified 50,000x). For each blend, domains were measured on two to five micrographs, and from 140 to 400 domains were measured for each set of blend conditions. According to Geblizlioglu, Argon, and Cohen (1985), the lower limit on the variance of volumes $\sigma(c_v)$ calculated from measuring areal projections of the domains is given by

$$\sigma(c_v)/c_v > 1.1/\sqrt{N_d} \qquad 5.2$$

where N_d is the number of domains that have been measured. For N = 140 to 400 from the measurements here, the variance or relative error is 9 to 5%. Note that equation 5.2 is a lower limit on the variance and the error could actually be greater. However, the

calculated values from one micrograph to the next for the same blend conditions varied by less than 10%, so the error limit calculated from equation 5.2 seems to be applicable. There is another error in domain measurements that results from truncation of spheres during sectioning. The sphere radii in a two-dimensional projection appear to be smaller than the actual radii due to this truncation. Berney, Cohen, and Bates (1982) showed that the measured radius is corrected for this truncation error by

$$R_{measured}/R_{actual} = (1 + R_{actual}/2t_s)/(1 + 2R_{actual}/t_s) \qquad 5.3$$

where t_s is the sample thickness. Berney et al. did studies in which they compared the results of domain sizes determined from small-angle scattering (SAXS) to those determined from transmission electron microscopy (TEM) and concluded that for transmission electron microscopy $R_{SAXS} = 1.3R_{TEM}$. Berney et al. suggested that R_{SAXS} is the actual domain size and that R_{TEM} is in error, possibly due to the staining procedure used for TEM samples or the mechanism of obtaining n transmission electron micrograph. It still is not conclusive that the radius measured during SAXS is the actual radius of a domain. For instance, Rigby and Roe (1986) used SAXS to determine styrene-butadiene diblock micelle core sizes in a matrix of low molecular weight polybutadiene. They found that at low temperatures the volume fraction of micelle cores exceeded the volume fraction of styrene in the blend by 10 to 20%. Since at low temperature there is high incompatibility between styrene and

butadiene, it is unlikely that there was much butadiene dissolved in the micelle core. This suggests that SAXS over-determined the size of the cores. It was found that the correction suggested by Berney et al. appeared to over-predict the size of the micelle cores here also, so equation 5.3 was used to correct the characteristic radius obtained with equation 5.1. A computer program was written that, from an input of domain dimensions, determined the number of domains, the characteristic radius of a domain, the mean characteristic radius, the standard deviation of domain sizes, the total volume occupied by domains, and a histogram of domain sizes for each micrograph. The results of this analysis are described below.

Figures 5.9 through 5.11 show the distribution of measured characteristic domain diameters for the 5%, 10%, and 20% blends annealed for one hour at 130^{o}C and 200^{o}C. No correction has been applied to the data on Figures 5.9 through 5.11. These figures show that the distribution of domain sizes appears to be Gaussian. The standard deviation in domain sizes decreased with increase in diblock content for the blends, where the standard deviation for the 5%, 10%, and 20% blends was 6 nm, 5 nm, and 4 nm, respectively. The standard deviation did not vary much with temperature of annealing for a given blend.

Figure 5.12 shows a plot of the corrected characteristic radius versus weight percent diblock for the blend samples annealed for one hour at 130^{o}C or 200^{o}C. The error bars result from applying equation 5.2. The radii of the domains in the 200^{o}C blends are on

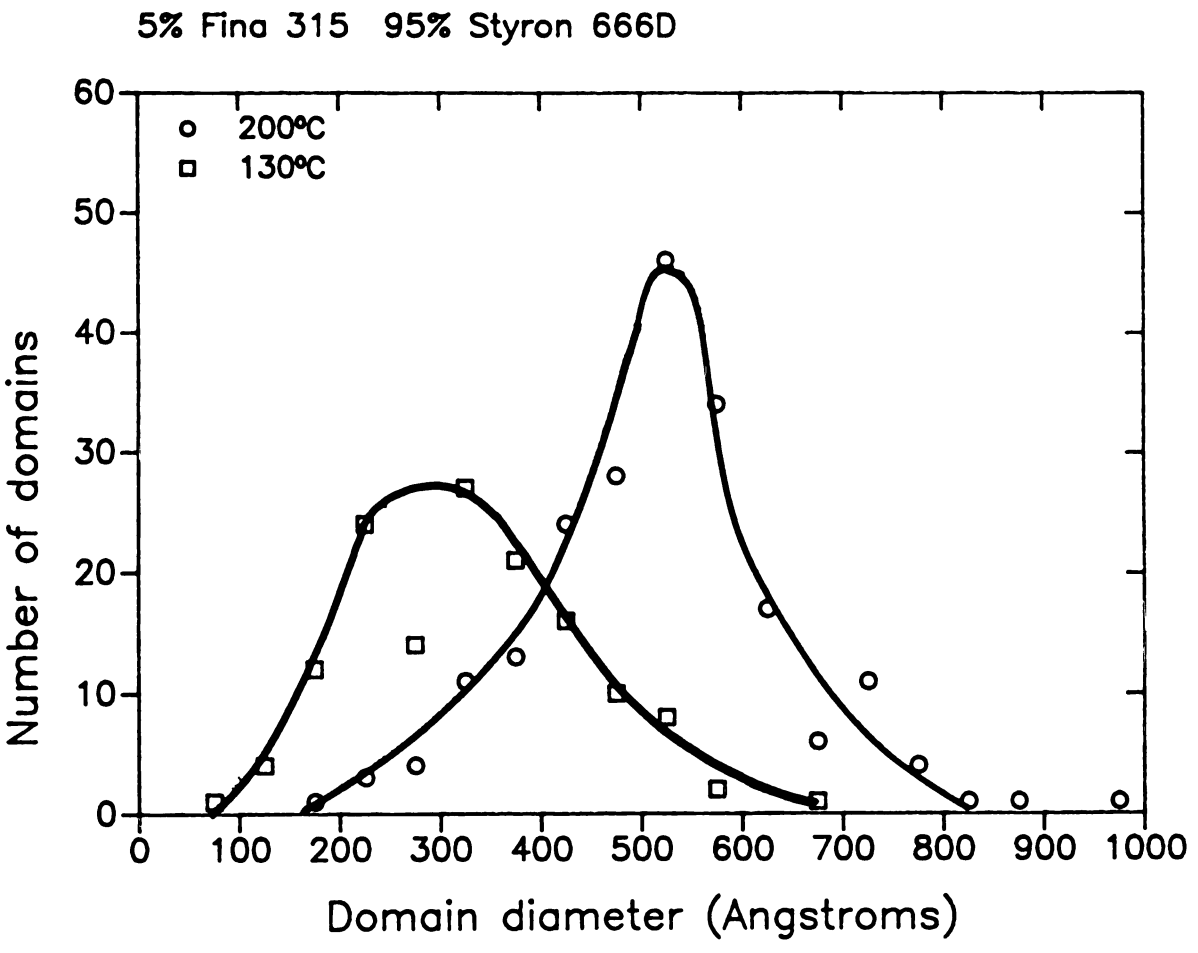

Figure 5.9 Distribution of domain sizes for 5 weight % Fina 315 in Styron 666D for samples annealed at 200°C or 130°C.

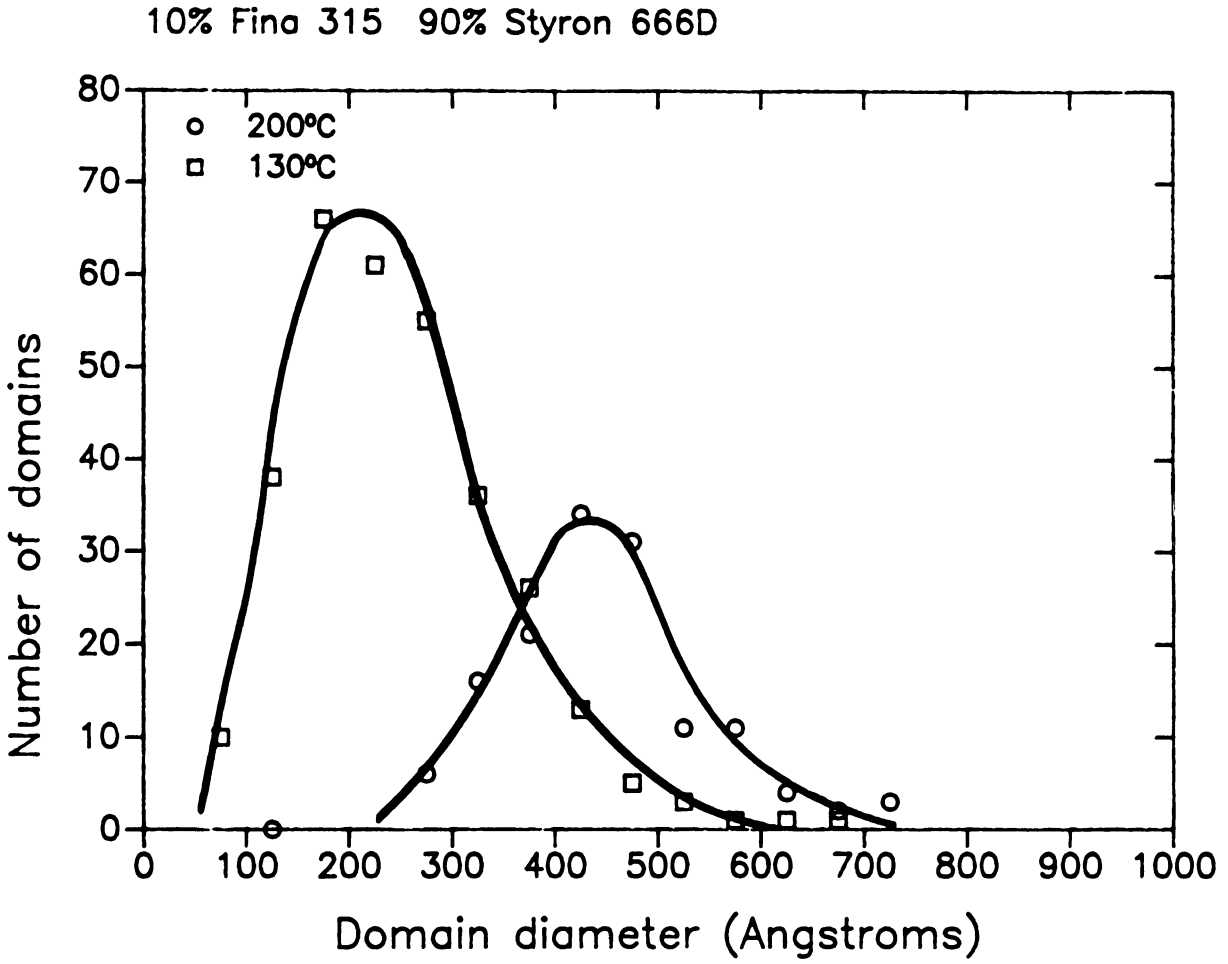

Figure 5.10 Distribution of domain sizes for 10 weight % Fina 315 in Styron 666D for samples annealed at 200°C or 130°C.

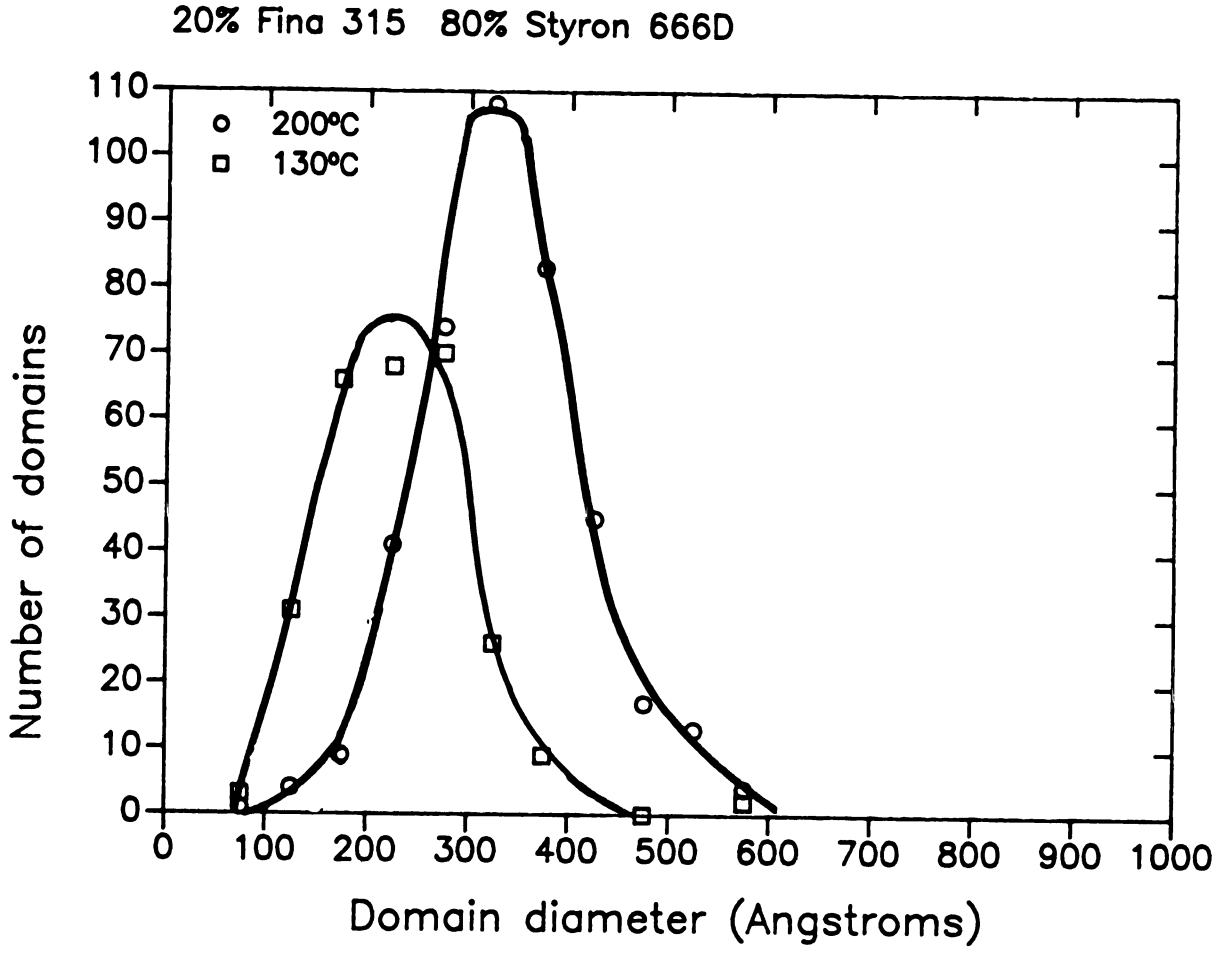

Figure 5.11 Distribution of domain sizes for 20 weight % Fina 315 in Styron 666D for samples annealed at 200°C or 130°C.

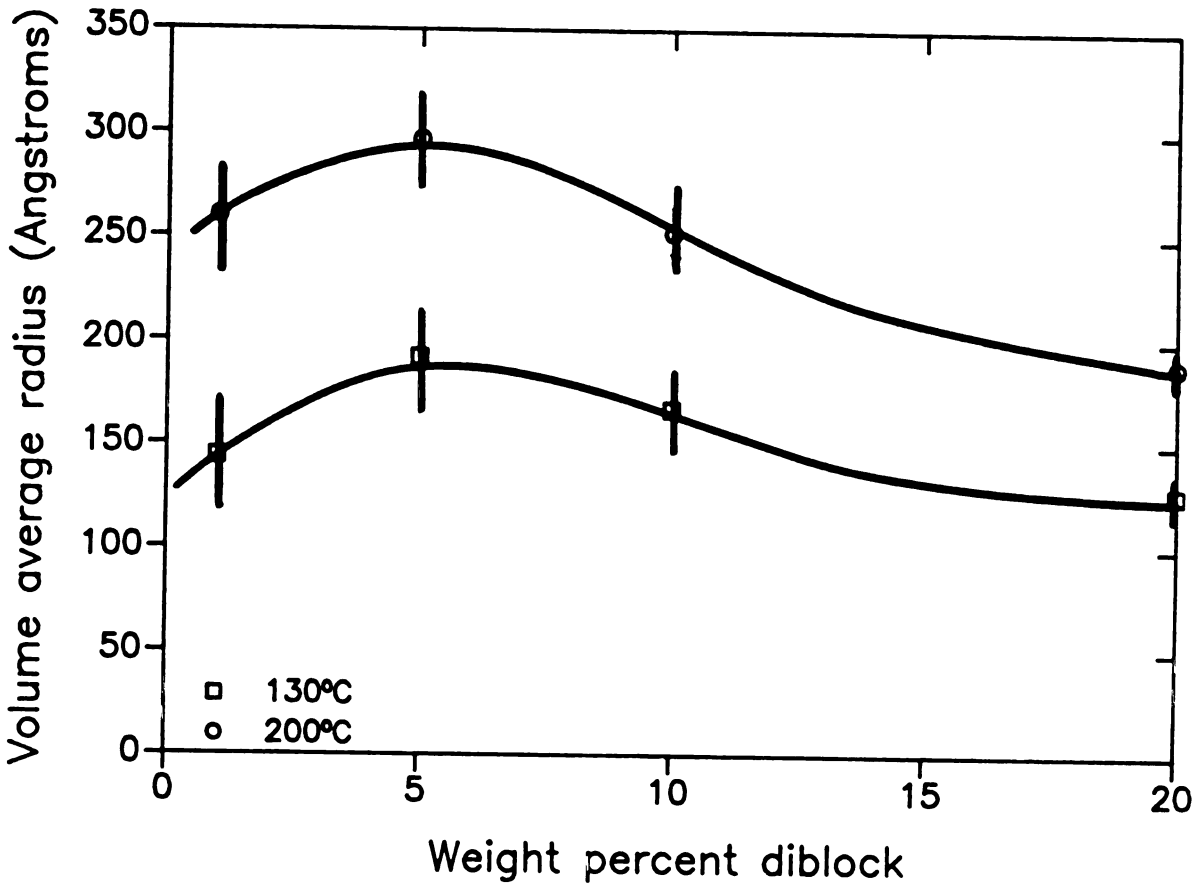

Figure 5.12 Volume average radius of domains in blends of Fina 315 with Styron 666D for samples annealed at 130^0C and 200^oC.

the same order of magnitude as the radii of domains Bates, Berney, and Cohen (1983) saw for the high molecular weight pure styrene/ butadiene diblocks that contained spheres of butadiene. Figure 5.12 demonstrates two trends for the size of the micelle core. First, for both equilibrium (200^{o}C) and melt stressed blends (130^{o}C), the size of the micelle core increased from 1% to 5% diblock. As diblock content increased above 5%, the size of the micelle core decreased. Second, processing caused the blends to have a smaller micelle core size than they do at equilibrium. As mentioned earlier, Selb et al. (1983) saw the same trend of a decrease in micelle core size with increased diblock content that was seen here. Selb et al. attributed this decrease to the way they measured domain radius. For instance, neither the thickness of the interface nor interparticle scattering is taken into account in small-angle neutron scattering, which may have affected Selb et al.'s results. In transmission electron microscopy, the interparticle scattering effects do not exist, so interparticle scattering will not explain the results obtained here. Selb's hypothesis of an interface thickness that varies with diblock concentration does not agree with the results of Bates et al. (1983), who showed that the interface thickness stays constant at approximately 2 nm for styrene-butadiene mixtures. Since the change in domain size with copolymer concentration was greater than 2 nm here (and for Selb et al.), the measured change in domain size does not appear to be due to a change in interface thickness. In other words, the decrease in domain size with increase in copolymer concentration appears to be real. It is

interesting to note that for melt stressed blends the characteristic radius approaches the width of the butadiene block in the pure Fina 315 diblock copolymer (12 nm) as concentration of diblock in the blend increases. For the equilibrium blends, the fact that the characteristic radius is much larger than the width of the butadiene block in the pure Fina 315 suggests the butadiene block is stretched a great deal during micelle formation. As mentioned earlier, it is probably because of this stretching that there is a transition from a spherical to cylindrical micelle shape. According to existing theories on micelle formation in AB/A blends, the size of spherical micelles should remain the same and the size of cylindrical micelles should increase with increasing diblock content in the blends. Clearly, the above data do not support this.

As mentioned earlier, a value of interest when comparing experimental results to theoretical results for micelle formation in AB/A blends is the number of diblock molecules making up a single micelle, p. Roe (1986) and Whitmore and Noolandi (1985) both theoretically explored the possibility of matrix homopolymer being dissolved in the micelle core and found that minuscule amounts are dissolved. In other words, one may assume the micelle core is made up entirely of the butadiene block of diblock. This being the case, the number of diblock molecules in a micelle can be determined by dividing the volume of the core by the molecular volume of a

butadiene block. For this calculation, the specific volume as given by Rigby and Roe (1986)

$$v_{PB} = 1.1138 + 8.24 \times 10^{-4} T_C \ cm^3/g \qquad 5.4$$

where T_C is temperature in centigrade was used. The calculated values of p are given in Table 5.1.

Table 5.1.--Number of diblock molecules in a single micelle.

Blend	Temperature of Annealing	p
1%	130°C	163
5%		391
10%		255
20%		111
1%	200°C	963
5%		1429
10%		877
20%		371

5.4 Clustering of Micelles

Figures 5.4 through 5.6 show that at equilibrium there appears to be a tendency for micelles to agglomerate, whereas for the stressed blends the micelles are well separated. There is some controversy as to what the long-range order is in AB/A blends containing micelles. According to Leibler and Pincus (1984), the interaction of cilia of different micelles is unfavorable due to entropic considerations, which causes the micelles to want to stay separated at equilibrium. In a completely different view to that of

Leibler and Pincus, Watanabe et al. (1982) hypothesized that AB diblock micelles will only tend to stay strongly separated if a concentration gradient of A monomer would exist if they did not. In other words, AB diblock micelles tend to separate in selective solvents (in these mixtures a solvent that dissolves one of the blocks and precipitates the other block is used, and therefore micelles form) because there would be areas of the solution rich in A-monomer if they did not. Formation of this type of concentration gradient is energetically unfavorable. This concentration gradient cannot exist for AB/A blends, so the micelles are much freer to interact. The results obtained here seem to agree with the hypothesis of Watanabe et al. Rigby and Roe (1986) suggested that the strong repulsion predicted by Leibler and Pincus probably only develops after some degree of overlap for the micelle corona has been realized. If the coronae from two different micelles overlap, the cilia from the two different coronae will become tangled. It will then take a large amount of time for the cilia to become untangled so that the micelles can separate. It appears for the blends studied here that there is a movement of micelles in the one hour annealing period at 200^{o}C, which causes many micelles to become entangled. A characteristic time for Brownian diffusion of micelles is given by $t_p = 6\pi\mu R^3/kT$, where μ is the viscosity of the matrix ($\mu \sim 10^5$ poise) and R is the radius of the micelle (R ~ 440A), which yields t_p ~ 40 minutes for the blends studied here. This implies that the micelles will move about 1.5 micelle diameters in the one hour annealing period. At high diblock concentrations, many

micelles must be less than 1.5 diameters apart, which leads to a large interaction of micelles. The expression for Brownian diffusion time shows that for the very high viscosities at 130°C, micelles will not move very much in the one hour annealing period.

5.5 Verification of Equilibrium at 200°C

To compare the results of experiment to theory for micelle formation in AB/A blends, one needs to establish that the structures obtained experimentally are thermodynamic equilibrium structures. To compare the difference in morphology between solution casting and melt mixing, a solution cast 5% blend was prepared, and it would seem, after a comparison of the results for the solution cast 5% blend and the melt mixed 5% blend, that the morphology seen at 200°C must be the thermodynamic equilibrium structure for the blends. To see this, consider the quite different morphologies that were obtained by melt mixing and solution casting in Figures 5.4b-d and Figure 5.13b, respectively. Figures 5.4b-d show the melt mixed blends have small, well-dispersed disk-shaped micelles, while Figure 5.13b shows that solution casting resulted in domains that were very large bundles of cylinders or large onion-skin structures. Figures 5.4a and 5.13a show that after annealing for one hour at 200°C the solution cast 5% blend and melt mixed 5% blend both had a structure that consisted of ellipsoidal micelles that were agglomerated to some degree. In other words, the morphology seen for the 5% blend at 200°C was obtained from two original blend structures that were quite different in nature, which suggests that the structures seen

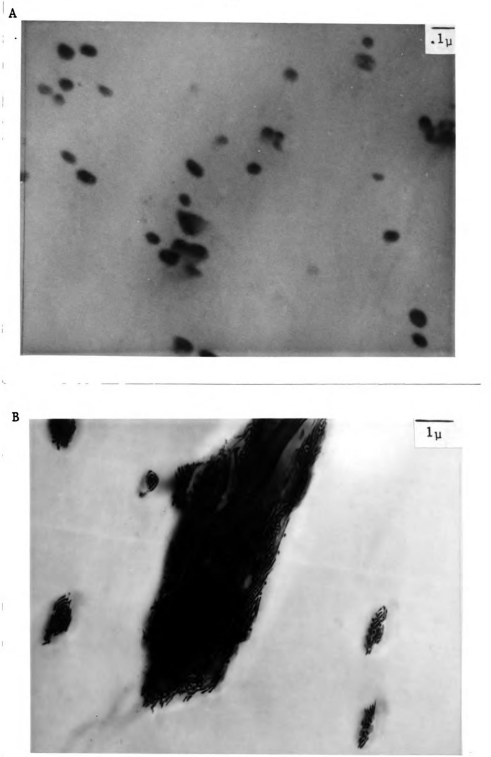

Figure 5.13 Transmission electron micrographs for a solution cast blend of 5 weight % Fina 315 in Styron 666D. Sample (A) was annealed for 1 hour at 200^{o}C, and sample (B) demonstrates the structure of the solution cast 5% blend without annealing.

for all blends that were annealed for one hour at 200°C must be equilibrium structures. As mentioned earlier, equilibrium is obtained because there is much motion of the polymer chains at 200°C.

There appears to be very little work done in the literature on kinetics of domain formation for polymer blends. Hadziioannou and Skoulios (1982) showed qualitatively that increasing temperature can decrease the time for phase transitions in pure block copolymers quite significantly. The results of Figure 5.13 demonstrate a large change in morphology for the solution cast blends has occurred in one hour. Figure 5.13 also shows that the compatibility between butadiene and styrene must be increasing quite a bit as the temperature is raised because the butadiene must pull out of the large domains seen in Figure 5.13b to form the much smaller domains seen at 200°C in Figure 5.13a. This would not happen unless the incompatibility between the styrene and butadiene diminishes. This result verifies that the blends created here have an upper critical solution temperature (USCT), which is in agreement with the results of Roe and Zin (1980) and Roe (1981) for other mixtures of polystyrene, polybutadiene, and corresponding diblock copolymer.

5.6 Composition of Micelle Corona

One question that arises for AB/A blends where the A homopolymer has a larger molecular weight than the A-block of the diblock is what the composition of the corona of the micelle is, i.e., what the value of n, the fraction of A-block in the corona,

is. Although this quantity cannot be measured directly, there is much evidence in the literature that when the A homopolymer has larger molecular weight than the A-block, there is little mixing of the two polymers. For example, Inoue et al. (1970), Eastmond and Phillips (1979), and Berney et al. (1988) all showed experimentally that the molecular weight of A homopolymer must be smaller than the molecular weight of the A-block of an AB diblock copolymer for the A homopolymer to be solubilized in A-block domain. Eastmond and Phillips (1979) suggested that the incompatibility of chemically identical blocks and homopolymers arises from an unfavorable entropy of mixing as a result of the blocks in the vicinity of the microphase interfaces adopting different sets of conformations than the randomly coiled chains in the bulk polymer. Since the styrene homopolymer here had a molecular weight about three times greater than the molecular weight of the styrene block of the diblock for the blends studied here, the results from Inoue, and so on, suggest that there is little mixing of the two polymers, and therefore n is fairly high. This also implies that the styrene blocks are compressed, because to exclude homopolymer from the corona the A-blocks must be compressed.

There is evidence here that the unfavorable entropy of mixing between the styrene-block and the styrene homopolymer increases as temperature is decreased. Figure 5.14, which is a micrograph of a blend that was annealed for one hour at 200^{o}C and then subsequently annealed for three hours at 130^{o}C, shows an interesting phenomenon, namely, some butadiene domains had inclusions of polystyrene.

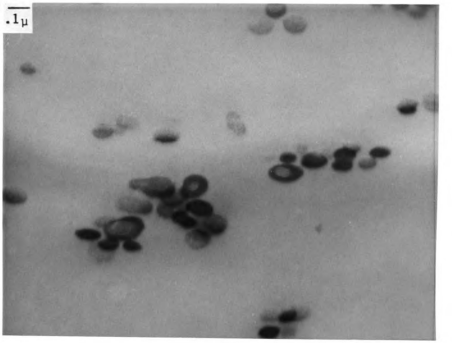

Figure 5.14 Transmission electron micrograph of 5 weight % Fina 315 in Styron 666D. Sample was annealed for 1 hour at 200^{o}C and then was subsequently annealed for 3 hours at 130^{o}C.

Whether this styrene came for the styrene block of the diblock or was matrix polystyrene is not obvious. Following the logic of Eastmond and Phillips (1979), mentioned above, it could be that the block polystyrene is assuming a different configuration, which makes it more incompatible with the matrix polystyrene as temperature is decreased. Along the same vein, it is evident in Figure 5.13 that the polystyrene in the diblock is forming a different phase from the matrix polystyrene for the solution cast blends. The structures created during solution casting would imply that the block polystyrene and the matrix polystyrene become extremely incompatible at lower temperatures.

Another possible explanation for the agglomeration of micelles seen here is if the block copolymer is forming different conformations than the matrix polystyrene, as suggested here, then mixing of the block polystyrene from different micelles may be more favored than mixing of block polystyrene and matrix polystyrene, and a driving force for agglomeration of micelles would exist.

Since it is hypothesized above that there is an unfavorable interaction between the matrix polystyrene and the styrene block of the diblock when the matrix polystyrene has a larger molecular weight than the styrene block, a consideration of the molecular weight distribution for the matrix polystyrene is in order. The molecular weight distribution for Styron 666D in Figure 4.1 reveals that the number average molecular weight is 93,420 and there is a large low molecular weight tail for the distribution. Since the molecular weight of the styrene-block for Fina 315 is 95,200, based

on the above hypothesis there are a fair number of matrix polymer chains that can mix favorably with the styrene-block. Eastmond and Phillips (1979) showed much experimental evidence that the molecular weight of the matrix polystyrene must be an order of magnitude less than the styrene-block before these two polymers will mix well. This implies that the matrix polystyrene would mix sparingly with the styrene-block for the blends considered there.

5.7 Degree of Micellization

The final parameter calculated from the micrographs obtained in this work was the degree of micellization ζ for each blend composition at both annealing temperatures. The degree of micellization was simply calculated by dividing the fraction of volume fraction of micelle cores ϕ_{core} in the blend by the total volume fraction of butadiene block ϕ_{PB} in the system. In this calculation the assumption is made that the micelle core consists solely of butadiene-block. The details of this calculation and the results are presented below.

By assuming the sample thickness was 90 nm (all samples considered here were sectioned at the same time to an ultramicrotome setting of 90 nm, so they should have roughly this thickness), the total volume corresponding to a micrograph could be calculated. The volume fraction of micelle cores ϕ_{core} was then calculated by dividing the average total volume of micelle cores for a micrograph by the total volume corresponding to a micrograph. It should be noted that in the calculation of volume fraction of micelle cores

the corrected characteristic radius given by equation 5.3 was used. Table 5.2 shows the volume fraction of micelle cores, the total volume fraction of polybutadiene, the volume fraction of diblock, and ζ for the various blends. The limits on ϕ_{core} in Table 5.2 were obtained with equation 5.2.

Table 5.2.--Volume fraction of micelle cores, polybutadiene, and diblock, and degree of micellization for blends.

Blend	Temperature	ϕ_{PB}	ϕ_{core}	$\phi_{diblock}$	ζ
1%	130°C	.0035	.0008 ± .0002	.011	.22
5%		.018	.012 ± .003	.053	.66
10%		.035	.013 ± .003	.106	.37
20%		.072	.012 ± .003	.211	.17
1%	200°C	.0035	.0033 ± .0007	.011	.94
5%		.018	.019 ± .005	.053	1.06
10%		.037	.027 ± .006	.108	.73
20%		.073	.033 ± .008	.212	.45
5%	200°C,1 hr/130°C hr	.018	.019 ± .005	.053	1.06

Table 5.2 shows the surprising result that the total volume fraction of micelle cores in the blend appears to stay approximately constant as diblock concentration increases above 5% for the blends annealed at 130°C or 200°C. Remember that the morphology at 130°C was created during extrusion. With the assumption that domains consist only of butadiene, the results of Table 5.2 suggest that above a certain concentration of diblock a constant number of diblock molecules are involved in domain formation, and the

remainder of the diblock molecules are dissolved. This means that the degree of micellization decreases with increase in diblock content for the blends as Table 5.2 indicates. Of course, if the micelle cores consist of polystyrene also, this logic does not hold. The results obtained with the blends here are in sharp contrast to the predictions of the theories of Leibler et al. (1983) and Whitmore and Loolandi (1985), which show that after a certain amount of diblock is dissolved in the matrix, as diblock is added to the blend, it forms micelles. Clearly, there is an effect that causes the formation of domains after a certain point to be a hindered process. One idea for this effect is seen by looking at the micrographs for the various blends as a function of concentration. It can be seen in the micrographs that as diblock content increases, the space available for formation of new domains becomes much smaller. It may be that this accounts for the decrease in degree of micellization with diblock content, although how is not obvious.

5.8 Summary of Results for Morphology Experiments

Micelle structures have been examined for blends of styrene-butadiene diblock/styrene homopolymer where the matrix styrene had larger molecular weight than the styrene block, and the following results were obtained. First, the shape of the micelles changed from spherical to cylindrical as the diblock content in the blend was increased both at equilibrium and during melt mixing. Second, the average size of the micelles went through a maximum with diblock concentration for both equilibrium and melt mixed blends, and at a

given diblock composition, the sizes of the domains at equilibrium were larger than during melt mixing. Third, there was a tendency for the micelles to agglomerate at equilibrium, which disappeared when the blends were processed. Fourth, the degree of micellization decreased with an increase in diblock content both at equilibrium and during melt mixing. Finally, melt mixing caused the degree of micellization to decrease. The existing theories on micelle formation in AB/A blends do not predict any of the above trends, so much research is still needed for complete understanding of this phenomenon.

CHAPTER VI

RESULTS AND DISCUSSION OF RHEOLOGY EXPERIMENTS

6.1 Introduction

This chapter contains the results of dynamic mechanical tests performed on the blends studied here. One goal of the rheological tests performed here was to relate rheological behavior for the blends created here to the morphology seen in Chapter V for the various blends created here. Another objective here was to determine an expression for the amount of energy stored by the blends during flow, as a function of blend structural parameters. This expression is then used in the modification to the micelle formation theory for AB/A blends, to include effect of flow, presented in Chapter VII. This chapter is organized as follows. In Section 6.2 the effect of thermal processing on rheological properties is analyzed. Section 6.3 contains an analysis of the rheological properties of blends which have their equilibrium structure, and Section 6.4 contains attempts to relate the change from nonequilibrium structures to equilibrium structures with temperature, seen in Chapter V for the blends, to the blend's rheology. Section 6.5 contains a development of the relationship between structural parameters for the blend and the amount of energy

stored during flow by the blends. Finally, Section 6.6 contains a brief summary of the results obtained here.

6.2 Effect of Thermal Processing on Rheological Properties for the Blends

It is well known that both high shear and high temperatures can cause polymers to degrade, which in turn can alter the rheology of the polymer (see Grassie & Scott, 1985, for example). Since the blends studied here were prepared by melt mixing in a twin screw extruder where they experienced both high shear (900 sec^{-1}) and high temperatures ($170^{o}C$-$190^{o}C$) and the rheological tests were performed at high temperatures (130^{o}-$200^{o}C$), care must be taken when interpreting the results of the rheological tests that the role of degradation in determining the final blend rheology is understood. Specifically, for the blends studied here one must be wary of associating changes in rheology with changes in micellar structure without checking for degradation of polymers. Following are details showing degradation was avoided during melt processing and high-temperature rheological testing of the blends studied here.

Figure 6.1 illustrates that it was necessary to stabilize the polymers studied here in order to prevent serious degradation during blend preparation. It can be seen in Figure 6.1 that degradation due to processing results in a decrease in $\eta_0 = \lim_{\omega \to 0} \eta'$ of two orders of magnitude for the unstabilized polystyrene relative to stabilized polystyrene. Assuming that η_0 is proportional to $M_w^{3.4}$, this means that without stabilization melt processing in the extruder has chopped up the polymer so much that the average molecular weight has

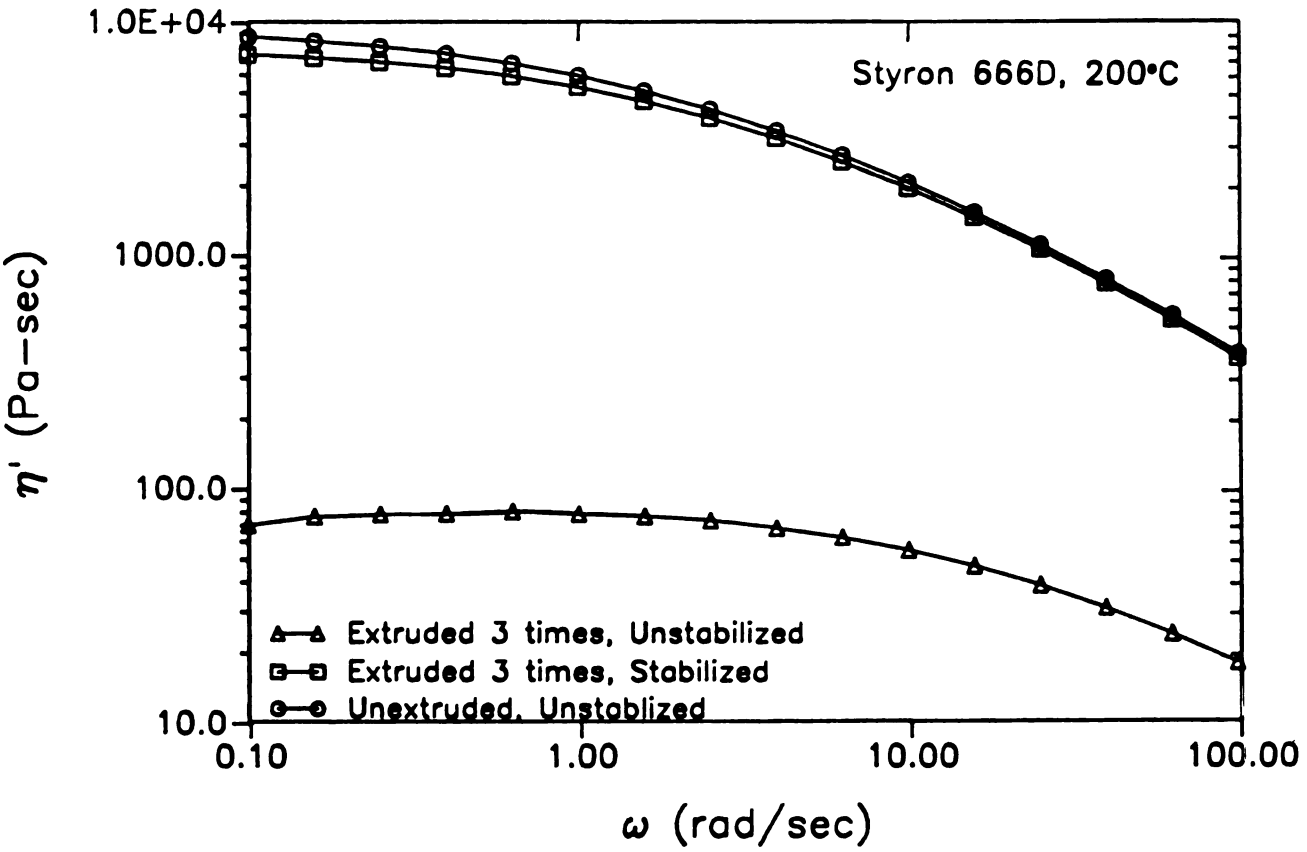

Figure 6.1 Effect of degradation during melt mixing on dynamic viscosity for stabilized and unstabilized Styron 666D.

dropped from 235,000 to 56,000. The results of Figure 6.1 are reassuring in that they show that the amount of stabilizer used in the study here has practically eliminated the effect of degradation due to processing.

During the rheological tests, the samples were annealed for one hour at high temperatures, and therefore the effect of thermal degradation must be considered. Experiments were performed in which the dynamic mechanical properties of the 5% blend and the 20% blend were monitored as a function of time for four hours. In these experiments the dynamic mechanical properties remained constant, so it is concluded that thermal degradation did not occur during the rheological tests.

As will be seen in more detail in Section 6.4, the results that were obtained for the 5% blend are peculiar in that the curves for G', G", and n' all lie below the results for pure polystyrene, while the results for the 10% and the 20% blend lie on or above the results for pure styrene. It is conceivable that this shift downward for the 5% data could have been due to degradation. To verify this trend was real, a 5% blend of Fina 315 with a different polystyrene (Dow 666 APR) was stabilized with .2 weight percent TNPP and .008 weight percent PHT (four times as much stabilizer as was used previously) and extruded twice instead of three times to reduce degradation. The pure polystyrene was stabilized and extruded in the same manner, and plots of G' for the processed and unprocessed polystyrene homopolymer, and the 5% blend are given in Figure 6.2. It can be seen in Figure 6.2 that the effect of degradation during

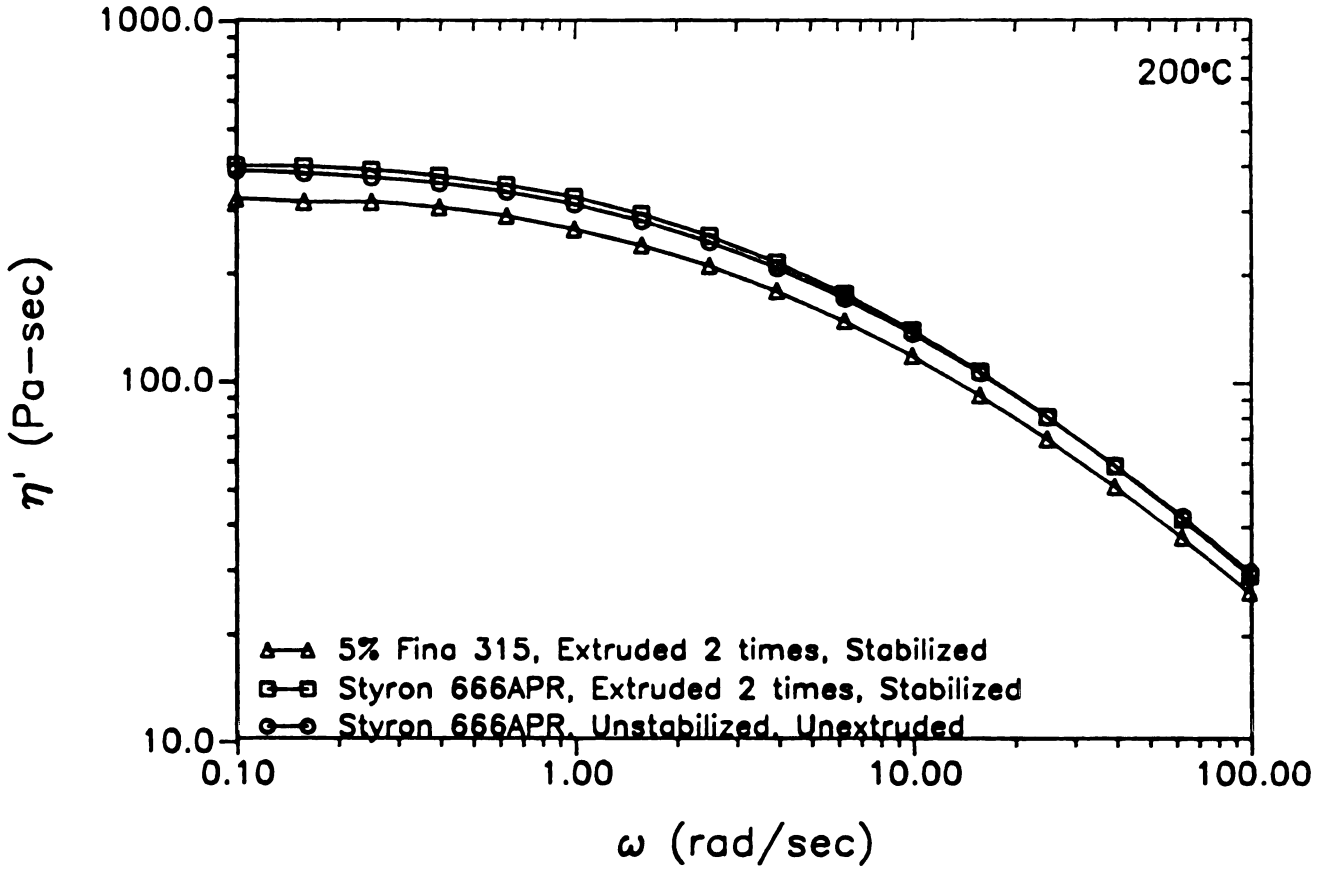

Figure 6.2 Verification that dynamic viscosity is smaller for 5 weight percent blends of Fina 315 with high molecular weight polystyrene than it is for the pure polystyrene.

processing has been eliminated, and the trend of decrease in G' for the 5% relative to the pure polystyrene still exists. Therefore, it is concluded that the trends seen with the blends here are correct.

6.3 Rheology of Blends With Equilibrium Structure

Recall from Chapter V that the blends studied here attained their equilibrium structure when annealed for one hour at 200°C, as the samples for rheological testing were. Since the low strains used in dynamic mechanical testing do not alter blend structure, the differences seen in rheology at 200°C must be due to the differences in morphology seen for blends at this temperature. In light of this, the rheological obtained at 200°C are analyzed in detail here.

Figures 6.3 and 6.4 show plots of G' and G" versus ω for the blends at 200°C. These curves illustrate that G" and G" are lower for the 5% blend relative to the pure polystyrene over the entire frequency range of the 200°C test (10^{-1} - 10^{2} rad/sec). As diblock concentration for the blends increases above 5 weight percent, the values of G' and G" also increase. It has already been established that these trends are not an artifact of the blend preparation technique.

The reason for the initial decrease in G' and G" when small amounts of diblock copolymer are added to the blend is not clear. Since the blend is composed mainly of polystyrene homopolymer at these concentrations, this result suggests that addition of diblock has increased the motion of the matrix polystyrene in some way. In Chapter V it was established that at concentrations up to 5 weight

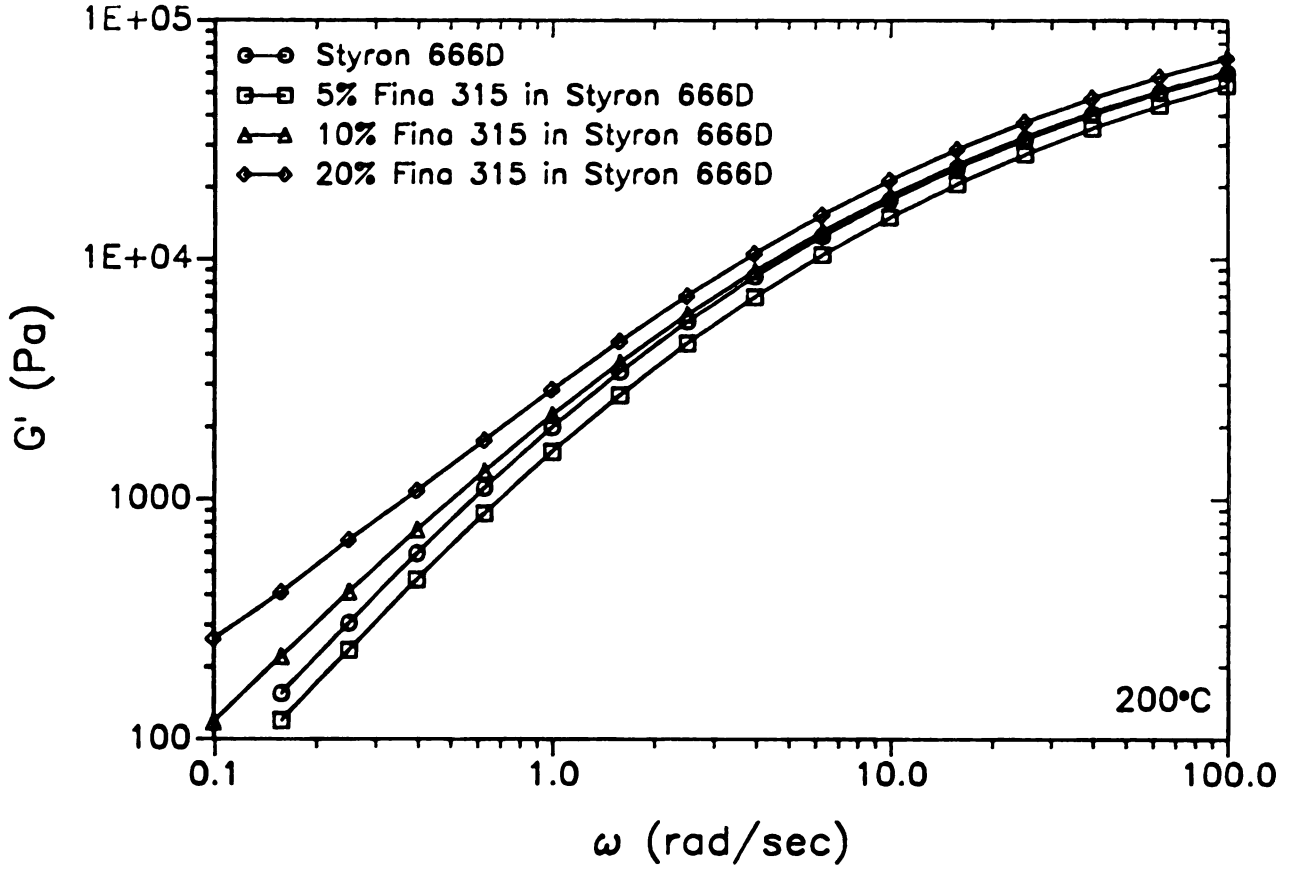

Figure 6.3 Storage modulus versus angular frequency for blends of Fina 315 with Styron 666D at 200°C.

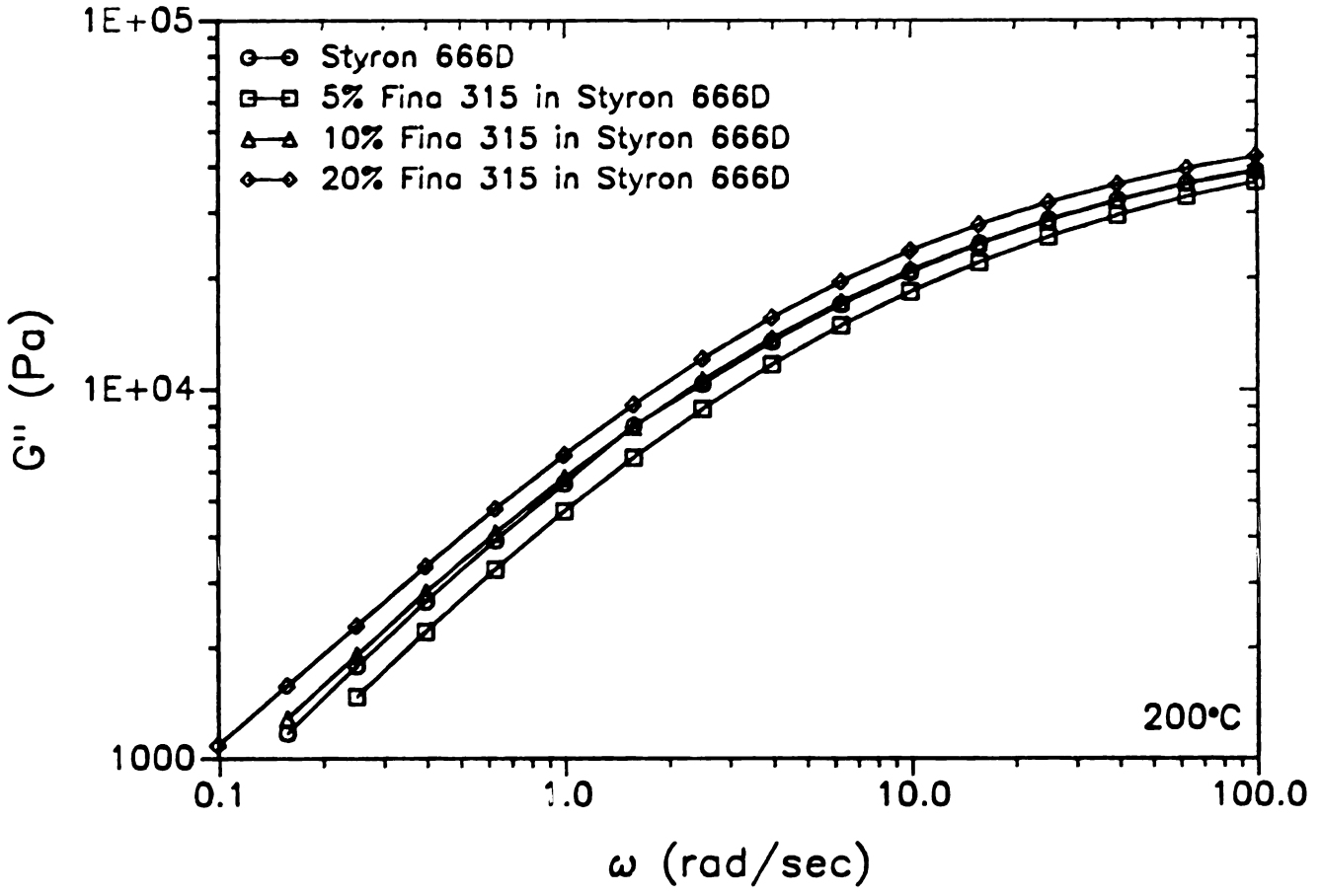

Figure 6.4 Loss modulus versus angular frequency for blends of Fina 315 with Styron 666D at 200°C.

percent diblock, the diblock added to the polystyrene is completely taken up in micelles so it is not diblock molecules dissolved in the matrix which causes the trends seen with G' and G". Another trend seen in Chapter V was that the size of the micelle core versus diblock concentration went through a maximum at approximately 5 weight percent diblock. The theoretical analysis in Chapter VII and the experimental results of Kinning and Thomas (1988) show that for a given diblock copolymer if conditions exist that cause the micelle core to increase, then the size of the micelle corona decreases. In other words, the micelle corona for the 5% blend appears to be thin, which suggests it is composed mostly of A-block from the diblock and does not contain much matrix polymer. It appears that the presence of micelles with "retracted cilia" has increased the motion of the matrix polystyrene molecules. Figure 3.5 shows that polymer chains can be viewed as reptating through a tube. Therefore, a possible explanation for the results obtained with the 5% blend is that as a matrix polystyrene molecule comes in contact with the corona of the micelle, the tube through which the molecule is reptating is altered (see Figure 6.A in the appendix). For instance, at the interface between the corona of the micelle and the matrix there is no entanglement of polymer, so the entanglement density of the matrix polystyrene is reduced in this local region. At a distance of one tube diameter from the corona a matrix polystyrene molecule is surrounded by other matrix polystyrene. Hence, the assumption made here is that the tube structure for the matrix polystyrene is only

altered for matrix polystyrene molecules that come in contact with the micelle corona (Figure 6.A). An analysis of the situation where entanglement density for the matrix polystyrene is reduced in the region of the micelle corona is given below.

From the tube model of Doi and Edwards (1978), the tube through which the matrix polystyrene reptates is considered to consist of N segments where each segment has a length a. The tube diameter is also equal to a. The value of N is usually determined from $N = 5M_{PS}/4M_e$ (Stuglinski & Graessley, 1985), where M_e is the molecular weight of the matrix polystyrene and M_e is the molecular weight between entanglements (usually taken as 18,000 for pure polystyrene). The lengths of tube segments a are determined from $r^2 = Na^2$, where r is the equilibrium end-to-end distance of the polystyrene (for polystyrene $r^2 = (.7(M)^{.5})^2$ (Roe, 1986). The total length of the tube is $L = Na$. The assumption made here is that the length of the tube through which the polymer molecule reptates does not change, but that the number of entanglements N making up the tube decreases when the matrix polystyrene tube contacts the micelle corona. Hence, from $L = NA$, as N decreases, the length of the tube segments and diameter of the tube, a, increase. For the pure matrix polystyrene which has $M_w = 235,000$, $N = 16.3$, $a = 8.41$ nm, and the length of the tubes L equals 137 nm.

From the tube model developed by Doi and Edwards (1978), the individual components in an entangled mixture contribute to stress in proportion to their weight or volume fraction. In other words, for the matrix polystyrene the stress-relaxation modulus is given by

$$G(t) = \phi_u G^o_{N,u} F(t/T_u) + \phi_m G^o_{N,m} F(t/T_m) \qquad 6.1$$

where ϕ_m is the volume fraction of polystyrene molecules whose tube structure behavior has been modified by contact with the micelle corona, ϕ_u is the volume fraction of matrix polystyrene whose tube structure is unmodified, G^o_N is the plateau modulus, F(t/T) is the probability distribution for the disengagement of a polymer chain from its initial tube as a function of time (Graessley, 1982), and T_u and T_m are reptation times. The disengagement times in equation 6.1 are defined as $T = L^2/\pi^2 D^*$ (Graessley, 1982), where D* is the diffusion coefficient along the tube. D* is defined as $D^* = kT/n_o \xi_o$, where n_o is the number of monomer units in the polymer chain and ξ_o is the friction coefficient per monomer unit. There is no apparent reason for D* to change for the matrix polystyrene in the vicinity of the micelle, and with the assumption that the length of the chain does not change, then $T_u = T_m$ in equation 6.1. This implies that $F(t/T_u = F(t/T_m)$ and a linear blending law exists for the plateau modulus given as

$$G^o_{N,blend} = \phi_u G^o_{n,u} + \phi_m G^o_{N,m} \qquad 6.2$$

Dividing both sides of equation 6.2 by $G^o_{N,u}$ using the fact that for the tube model the plateau modulus is given by $G^o_N = \rho R_G T/M_e$ yields

$$G^o_{N,blend}/G^o_{N,u} = \phi_u + \phi_m M_{e,u}/M_{e,m} \qquad 6.3$$

where $M_{e,m}$ is the average entanglement molecular weight for the matrix polystyrene whose tube structure is affected by the micelle

corona. $M_{e,u}$ is the entanglement molecular weight for unaffected matrix polystyrene (18,000). The ratio of $G^o_{N,blend}/G^o_{N,u}$ in equation 6.3 is determined for the 5% blend as follows. As can be seen in Figure 6.3, the curves of G' versus ω for the different blends and the pure polystyrene become parallel at high frequencies, and data taken at lower temperatures indicate these curves stay parallel throughout the plateau region. Therefore, Figure 6.3 suggests that there is a slightly different plateau modulus for the pure polystyrene and the 5% blend. The ratio of G' for pure polystyrene to G' for the 5% blend is approximately 1.1 at a frequency of 100 rad/sec. Assuming that this is a good estimate of the ratio of G^o_N for the two polymers, there are two unknowns in equation 6.3, ϕ_m and the ratio $M_{e,u}/M_{e,m}$. ϕ_u can be determined from $\phi_u = 1 - \phi_m$. The value of ϕ_m is estimated as follows.

The total volume of tube segments V_{tc} that come in contact with a single micelle corona is given by

$$V_{tc} = 4\pi/3([R + a_m]^3 - R^3) \qquad 6.4$$

where R is the radius of the micelle and a_m is the average radius (and segment length) of a modified tube. If the assumption is made that every tube segment that is in contact with a micelle corona belongs to the tube of a different matrix polystyrene molecule, then the maximum volume per micelle affected by a change in tube structure of matrix polystyrene molecules is $N_m(V_{tc})$ cm^3/micelle, where N_m is the average number of entanglements for the modified tube. The total volume fraction, ϕ_m, of matrix polystyrene affected by a change in tube structure is $N_m(V_{tc})$ times the number density of

micelles divided by the volume fraction of polystyrene in the blend 1 - ϕ. In Chapter V it was shown that all diblock molecules participate in micelles for the 5%, 200°C blend, and there were 1429 diblock molecules per micelle. With the assumption of no homopolymer in a micelle, the number density of micelles is equal to the volume fraction of diblock copolymer molecules in the blend divided by the volume of a single micelle. Using the specific volume of polystyrene (1.0367 cm^3/g) and the specific volume of polybutadiene (1.2786 cm^3/g) at 200°C, the molecular volume of the Fina 315 diblock is equal to 2.5047×10^{-19} cm^3/molecule, and the number density of micelles equals $.05/(1429)2.5047 \times 10^{-19} = 1.397 \times 10^{14}$ micelles/cm^3. Also, the radius of the micelle R is equal to $([3][1429]\ 2.5047 \times 10^{-19}/4\pi)^{1/3} = 4.41 \times 10^{-6}$ cm. Therefore, we have

$$\phi_m=(1.397x10^{14})(N_m)4\pi([4.41x10^{-6}+a_m]^3-[4.41x10^{-6}]^3)/(3)(1-\phi) \qquad 6.5$$

Using $N_m = 5(M_{PS})/4M_{e,m}$ and $a_m = L/N_m$ in equation 6.5 and combining equation 6.2 with 6.3 yields an expression in terms of $M_{e,m}$ alone. Solving this equation yields $M_{e,m} = 21{,}000$, which results in $\phi_m = .61$ and $N_m = 14$. To develop equation 6.5 the assumption was made that every tube segment that was touching a micelle corona belonged to the tube of a different polymer; i.e., a single polymer molecule can have only one tube segment touching the micelle corona. If instead the assumption is made that the tube segments that touch the micelle corona combine to form complete tubes for the matrix polystyrene (i.e., only entire matrix polystyrene molecules touch

the micelle corona), then the minimum volume fraction of matrix polystyrene affected by a change in tube structure at the micelle corona is given by replacing N_m in equation 6.5 by a value of one. Solving for M_e as before yields M_e = 51,000, which results in ϕ_m = .14 and N_m = 5.7.

The above calculations show that the rheology obtained for the 5% blend supports the notion of entanglement density being decreased for matrix polystyrene in the region of a micelle corona. Specifically, it was shown by using experimental values for the plateau modulus of the 5%, 200°C blend and the pure polystyrene that the average number of entanglements for a matrix polystyrene that comes in contact with a micelle corona in the 5%, 200°C blend is between 14 and 5.7 as compared to 16 for the pure polystyrene. An interesting aspect of the above calculations is that although there is only 5% diblock copolymer in the 5% blend, the micelle structure may affect the tube structure of between 14% and 16% of the matrix polystyrene.

The zero shear viscosity is defined as $\eta_0 = \int_0^\infty G(t)\,dt$. Using this in equation 6.3 suggests that there is a linear blending law for η_0, and with the assumption of $F(t/T_u) = F(t/T_m)$ used above the experimental value for the ratio of $\eta_{0,blend}/\eta_{0,u}$ should be the same as the experimental results for $G^o_{N,blend}/G^o_{N,u}$. However, the experimental ratio of zero shear viscosity for the 5%, 200°C blend to the zero shear viscosity for the pure polystyrene is .82, whereas the ratio of plateau moduli is .91. This suggests that a linear blending law does not apply for η_0. This is in line with

Struglinski and Graessley (1985), who suggested a blending law for η_o given by

$$\eta_{o,blend} = [\phi_u \eta_{o,u}^{1/3.4} + \phi_m \eta_{o,m}^{1/3.4}]^{3.4} \qquad 6.6$$

G' and G" increase as concentration of diblock increases above 5% for the blends, and the moduli for blends with 10% and 20% diblock show a greater divergence from the pure polystyrene moduli at frequencies below 1 rad/sec in Figures 6.3 and 6.4. Both of these results are similar to the results of Watanabe and Kotaka (1983), who studied styrene/butadiene diblock-low molecular weight polybutadiene blends and showed that G' and G" increase with increasing diblock content in their blends, and a shoulder occurred in their G' versus ω curves when micelles started to overlap. More specifically, Watanabe and Kotaka associated the shoulder in their G' versus ω curves with a slow relaxation mechanism attributable to formation and dissociation of aggregates of micelles. The micrographs of Chapter V show there is much aggregation of micelles for 10% and 20% blends, so the reason for the apparent shoulder in the G' versus ω curves here is also probably due to the interaction of micelles. Also, the increase in G' and G" with increased concentration of diblock for the blends here can probably be traced to the increased structure of the blend as diblock is added. Watanabe and Kotaka found a characteristic relaxation time for formation and dissociation of aggregates of micelles in their blends

from the location of the inverse frequency at the location of the shoulder in their G' versus ω plots. This time was approximately 10 seconds at 5 to 10 weight percent diblock in their blends and increased rapidly with increasing diblock concentration. Since, as Figure 6.3 indicates, the shoulder of the G' versus ω curve is not fully developed at the lowest frequency of testing (ω = .1 rad/sec), the relaxation time for the formation and dissociation of micelle aggregates at 200^{o}C must be greater than 10 seconds for the 10% and 20% blends.

Using Cole-Cole plots, a relaxation time for each blend may be determined and related to the blend's morphology. Monfort, Marin, and Monge (1984) detailed the problems involved in determining a relaxation time for polystyrene samples and showed that these problems become exaggerated for polystyrenes that are polydisperse, such as the polystyrene studied here. Monfort et al. found the best way to determine an average relaxation time for polystyrene was through the use of plots of the imaginary part of the complex viscosity η'' versus dynamic viscosity η' (also known as Cole-Cole plots). In other work, Monfort and Monge (1975, 1976) showed that the reciprocal of the frequency at the maximum of η'' in the Cole-Cole plot represents an average relaxation time for homopolymers no matter what the molecular weight distribution. It is this relaxation time that was determined here.

As an aside, Figure 6.5 shows a Cole-Cole plot for the pure Fina 315. Recently, Diogo, Marin, and Monge (1987) studied the rheology of a SBS triblock copolymer with cylindrical domains. The

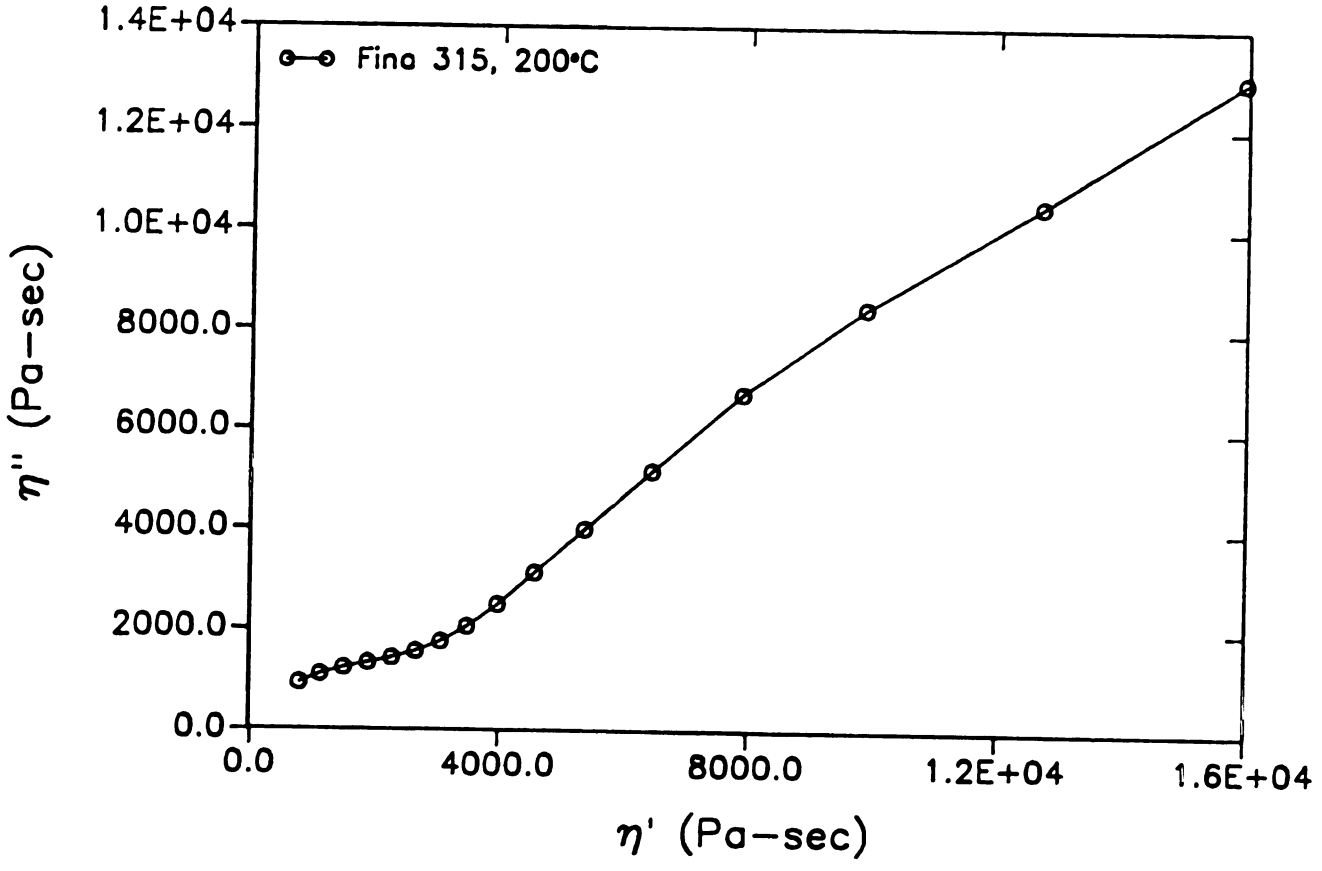

Figure 6.5 Cole-Cole plot for pure Fina 315 at 200^{o}C.

results of Figure 6.5 are similar to that of Diogo et al. in that two different sets of relaxation times seem to exist, separated by the branch in the η'' versus η' plot. Diogo et al. related the two relaxation mechanisms they saw to the reptation behavior of polybutadiene and the constraint release of the polystyrene. Since the diblock studied here is lamellar, it is likely that the two relaxation modes seen here were related to the butadiene chain motion and the polystyrene chain motion. Further analysis of pure diblock copolymer is outside the scope of this work.

Figure 6.6 shows Cole-Cole plots for the blends. The average relaxation times determined from the Cole-Cole plots are given in Table 6.1, which shows the average relaxation time initially decreases with increase in diblock concentration and then increases as diblock concentration is increased further. This result is the same as the trend seen with G' and G" noted earlier.

Table 6.1.--Relaxation times for the blends determined from Cole-Cole plots.

Blend	t(sec)	t_{160}(sec)	Marin et al. (1975) t_{160}(sec)
0%	.41	14.1	10.4
5%	.36		
10%	.49		
20%	.77		

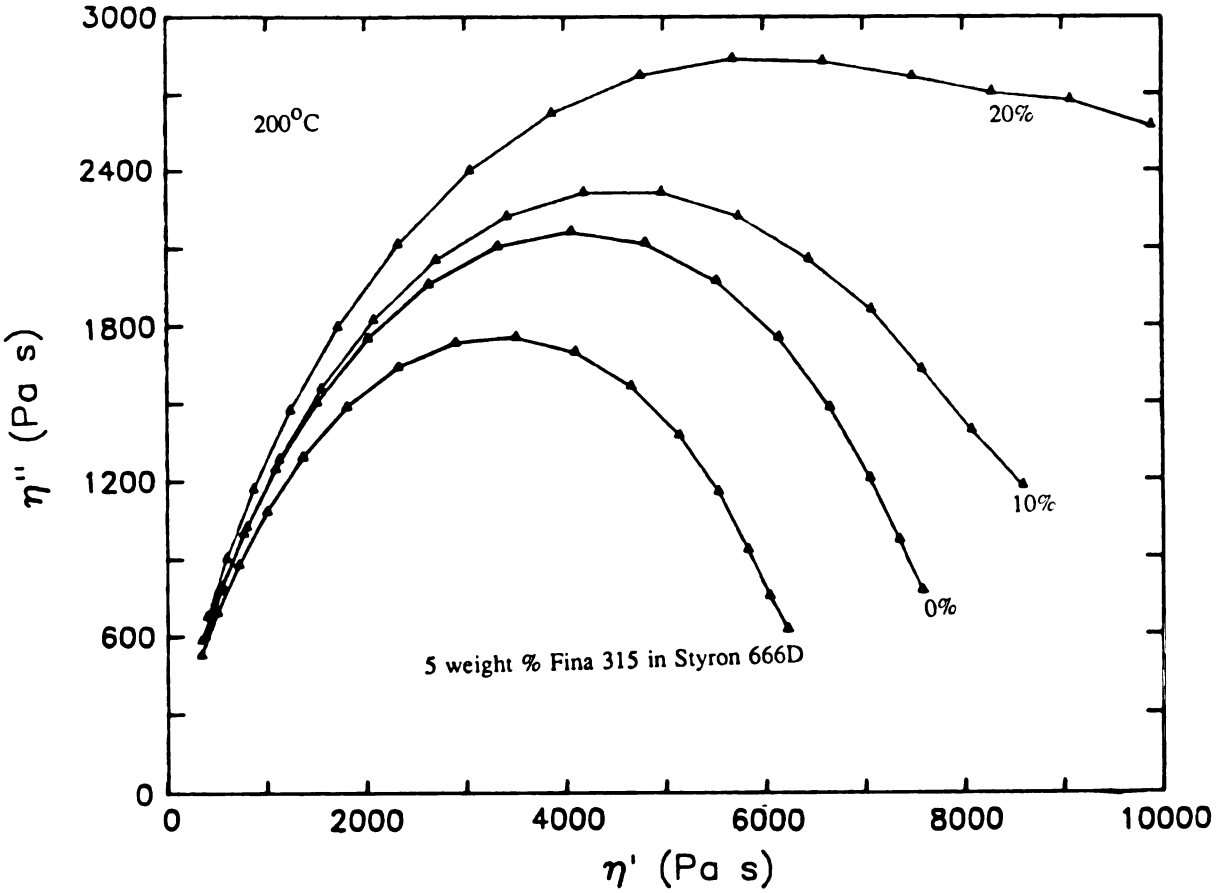

Figure 6.6 Cole-Cole plots for blends of Fina 315 with Styron 666D at 200°C.

Marin et al. (1975) experimentally showed that the average relaxation time for polystyrene samples with a polydispersity of 3.5 is given by

$$\log t_{192} = 6.22 \log M_w - 33.69 \qquad 6.7$$

at 192°C. Using M_w 235,000 for the polystyrene used here, which had a polydispersity of 2.5, in equation 6.7 yields t = .52 seconds. Shifting this value of t to 160°C with $t_{160} = t/a_t$, where the a_t is given by equation 6.9 to yield t_{160} = 10.4 seconds. This is comparable to t_{160} = 14.1 seconds obtained from the 200°C experimental data here.

From the Cole-Cole plots, an angle β can be determined as shown in Figure 6.7. For every blend and polystyrene (including those in Figure 6.1) analyzed here, β was equal to 56°. The angle β is related to the breadth of the relaxation time distribution, where a constant β implies a constant spread of relaxation times. Following is a discussion of the possible reasons for the trends seen in β and the relaxation times presented in Table 6.1.

The result of constant β obtained here implies that addition of up to 20 weight percent diblock to the polystyrene does not change the relaxation time distribution from that seen for the pure polystyrene. This means that although, as seen in Chapter V, 60% of the total diblock in the blend is dissolved in the matrix for the 20% blend, the apparent polydispersity of the matrix polymer does not change. It is interesting that the polystyrene shown in Figure

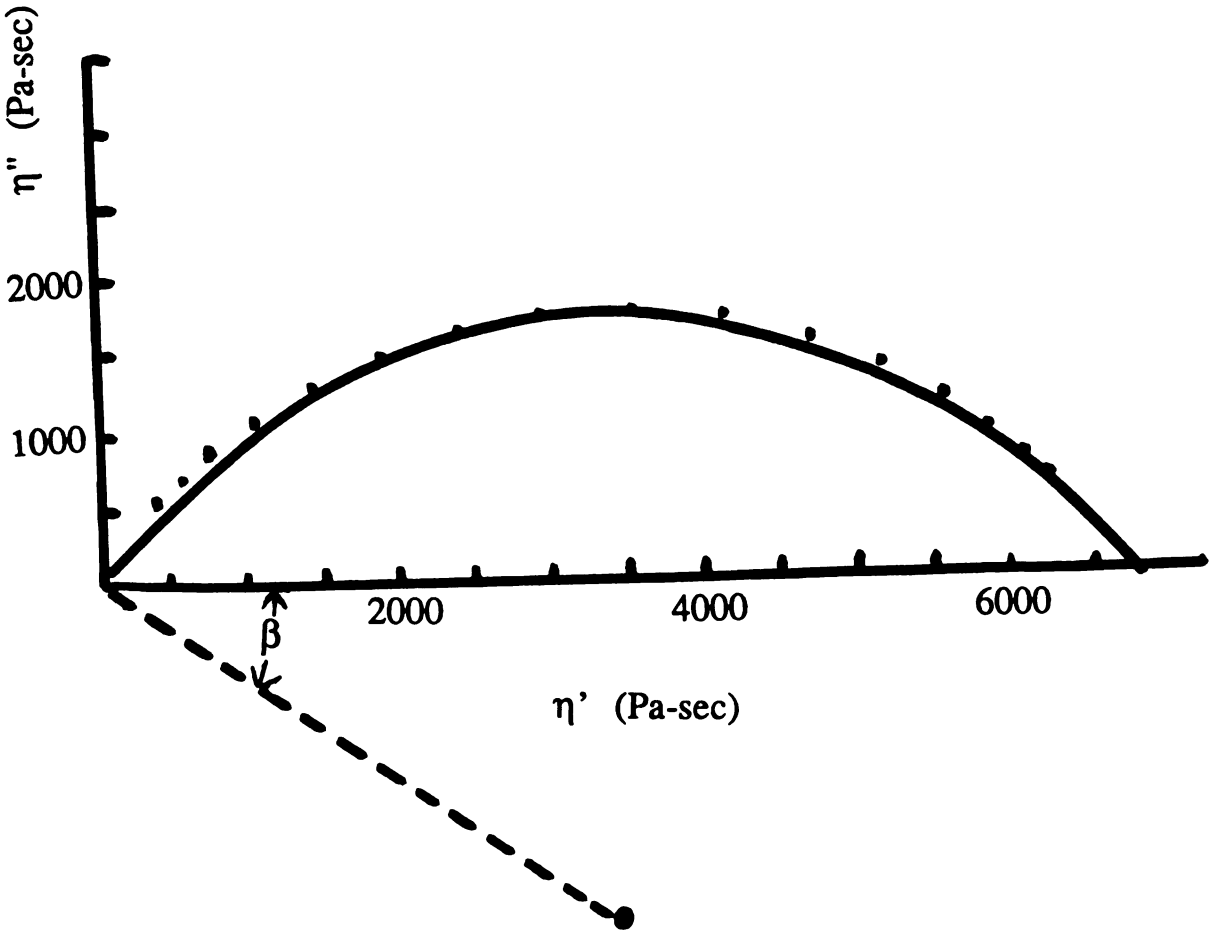

Figure 6.7 Determination of β for blend of 5 weight % Fina 315 with Styron 666D at 200°C.

6.1 which was severely degraded during processing had the same value of β as the unprocessed polystyrene. According to Marin et al. (1975), this would indicate the polydispersity of these two samples was the same. In other words, although processing has decreased the apparent average molecular weight from 235,000 to 56,000 as detailed earlier, the shape of the molecular weight distribution is the same for the two samples.

If one assumes that the slowest relaxation processes for the bulk polystyrene are governed by reptation of the polymer chains through topological constraints as introduced by de Gennes (1971) and analyzed by Doi and Edwards (1978, 1979), then there are two possible explanations for the effect of addition of diblock on the bulk polystyrene seen in Table 6.1. First, the addition of diblock could affect the average reptation time for the matrix polymer, or, second, the effect of addition of diblock on the topological constraints for the matrix polymer chains may be reflected in the results. If one assumes that reptation and relaxation due to tube modification are uncorrelated, then as Monfort et al. (1984) showed,

$$1/t = 1/t_{rep} + 1/t_{mod} \qquad 6.8$$

where t is given in Table 6.1, t_{rep} is the relaxation time due to reptation, and t_{mod} is the relaxation time due to tube modification.

Monfort et al. (1984) showed that $t_{rep}/t_{mod} = 6 \times 10^{-5} M_w^{.9}$ for monodisperse polystyrenes. This ratio probably does not change a great deal for polydisperse polystyrenes and yields $t_{rep}/t_{mod} \sim 4$ for the polystyrene considered here. Since t_{rep} and t_{mod} have the

same order of magnitude for the polystyrene used in this study, it is intuitive that the addition of diblock could affect either t_{rep} or t_{mod} for the matrix polystyrene and hence alter t to produce the trend seen in Table 6.1. Arguments were given earlier which show that the micelle structure for the 5% blend causes the number of entanglements to decrease. This suggests t_{mod} may be changing in the vicinity of micelle corona. As equation 6.8 indicates, this will result in a decrease in t, which was seen experimentally. The increase in t with diblock concentration is probably linked to the long time relaxation process of formation and dissociation of agglomerates of micelles described earlier.

6.4 Rheology as a Potential Probe for Structural Differences

In Chapter V, it was shown that as the temperature of annealing was increased from 130°C to 200°C, the structure of all blends changed from small, well-dispersed micelles to larger agglomerated micelles. Guinlock and Porter (1977) and Widmaier and Mayer (1980) studied the rheology/morphology relationship for SBS block copolymers as a function of temperature and reported that below a critical frequency, linear viscoelastic data may be collapsed into one of two branches when using time-temperature superposition above and below the phase transition temperature. Therefore, time-temperature superposition was employed here to determine if the changes in morphology with temperature for the blends were evident in the master curves.

Figures 6.8 and 6.9 show the master curves of G' and G" at 160°C. To form the master curves shown in Figures 6.8 and 6.9, the shift factors a_t calculated by the WLF equation (Ferry, 1980), defined as

$$\log a_t = -C_1^0(T - T_0)/C_2^0 + T - T_0) \qquad 6.9$$

with $C_1^0 = 5.760$ and $C_2^0 = 109.8$ for $T_0 = 160^0C$, worked equally well for the pure polystyrene homopolymer and the blend. The values of C_i^0 used are those suggested by Ferry (1980) for polystyrene. The a_t's calculated using equation 6.9 had to be altered less than 3% to create the master curves shown in Figures 6.8 and 6.9. The shapes and magnitudes of the G' and G" curves in Figures 6.8 and 6.9 are similar to those published (Onogi et al., 1970; Monfort et al., 1984) for polydisperse polystyrenes of comparable molecular weight (235,000) to the polystyrene homopolymer used here. As can be seen from Figures 6.8 and 6.9, the change in morphology with temperature seen in the present study of AB/A blends did not result in two different branches in the master curve. This implies that either the transition that was seen here with temperature occurred smoothly with temperature, or these rheological measurements were being overwhelmed by the response of styrene and were not sensitive enough to detect the change in morphology that occurred.

Recently, Kim, Han, and Chu (1988) demonstrated that a plot of G' versus G" is very sensitive to the structure of block copolymer-homopolymer blends. Specifically, when a plot of log G' versus log G" ceases to vary with temperature, then the morphological state of

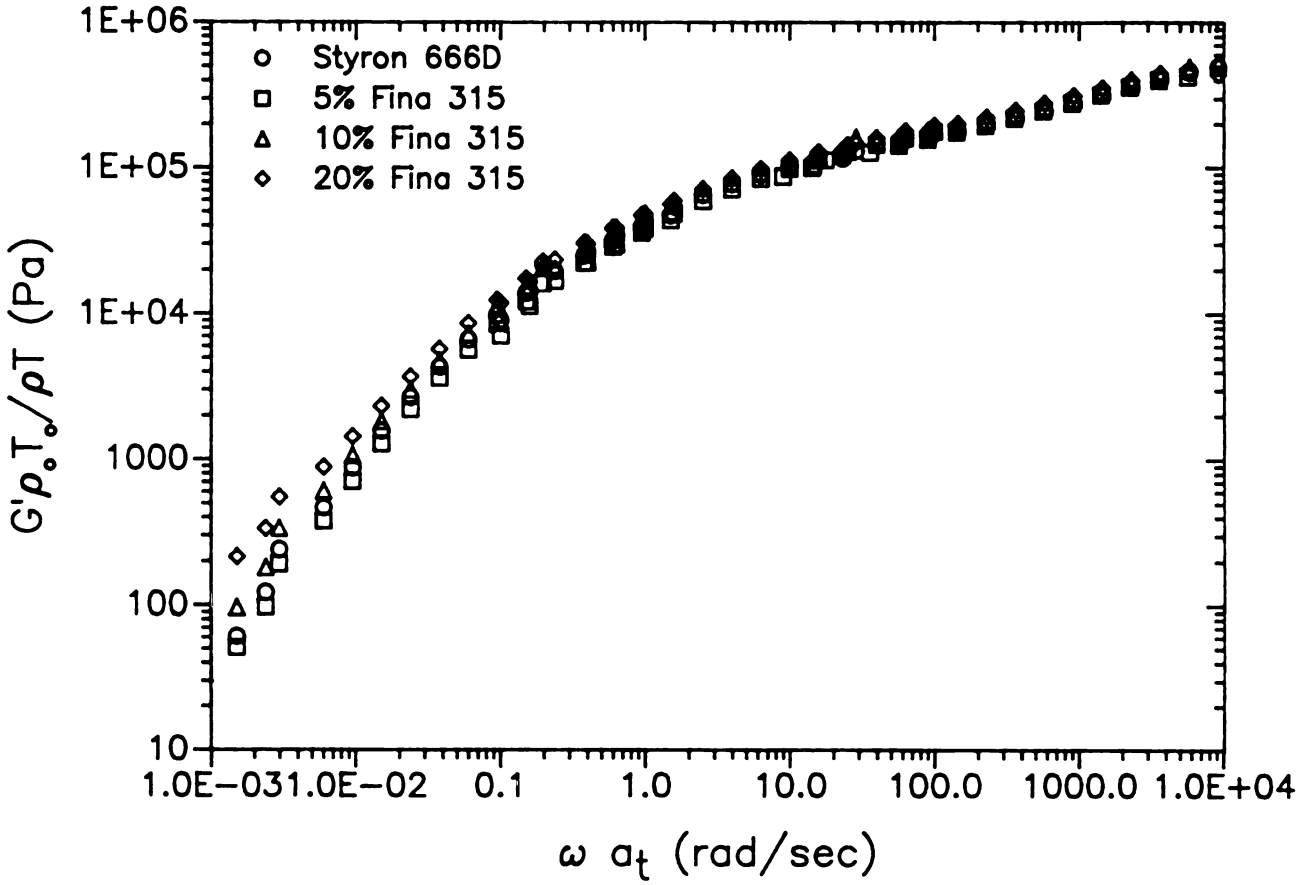

Figure 6.8 Master curves of storage modulus versus angular frequency for blends of Fina 315 with Styron 666D at 160°C.

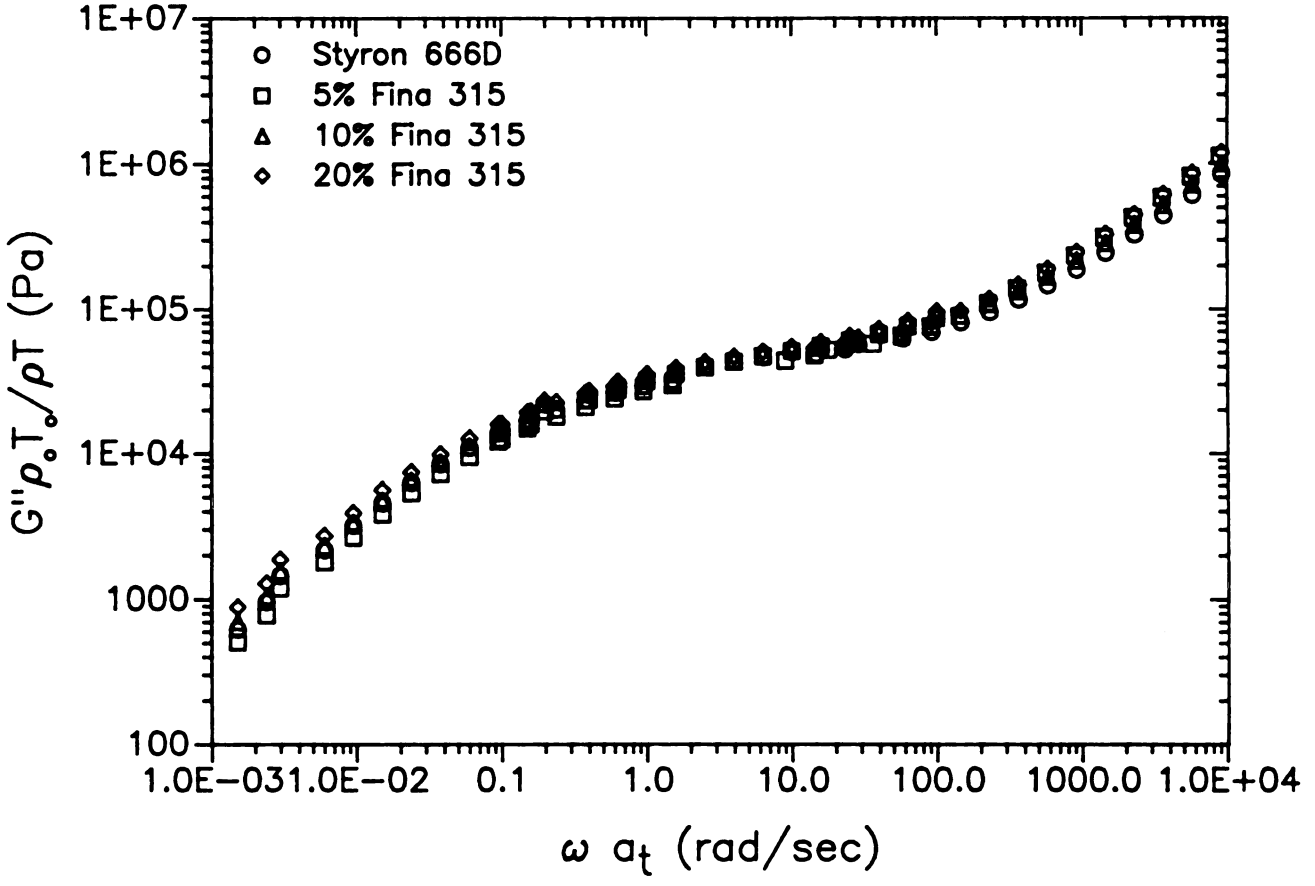

Figure 6.9 Master curves of loss modulus versus angular frequency for blends of Fina 315 with Styron 666D at 160°C.

the polymer is also invariant with temperature. Figure 6.10 shows a plot of G' versus G" for the polystyrene homopolymer and the 20% blend studied here. It can be seen in Figure 6.1 that the polystyrene data superimpose for all temperatures. However, for the 5% blend, the G' versus G" data obtained at 130°C do not superimpose on the data obtained at 160°C and 200°C. This same trend was seen for the 10% and 20% blends. According to Kim et al., this correctly implies that the morphology at 130°C is quite different from the morphology at 200°C. The fact that the 160°C data and 200°C data superimpose suggests the morphology at 160°C must be similar to that at 200°C. It follows that the polymer chain diffusion is sufficient in the one hour annealing period at 160°C to cause the morphology at 160°C to be similar to the morphology at 200°C for all of the blends studied here. To verify this conclusively, micrographs of the 160°C blend would have to be obtained. Finally, it appears that plots of G' versus G" may be more convenient for detecting changes in microstructure of blends similar to those studied here than for plotting data in master curves. More work needs to be done to establish that this is a universal conclusion.

It was of interest here for use in the theory presented in Chapter VII to establish how the rheology changed as the amount of diblock copolymer in micelles increased. The morphology results from the last chapter show that the total amount of diblock copolymer in micelles increased as the annealing temperature increased. This result occurred because copolymer that had dissolved in processing precipitated back into micelles as the blend

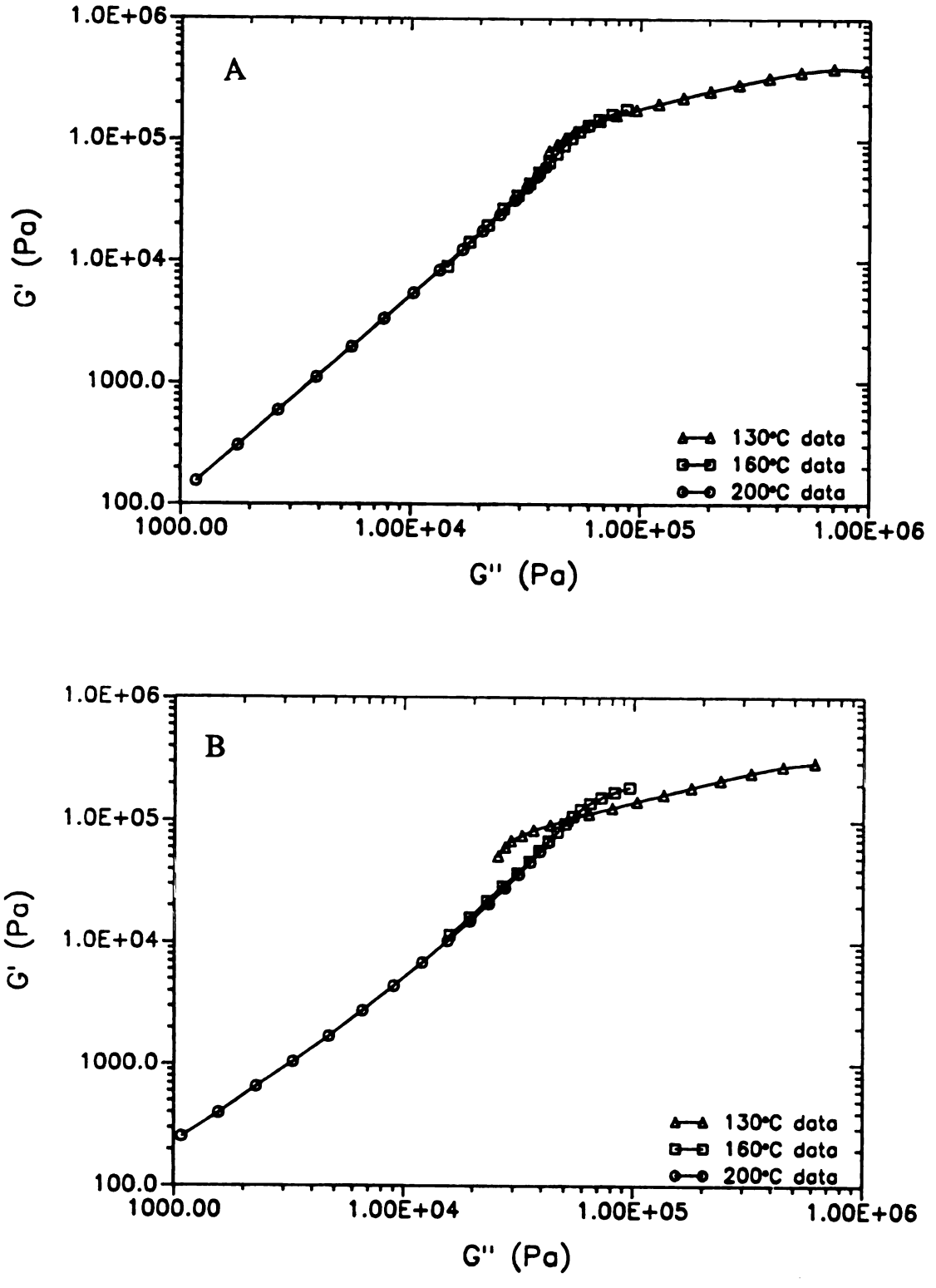

Figure 6.10 Storage modulus versus loss modulus for (A) pure Styron 666D and (B) 20 weight % Fina 315 in Styron 666D.

was annealed in a quiescent environment at a high temperature. Attempts were made here to monitor rheological properties versus time at temperatures between 140°C and 200°C with the hope that the change in rheology with respect to time could be related in some way to the amount of diblock that was precipitating into micelles. In all of these tests, after the desired temperature was achieved the rheology did not change much over a two hour period. Therefore, an alternative approach relating the amount of energy stored during flow to morphology of the blends at equilibrium is presented in the next section.

6.5 Amount of Energy Stored During Flow as a Function of Blend Structure

The theory presented in the next chapter requires a calculation of the added free energy during a steady-deformation process. As detailed by Rangel-Nafaile et al. (1984), for a steady shear process, this free energy is given by

$$\Delta G^S = 1/2 \text{tr } \underline{\underline{\tau}} = N_1/2 \qquad 6.10$$

where $\underline{\underline{\tau}}$ is the deviatoric stress tensor and N_1 is the first normal stress difference. The objective here is to determine G at constant shear stress for a given blend.

In terms of the quantities that are used to describe the micelle system, it seems logical that tr $\underline{\underline{\tau}}$ will depend on the total volume fraction of copolymer in the system ϕ and on the volume fraction of this copolymer which is in micelles ζ. The problem, then, was to determine N_1 as a function of ϕ and ζ. For pure

polystyrene, N_1 is easily obtained from steady shear measurements. However, it has been established in the last chapter that stress changes the structure of the blends studied here, so N_1 as a function of ϕ and ζ cannot be unambiguously determined from steady shear tests. The alternative was to determine ΔG^s for the blends from dynamic mechanical tests which do not alter the structure of the blends during testing. Rangel-Nafaile et al. (1984) showed that N_1 is related to dynamic mechanical properties by

$$N_1 = 2J_e^o \sigma^2 \qquad 6.11$$

where J_e^o is the steady-state creep compliance and σ is shear stress. From Ferry (1980), J_e^o can be calculated from

$$J_e^o = (1/n_o^2) \lim_{\omega \to o} G'/\omega^2 \qquad 6.12$$

Equation 6.12 may be used when sufficiently low frequencies are accessible where $G' \alpha \omega^2$. Figure 6.5 shows log G' versus log ω at the lowest frequency used (.1 rad/sec) does not have a slope of 2 for any of the blends studied here, so an alternative to equation 6.11 was found.

By definition (Ferry, 1980), G' is a measure of the amount of energy stored and recovered per cycle, when different systems are compared at the same strain amplitude during dynamic mechanical tests. By the same token, G" is a measure of the energy lost due to viscous dissipation. Therefore, tan δ = G"/G' is the ratio of the

energy lost to the energy stored during a cycle. The complex modulus G* is given by the following expressions

$$G^* = \sqrt{G'^2 + G''^2} = \sigma_0/\gamma_0 \qquad 6.13$$

where σ_0 is the stress amplitude and γ_0 is the strain amplitude. At a constant G*, with σ_0 constant, the stress amplitude is also constant. The logic used here, then, is at a constant G*, cot δ = 1/tan δ is a relative measure of ΔG^S at a shear stress of $\sigma_0 = G^* \gamma_0$. For a given blend with constant G*, as cot δ increases the amount of energy stored by the blend increases.

With the above assumptions, a first approximation for the dependence of tr $\underline{\underline{I}}$ on structure is given by

$$N_{1,blend} = N_{1,PS} (1 + b_1 \phi\zeta) \qquad 6.14$$

where $N_{1,PS}$ is the first normal stress difference for pure polystyrene. The constant b_1 is estimated by using the morphological results from the last chapter and a plot of tan versus G* (Figure 6.11) as follows. If one assumes that the domains seen in the micrographs for the blends annealed at 200°C consist entirely of butadiene, then Table 6.2 results.

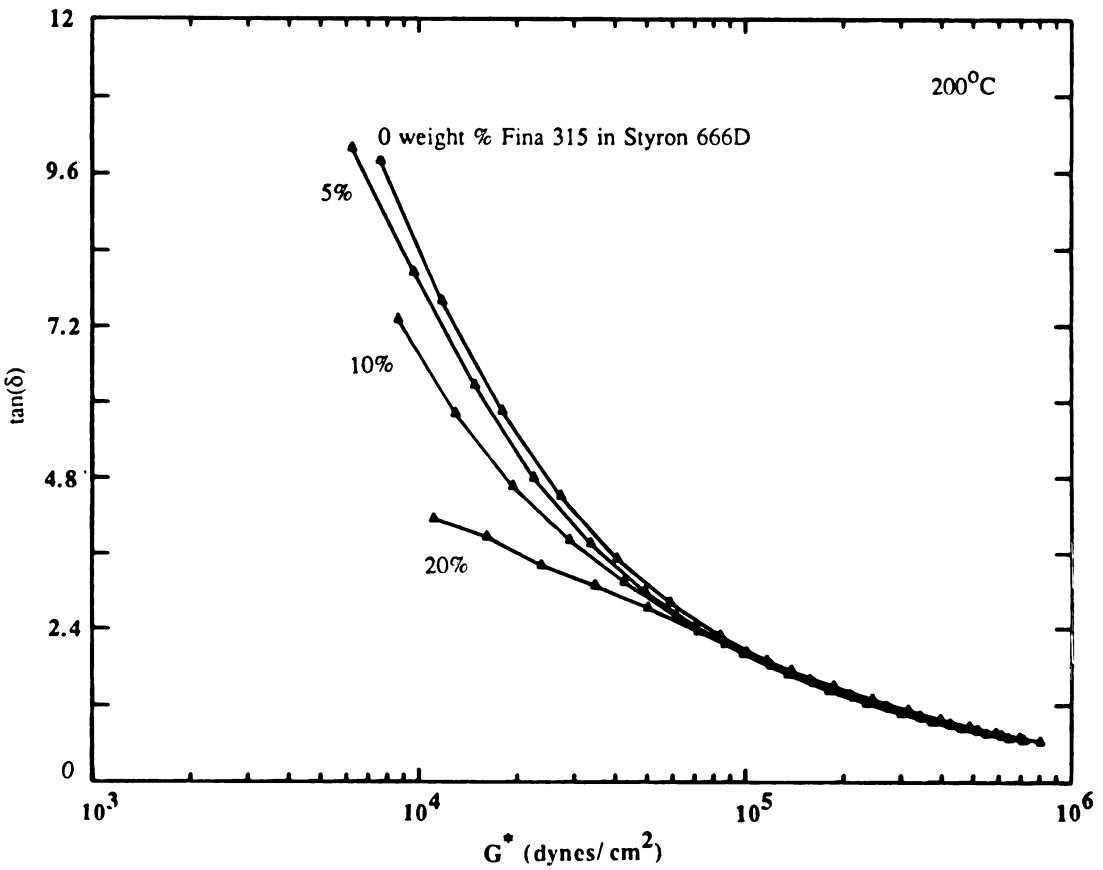

Figure 6.11 Tan(δ) versus complex modulus for blends of Fina 315 with Styron 666D at 200°C.

Table 6.2.--Degree of micellization and volume fraction of diblock for blends at 200°C.

Blend	ϕ	ζ	$\phi\zeta$[a]
5%	.053	1.00	.053
10%	.106	.59	.059
20%	.211	.38	.076

[a] $\phi\zeta$ is volume fraction diblock copolymer participating in micelles.

From the plots of tan versus G* in Figure 6.11, the relative change in N_1 with concentration of diblock can be determined from

$$N_{1,blend} = N_{1,PS} \tan\delta_{PS}/\tan\delta_{blend} \qquad 6.15$$

As an example, consider the case when G* = 10^4 dynes/cm^2. Figure 6.13 shows a plot of $N_{1,blend}/N_{1,PS}$ versus $\phi\zeta$ for G* = 10^4 dynes/cm^2 and T = 200°C. For low $\phi\zeta$ it appears that N_1 is linear with $\phi\zeta$. No data were obtained for $\phi\zeta$ between 0 and .05, but it seems unlikely that N_1 for blends with low diblock content is going to vary much from a linear relation because at $\phi\zeta$ = .05 the first normal stress difference is already close to that of pure polystyrene. For higher values of $\phi\zeta$, a quadratic relation between N_1 and $\phi\zeta$ is more appropriate.

The values of $N_{1,PS}$ for use in equation 6.14 were correlated with the shear stress according to a relation used by Han and Jhon (1986)

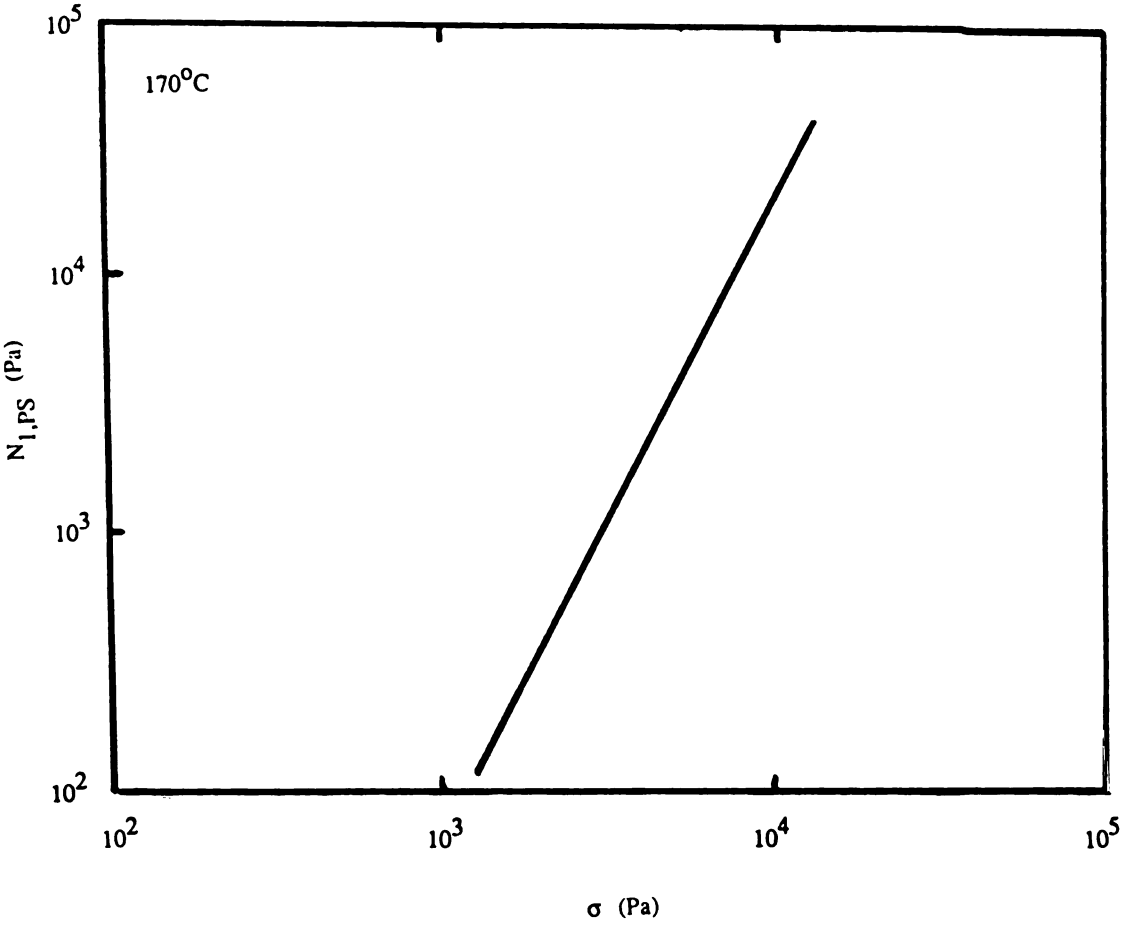

Figure 6.12 First normal stress difference versus shear stress for Styron 666D at 170°C.

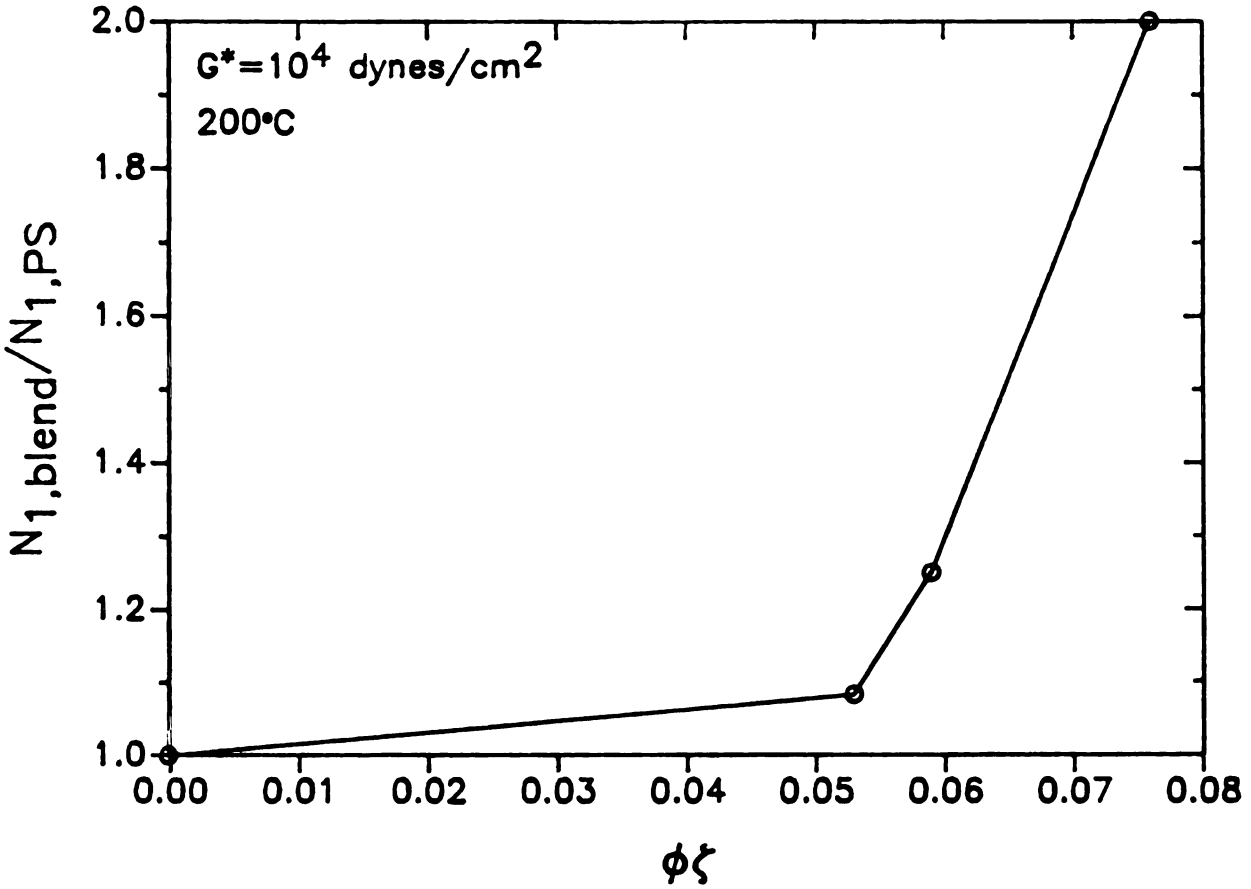

Figure 6.13 $N_{1,blend}/N_{1,PS}$ versus volume fraction of total diblock participating in micelles for $G^* = 10^4$ dynes/cm^2 and T=200°C.

$$N_1 = a_N(\sigma)^{b_N} \qquad 6.16$$

where a_N and b_N depend on molecular weight and molecular weight distribution. As Figure 6.12 shows, the empirical relation of equation 6.12 holds for the polystyrene homopolymer used here with $a_N = 5.218 \times 10^{-8}$, $b_N = 2.522$, and stress has units of dynes/cm^2. Equation 6.16 can be used to calculate $N_{1,PS}$ at constant stress for use in equation 6.14.

6.6 Summary of Results

It was shown here that melt mixed blends can be formed in which the effect of degradation during processing on rheology can be eliminated. It was found that G', G", and an average relaxation time for the blends went through a minimum with diblock concentration at a diblock concentration of $\phi \sim .05$. It is suggested that the reason for the initial decrease in G', G", and the relaxation time is due to the micelle structure for the 5% blend causing the distance between entanglements for the matrix polymer to increase. The subsequent increase in these G' etc. is attributed to the formation and dissociation of micelle agglomerates. It was found that a plot of G' versus G" seems to be more sensitive to changes in morphology with temperature, seen in Chapter V, than master curves are, which have been used in the past to detect this change. Finally, an expression was developed that related the energy stored by the blends in a stationary shear flow to the equilibrium structure of the blends at 200^{o}C.

CHAPTER VII

THEORY FOR THE EFFECT OF CILIA-MATRIX INTERACTIONS AND EFFECT OF FLOW ON MICELLE FORMATION IN AN AB/A BLEND

7.1 Introduction

In this chapter, the theory of micelle formation in blends of excess A homopolymer with AB diblock presented by Leibler, Orland, and Wheeler (LOW) (1983) is modified to account for the effect of unfavorable interaction between the A homopolymer and the A-block of the copolymer when the homopolymer has equal or larger molecular weight than the A-block. Another theoretical consideration here is an analysis of the effect of energy stored by the blend during a stationary shear flow on micelle formation. The theory of LOW is also modified, by a procedure similar to that used to Roe (L986) and Mayes and de la Cruz (1988), to allow the homopolymer and the blocks of the diblock to have arbitrary degrees of polymerization.

There have been some experimental studies (Selb et al., 1983; Rigby & Roe, 1986; Kinning & Thomas, 1988) that looked at equilibrium micelle structures in solution cast AB/A blends. Nevertheless, in industry it is more common to prepare blends by high temperature nonequilibrium melt mixing rather than by low temperature solution casting. A number of results for micelle structure obtained with melt mixed styrene-butadiene diblock/styrene

homopolymer blends in Chapter V were motivation for the theory developed here. First, evidence is presented in Chapter V that an equilibrium structure can be achieved at high temperatures for an AB/A blend when the A homopolymer has a larger molecular weight than the A-block of the copolymer. Several experimental studies (e.g., Inoue et al., 1970; Eastmond & Phillips, 1979; Berney, Cheng, & Cohen, 1988) have suggested that when such a ratio of molecular weights exists, unfavorable interactions between the A homopolymer and A-block hinders the two polymers from mixing freely at equilibrium. Therefore, an interaction parameter χ_{AH} for the A homopolymer and A-block is included in the theory developed here. A second experimental result noted in Chapter V and by Selb et al. (1983) is a decrease in the size of the micelle core with increase in diblock copolymer concentration. A third experimental result found in Chapter V was that the degree of micellization as well as the size of the micelle core decreased when the blend was processed under high shear. As an attempt to explain these results, a semi-empirical expression for the effect of energy stored during flow was developed here. It should be briefly noted here that a final experimental result obtained in Chapter V is that at equilibrium and under processing conditions the degree of micellization decreased with increase in diblock content. Also, the tendency for micelles to agglomerate decreased during processing. These final experimental aspects are not currently predicted by existing theories and are not predicted by the theory developed here.

Since the introduction of the theory of LOW (1983), there have been many enhancements to the theory of LOW (Leibler & Pincus, 1984; Roe, 1986; ten Brinke & Hadziioannou, 1987; Mayes & de la Cruz) and an alternative theoretical development (Whitmore & Noolandi, 1985) which have greatly increased the theoretical understanding of micelle formation in block copolymer-homopolymer blends. This theory has been extended to account for homopolymer and blocks of the diblock copolymer with different degrees of polymerization (Whitmore & Noolandi, 1985; Roe, 1986; Mayes & de la Cruz, 1988), swelling of the micelle core by matrix homopolymer (Whitmore & Noolandi, 1985; Roe, 1986), the effect of micelle-micelle interactions (Leibler & Pincus, 1984), and the different packing of chains between cylindrical and spherical micelles (Mayes & de la Cruz (1988). There is fairly good quantitative agreement between the predictions of the above theories and experimental results for micelle radii as a function of blend molecular characteristics, but the theories fail to predict such experimental trends as decrease in micelle core size with increase in diblock concentration (Selb et al., 1983) and swelling of micelle cores with temperature (Rigby & Roe, 1986). Since Roe (1986) and Whitmore and Noolandi (1985) have both developed theories of micelle formation that allow matrix polymer to swell the core of the micelle and have shown that these theories predict that virtually no homopolymer swells the core, this phenomenon is not included in the theory presented here.

It is the objective of this chapter to show that straightforward modifications of the theory of LOW to account for the effect of interactions between matrix A homopolymer and A-blocks in the corona of the micelles and inclusion of elastic normal stresses as an addition to free energy can explain many of the experimental observations described in Chapter V.

7.2 Theoretical Model With Interaction Between the A Homopolymer and A-Block

The physical picture of the micelle structure considered here is shown in Figure 7.1, where the core (region 1) has radius R_B and contains B-block monomers, the corona has a thickness of $R_A = R - R_B$ and contains A-block monomers and A homopolymer monomers, and the matrix contains A homopolymer and dissolved AB diblock monomers. Let p equal the number of diblock copolymers in a micelle and η equal the fraction of A-block monomers in the corona; then assuming incompressibility conditions exist, the following volume balances hold:

$$4/3\pi R_B^3 = pN_Ba^3 \qquad 7.1$$

$$4/3\pi (R^3 - R_B^3)\,\eta = pN_Aa^3 \qquad 7.2$$

where N is the number of segments and a is the length of a segment in the blocks.

The free energy of formation of a single micelle is given by

$$F = 4\pi R_B^2\,\gamma + F_d + F_{mA} + F_j \qquad 7.3$$

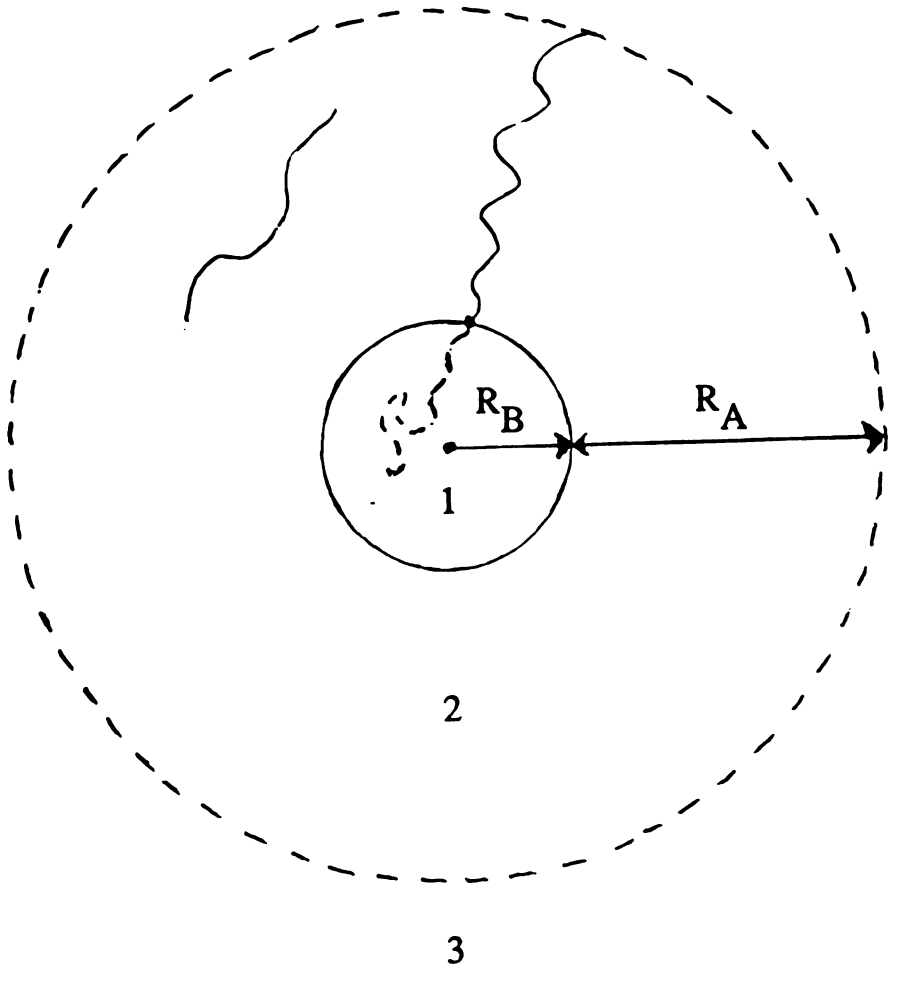

Figure 7.1 Schematic of a spherical micelle in an AB diblock/A homopolymer blend. Region 1 is the core and contains B-blocks. Region 2 is the corona and is composed of A-block mixed with A homopolymer. Region 3 is the matrix and consists of A homopolymer mixed with AB diblock copolymer.

where the first term on the right hand side of equation 7.4 is the interfacial energy and γ is the interfacial tension given by LOW as

$$\gamma = (kT/a^2)(\chi_{AB}/6)^{1/2} \qquad 7.4$$

The free energy of deformation F_d, the free energy of mixing F_{mA}, and the joint localization energy F_j in equation 7.3 are considered separately below.

F_d in equation 7.3 is the free energy due to deformation of diblock copolymer chains and is given by

$$F_d = \frac{3}{2} kTp \left[\frac{R_A^2}{r_A^2} + \frac{r_A^2}{R_A^2} + \frac{R_B^2}{r_B^2} + \frac{r_B^2}{R_B^2} - 4\right] \qquad 7.5$$

In equation 7.5, r_A and r_B are taken to be the unperturbed end-to-end distance of the A-block and B-block chains of the diblock, and F_d is then the energy due to deformation of these chains away from these dimensions during domain formation. The values of r used here are calculated from

$$r^2 = N\, a^2 \qquad 7.6$$

where a is taken to be an average Kuhn statistical length. During the derivation of their theory, LOW employed the concept of the monomer units of the homopolymer and both blocks of the diblock copolymer having a length of a. In general, this is not a good assumption because the chemically different B polymer will have a different length than the A polymer. Also, Roe (1986) made the

valid point that there is no theoretical basis for choosing a to be equivalent to the monomer length, and when a theory includes a consideration of interfacial effects, the numerical results obtained depend on the definition of a. Nevertheless, the theory developed here will use the assumption that a is equal to an average Kuhn statistical length, because this allows a verification of the numerical calculations here with the data presented by LOW while also giving theoretical results that can be checked against the experimental results presented in Chapter V. The assumption of constant a is reasonable for styrene/butadiene blends because the Kuhn statistical lengths for polystyrene and polybutadiene are .71 nm and .68 nm, respectively. In this work, the values of N_H, N_A, and N_B, determined from equation 7.6, are the number of statistical segments for the homopolymer, A-block, and B-block chains, respectively. It turns out that the N_i are close to the degree of polymerization for the styrene-butadiene systems considered here. With the above definition of N_H, N_A, and N_B, the number of statistical segments of the diblock is given by $N = N_A + N_B$, α is defined as $\alpha = N/N_H$, and $f_A = N_A/N$ is the fraction A polymer in the diblock. It should be reiterated here that contrary to LOW and Mayes and de la Cruz (1988), the case of $\alpha < 1/f_A$ has been examined by Whitmore and Noolandi (1985) without the modifications to the theory given here.

F_{mA} in equation 7.3 is the free energy of mixing the A homopolymer monomers and the A-block monomers in the corona and is given from the Flory-Huggins expression for free energy of mixing as

$$F_{mA} = \frac{4\pi}{3a^3}(R^3 - R_B^3)\, kT \left[\frac{\eta}{N_A} \ln \eta + \frac{1-\eta}{N_H} \ln (1-\eta)\, \chi_{AH}\, \eta(1-\eta)\right] \qquad 7.7$$

Although LOW have neglected the first term on the right hand side of equation 7.7, the whole free energy expression must be kept when considering the localization of the A-B joint at the interface as described by Mayes and de la Cruz (1988). It is interesting to note that the first term on the right hand side of equation 7.7 can cause a significant contribution to the free energy as N_H increases relative to N_A. χ_{AH} in the last term of equation 7.7 constitutes an interaction function into which all deviations from purely combinatorial behavior are incorporated (see Prausnitz, 1969, for example). Usually χ_{AH} is taken to be zero for mixing of chemically identical species, such as the A-block and A homopolymer, but as mentioned earlier, there is much experimental evidence that the A-block and A homopolymer molecules do not mix freely when $\alpha < 1/f_A$. Therefore, it is assumed here that χ_{AH} is unequal to zero when $\alpha < 1/f_A$. It has been hypothesized by Eastmond and Phillips (1979) that the incompatibility between A-block and matrix homopolymer when $\alpha < 1/f_A$ arises from an unfavorable entropy of mixing as a result of the A-blocks which are tethered to an impenetrable interface adopting different sets of conformations than randomly coiled chains in bulk polymer. Meier (1969) calculated the chain statistics for block molecules in pure block copolymers which are constrained to remain in their respective phases. Meier found it necessary to use the diffusion equation, rather than a lattice-type model from which

equation 7.7 arises, to develop his theory, and an extension of Meier's work to analyze mixing in the corona may reveal exactly how the conformations of the tethered A-block act to exclude homopolymer from the corona. Nevertheless, the assumption is made here that the deviations from ideal mixing due to conformation effects can be incorporated into χ_{AH}, and appropriate values of χ_{AH} are determined by comparing theoretical calculations to experimental results.

F_j in equation 7.3 is the joint localization energy which arises from the decrease in entropy associated with fixing the A-B joint of the diblock copolymer at the interface between the micelle core and corona. The expression for this energy is given by Mayes and de la Cruz (1988) as

$$F_j = kTp \ln \left[\frac{R^3 - R_B^3}{3R_B^2 a}\right] \qquad 7.8$$

LOW neglected F_j in their development on the grounds that it gave a negligible contribution to the free energy of the micelle. In the calculations here it was found that F_j can have a noticeable effect on the numerical results, so after neglecting F_j to check the results of the calculation here with those of LOW, F_j was kept in all other calculations done here.

The above equations can be combined to yield

$$F/kT = pf = A_1 \chi_{AB}^{1/2} p^{2/3} N_B^{2/3} + A_2 (1+C) p^{5/3}/N_B^{1/3} + A_3 p^{1/3} N_B^{1/3} (1+\frac{1}{C})$$

$$+ p \frac{N_A}{\eta} [\frac{1-\eta}{N_H} \ln(1-\eta) + \frac{\eta}{N_A} \ln[\frac{A_4 p^{1/3} N_A}{N_B^{2/3}}] + \eta(1-\eta) \chi_{AH} \qquad 7.9$$

where $A_1 = 6^{1/6}\pi^{1/3}$, $A_2 = 3^{5/3}/2^{7/3}\pi^{2/3}$, $A_3 = 6^{1/3}\pi^{2/3}$, $A_4 = \frac{1}{(4\pi)^{1/3}3^{2/3}}$,

and $C = \frac{N_B}{N_A} [(\frac{N_A}{N_B \eta} + 1)^{1/3} - 1]^2$ 7.10

where kTf is the free energy per copolymer chain in a single micelle. Defining Ω as the number of monomers in the system, ϕ as the fraction of AB diblock copolymer, and ζ as the fraction of diblock that participates in micelles, then the total free energy due to formation of micelles is equal to $(\Omega\phi\zeta/N)kTf$.

The total free energy of the system F_M can now be written as

$$F_M = \frac{\Omega\phi\zeta}{N} kTf + F_{mix,bulk} - T S_m \qquad 7.11$$

In equation 7.11, $F_{mix,bulk}$, the free energy of mixing A homopolymer monomers and AB diblock copolymer monomers in the bulk, is given by

$$F_{mix,bulk} = \Omega kT (1 - \xi\phi\zeta) [\frac{\phi_1}{N} \ln \phi_1 + \frac{1-\phi_1}{N_A} \ln (1 - \phi_1) + \qquad 7.12$$

$$\frac{N_B}{N} \chi_{AB} \phi_1 (1 - \frac{N_B}{N} \phi_1)]$$

where the interaction between A and B monomers is taken to dominate over other interactions. S_m, the translational entropy of the micelles, is given by

$$S_m = - \Omega k \left[\frac{\phi\zeta}{pN} \ln (\xi\phi\zeta) + \frac{1-\xi\phi\zeta}{\xi pN} \ln (1-\xi\phi\zeta)\right] \qquad 7.13$$

where

$$\xi = \frac{1}{N} \left[\frac{N_A}{\eta} + N_B\right] \qquad 7.14$$

is the ratio of micelle volume including the corona to the volume occupied by block copolymer alone, and

$$\phi_1 = \frac{\phi (1 - \zeta)}{1 - \xi\phi\zeta} \qquad 7.15$$

is the volume fraction of diblock molecules in the matrix.

To determine the equilibrium values of the parameters p, η, and ϕ_1, a FORTRAN program, incorporating the IMSL minimization subroutine DCONG, was used to minimize the total free energy (equation 7.13). The results of the calculations are tabulated in Appendix A.

7.3 Predictions of Theory With χ_{AH} Included

The numerical procedure used here to evaluate equation 7.11 gave results that were in exact agreement with those presented by Leibler et al. (1983) (LOW), as can be seen in Figure 7.2. Figure 7.2 also demonstrates that introducing the joint localization energy of equation 7.8 and comparing to the results of Mayes and de la Cruz

	LOW	Mayes and de la Cruz
p	78	68
η	0.195	0.182

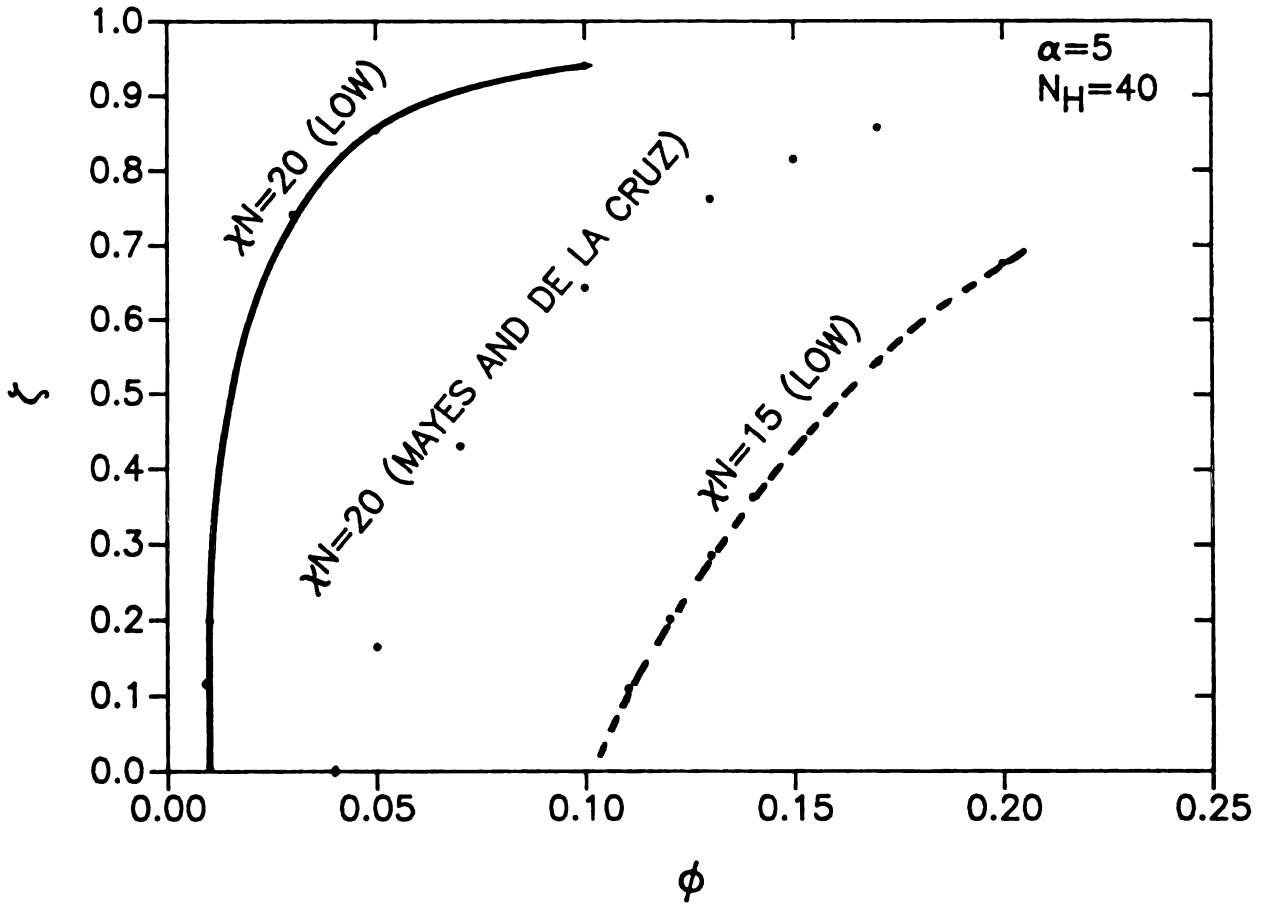

Figure 7.2 Comparison of numerical calculations to data of Leibler, Orland, and Wheeler (LOW) (1983) and Mayes and de la Cruz (1988). The curves represent literature data and the points were calculated. The criticial micelle concentration (ϕ at ζ=0) obtained using the theory of Mayes and de la Cruz is similar to the value reported by these authors.

(1988) yielded critical micelle concentrations that were in close agreement. A noteworthy result of introducing the joint localization energy is that it causes the degree of micellization ζ, the number of chains in a micelle p, and the volume fraction of A-block in the corona η, to decrease when compared to the prediction of LOW. This is contrary to the statement of LOW that the effect of joint localization is negligible.

Before considering the prediction of the theory with the modification of equation 7.7, a discussion of the case considered here is in order. In all of the plots shown here, the case of N_A = 966, N_B = 684, and N_H = 2383 is considered because these values apply to the blends studied experimentally in Chapter V. The values of N were determined by using equation 7.6 with $r = .7(M_w)^{.5}$ for polystyrene, $r = .9(M_w)^{.5}$ for polybutadiene (Roe, 1986), and an average Kuhn statistical length of .695 nm. It was found in Chapter V that the expression used to determine r for the butadiene block may actually yield an r that is too high, but for the purpose of the calculations here, the expression proposed by Roe is adequate. In this work, the effect of χ_{AH} and energy stored by the blend during a stationary flow on p, η, and ζ are of most interest, and it turns out that the observed trends with the single blend considered here were also seen in numerous calculations with other values of N_A, N_B, and N_H, so just one set of N_i's was used here.

Selection of unambiguous value of χ_{AB} for use in the theoretical calculations, to yield a direct comparison to experimental results, was not possible. Roe and Zin (1980) studied

mixtures of polybutadiene and polystyrene and arrived at the equation

$$\chi_{AB} = 73/T - .0835 \qquad 7.16$$

from the average of results for a number of mixtures. Equation 7.16 yields a result of $\chi_{AB} = .071$ at the experiment temperature of 200°C. This χ_{AB} yields $\chi_{AB}N = 116$ for the blends considered here, or in other words, equation 7.16 predicts a very high degree of incompatibility between polystyrene and polybutadiene for the blend considered here at experimental conditions. Roe and Zin (1984) demonstrated that for mixtures of styrene/butadiene diblock copolymers and styrene or butadiene homopolymers, χ_{AB} is actually much lower than that given by equation 7.16. The fact that Rigby and Roe (1986) calculated a critical micelle concentration much smaller than seen experimentally, when using equation 7.16, also suggests equation 7.16 overpredicts χ_{AB}. The experimental results in Chapter V also indicate the ability to solubilize diblock in the matrix to a much greater degree than a value of $\chi_{AB}N = 116$ would suggest. Hence, another lower value for χ_{AB} of .015 has been considered in addition to the value of .071 in simulations here. The corresponding values of $\chi_{AB}N$ are 28.5 and 115, respectively.

Figure 7.3 shows that as χ_{AH} increases, the fraction of A-block η making up the corona also increases. This is in line with the hypothesis that was used to introduce χ_{AH}, namely, as the entropy for mixing of the A-block and homopolymer becomes unfavorable due to

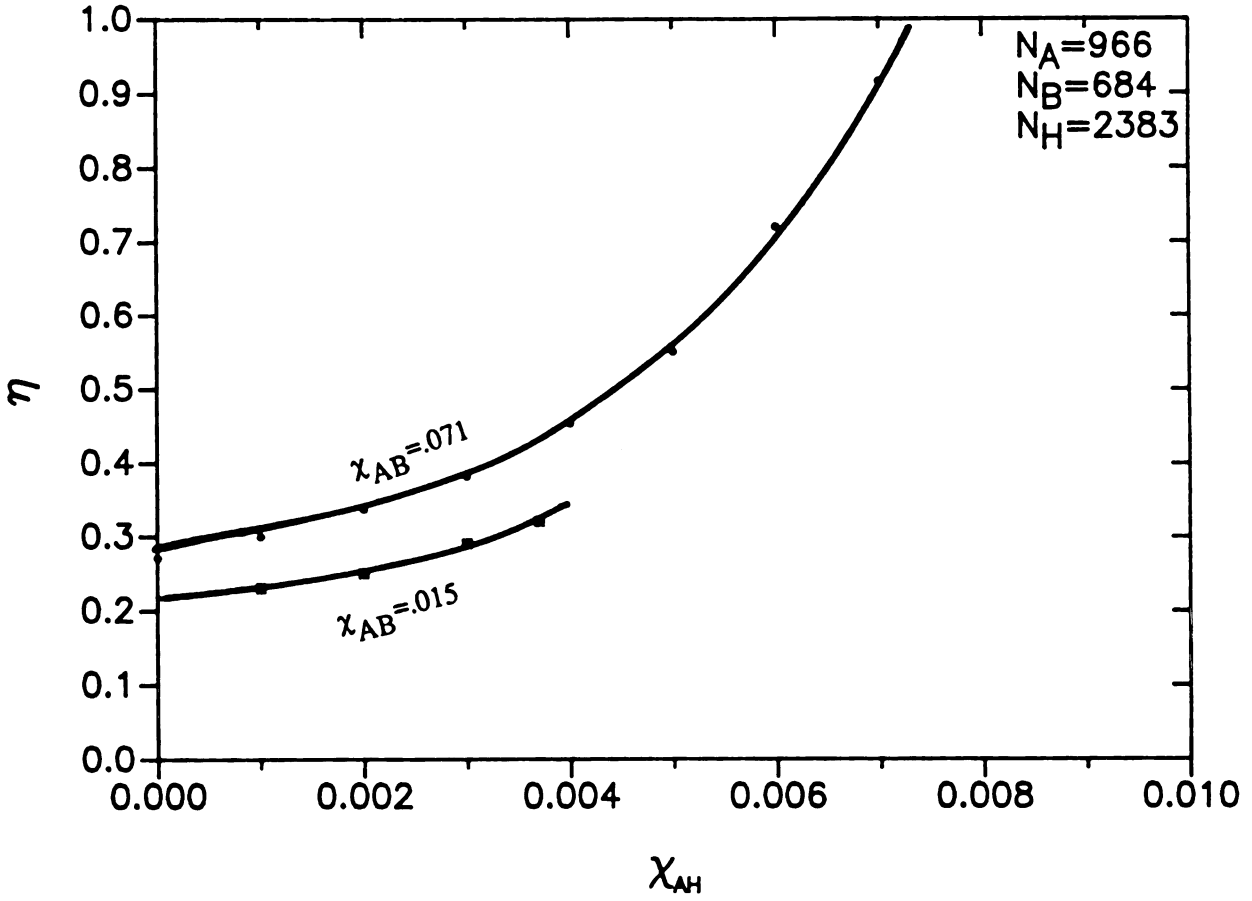

Figure 7.3 Fraction of A-block in micelle corona versus degree of incompatibility between A-block and A homopolymer molecules.

the conformation difference of the two polymers, the effect is to exclude matrix homopolymer from the corona. The curves for χ_{AB} = .015 and χ_{AB} = .071 in Figure 7.3 put limits on the possible values of χ_{AH}. The curve for χ_{AB} = .015 stops at a value of χ_{AH} = .0037 because the degree of micellization is zero above this value of χ_{AH} (see Figure 7.5). The curve for χ_{AB} = .071 shows that at χ_{AH} = .007 the value of n is approximately one. We see that as χ_{AB} decreases, the ratio of $\max(\chi_{AH})/\chi_{AB}$ increases, but the effect of possible values of χ_{AH} on n is also very limited. In other words, the theory predicts the physically intuitive result that as compatibility between A polymer and B polymer increases, the effect of incompatibility between A-block and matrix homopolymer becomes less significant.

Figure 7.4 demonstrates that as χ_{AH} is increased, the number of diblock molecules participating in micelles p is also increased. This result in conjunction with equation 7.1 implies that the radius of the micelle core R_B also increases, as shown in Figure 7.5. Figure 7.5 also shows that the radius of the corona R_A decreases accordingly as the micelle core radius increases, which keeps the overall size of the micelle $R = R_A = R_B$ constant. The trends seen in Figure 7.4 and 7.5 can be understood by examining the three effects that compete to determine the size of the micelle as described by LOW. The first effect is to decrease the interfacial tension which favors a large interfacial area. An increase in interfacial area occurs when the size of the micelle core radius increases, and therefore, as equation 7.1 shows, this effect favors

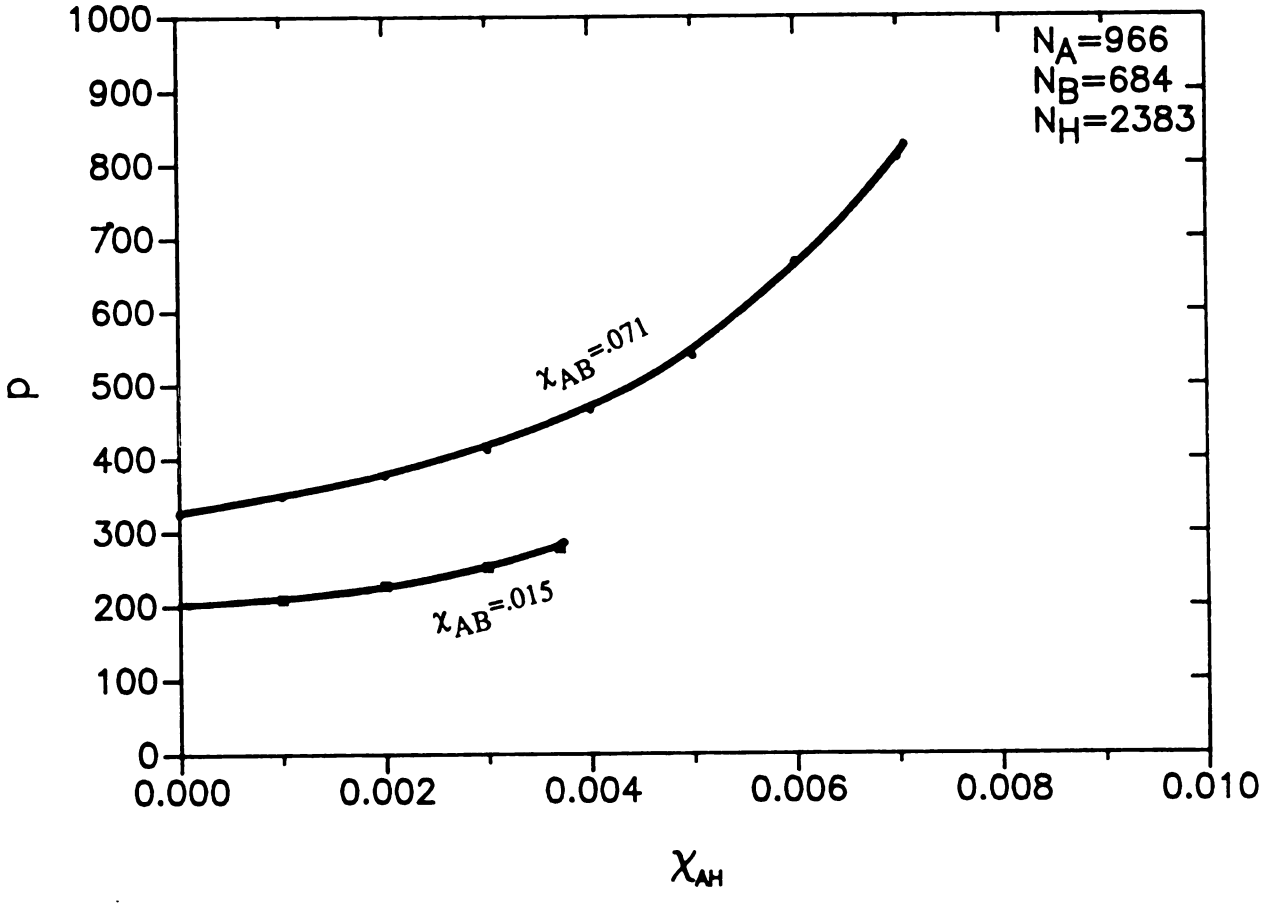

Figure 7.4 Number of AB diblock copolymer molecules in a single micelle versus degree of incompatibility between A-block and A homopolymer molecules.

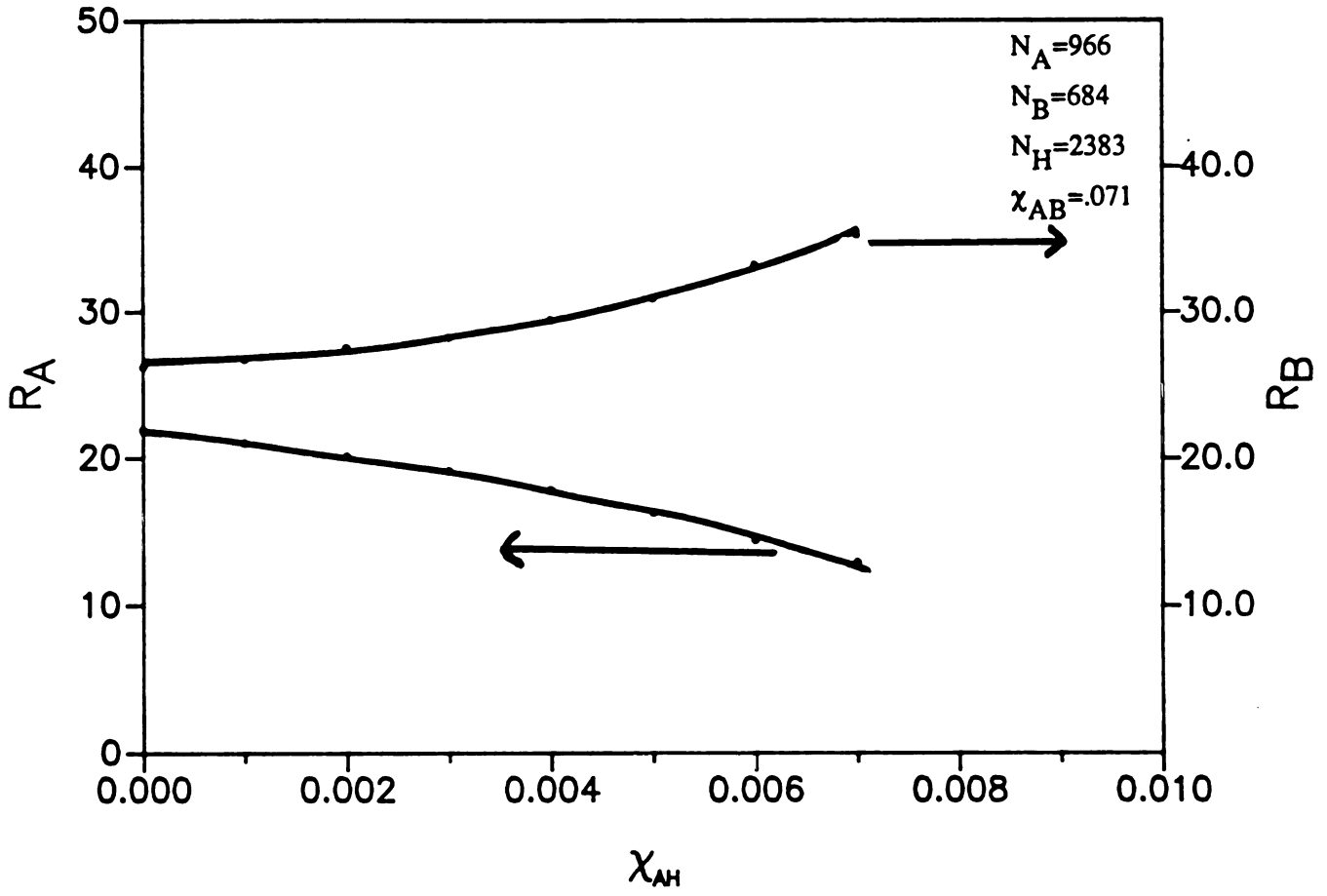

Figure 7.5 Size of micelle core and corona versus degree of incompatibility between A-block and A homopolymer molecules.

an increase in p. The second effect is the deformation of the blocks during micelle formation. To increase the core radius the B-block molecules must stretch, which is unfavorable toward an increase in R_B. For values of n such that the A-blocks are compressed, which is always the case for the blends studied here, addition of diblock to the micelle will cause less stretching of the micelle corona (see equation 7.2) and therefore be a favored process. Since the effect of increase in χ_{AH} is to increase n, the tendency to add diblock to the micelles to decrease compression of the A-block is responsible for the increase in p with increase in χ_{AH} seen in Figure 7.3. The third effect is an increase in the size of a micelle, which for the unmodified theory means an increase in p, increases the translational entropy of the micelle gas, and hence increases the total free energy F_M. This last effect is interesting in light of the calculations here in that p increases dramatically with χ_{AH} and yet the overall size of the micelle stayed constant, which implies the translational entropy remained constant. This indicates the translational entropy of the micelles may cause the micelle size to remain constant.

Leibler and Pincus (1984) developed a theory for the interaction between micelles based on the assumption that the interactions did not affect the number of diblock copolymer molecules in a micelle. The results of Leibler and Pincus's calculations show that the size of the corona changes as a result of micelle-micelle interactions. Figures 7.4 and 7.5 show clearly that terms that affect the size of the corona can dramatically affect the

number of diblock copolymer molecules in a single micelle. In fact, Leibler and Pincus showed that the initial result of micelle-micelle interactions is to compress the micelle corona, which according to the calculations here should result in an increase in p.

For χ_{AB} = .071, the calculated degree of micellization was equal to one and was not affected by the value of χ_{AH}. For χ_{AB} = .015, it can be seen in Figure 7.6 that an increase in χ_{AH} decreases the degree of micellization and increases the critical micelle concentration. This trend is expected because any energy that increases the free energy of a micelle as the energy due to χ_{AH} does results in formation of micelles being less favorable.

Figure 7.7 shows the experimental results for p versus ϕ. This plot shows that at equilibrium (200^{o}C curves) p versus ϕ goes through a maximum at $\phi \sim .05$. The results of the calculations revealed that for a given χ_{AH}, p, η, and ζ did not change with change in diblock content ϕ. These results indicate that if the experimental variations in p are to be explained with χ_{AH}, then χ_{AH} must vary with diblock content in the blend. Specifically, comparison of Figures 7.4 and 7.7 shows χ_{AH} must initially increase with diblock concentration, and then after $\phi \sim .05$ might be explained as follows. As Figure 7.8 indicates, it was found experimentally that the amount of diblock dissolved in the matrix increased considerably as diblock content increased above ϕ = .05. In fact, the diblock that appears to be dissolved in the matrix may actually be dissolved in the corona of the micelles, which would

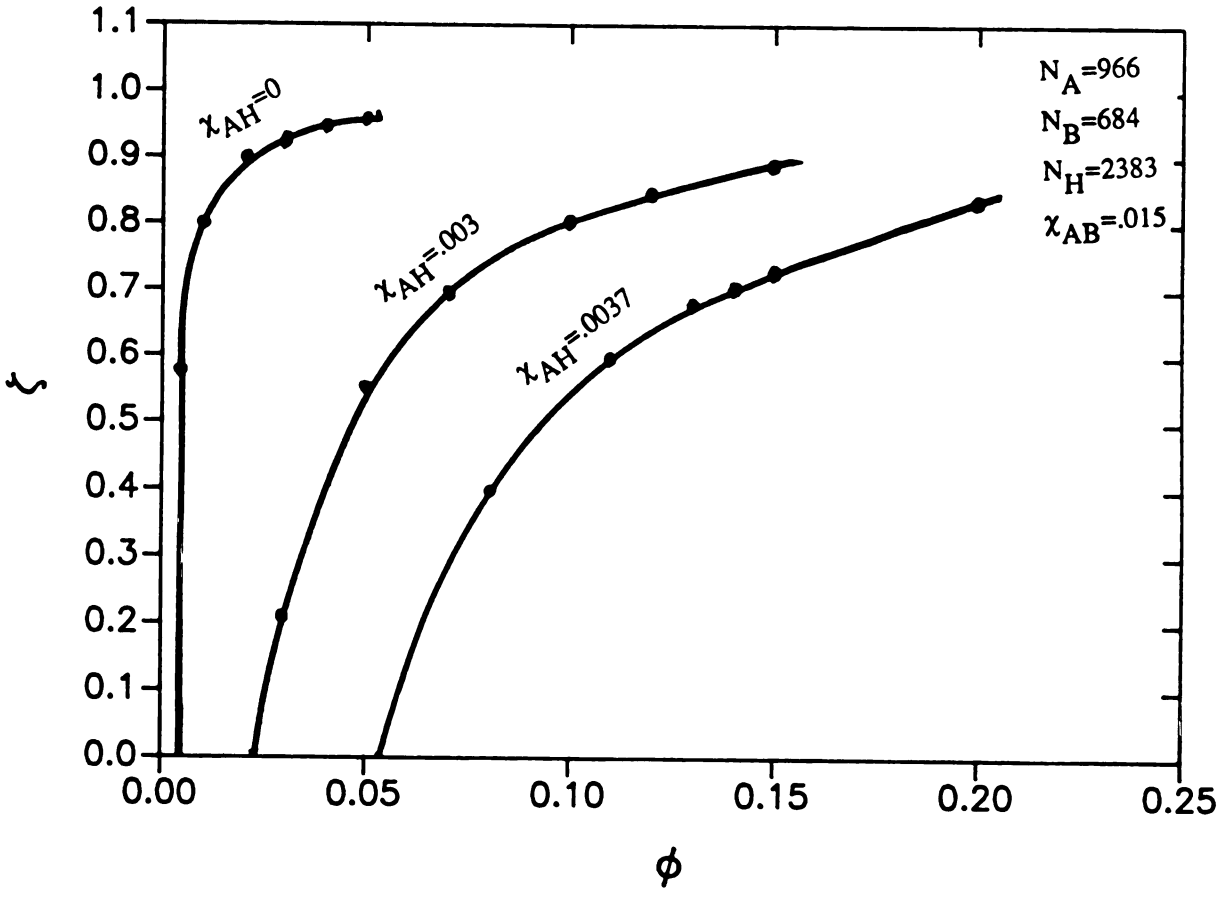

Figure 7.6 Degree of micellization versus volume fraction of AB diblock copolymer at different levels of incompatibility between A-block and A homopolymer molecules.

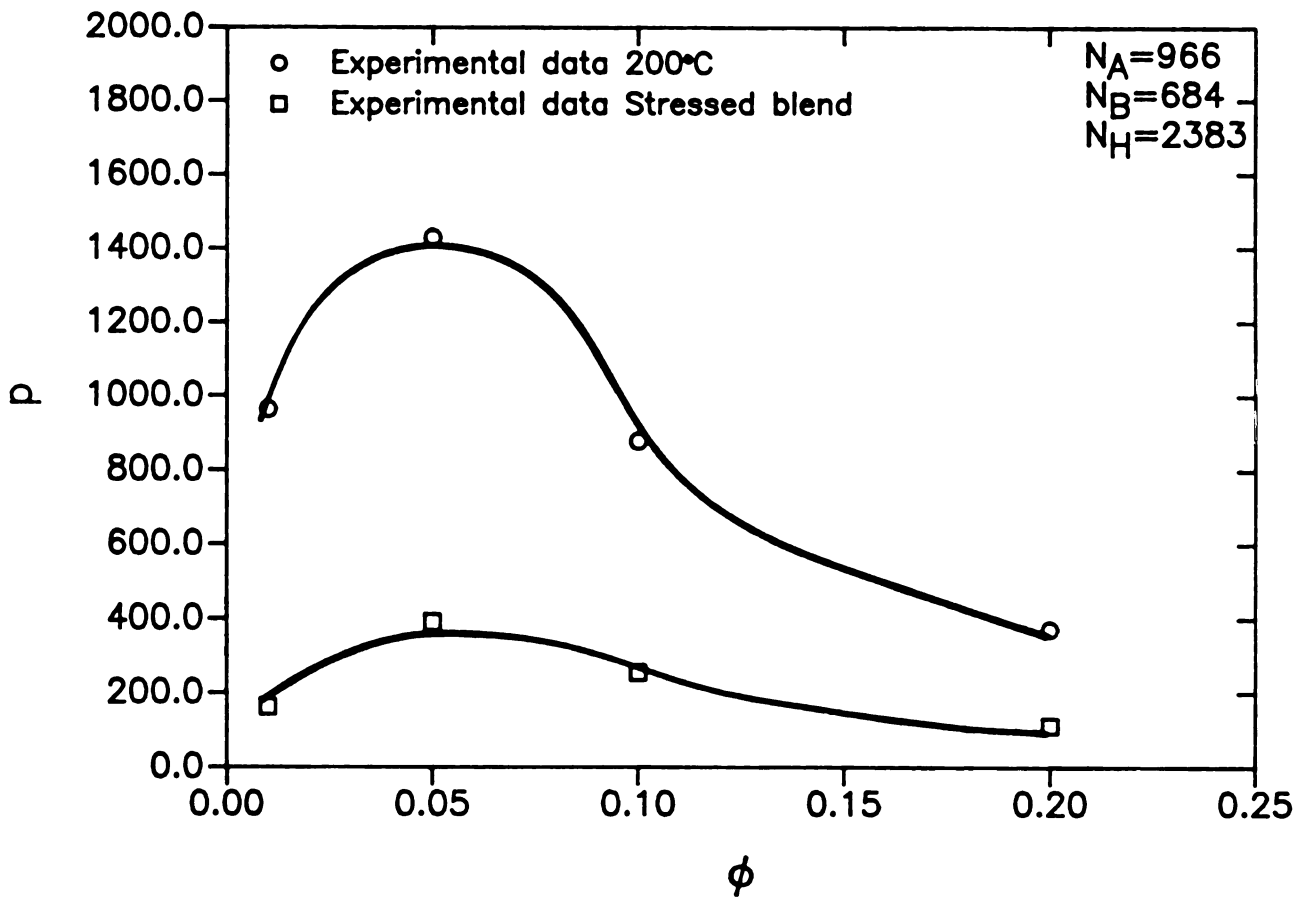

Figure 7.7 Number of AB diblock copolymer molecules in a single micelle versus volume fraction of AB diblock copolymer from experimental data.

swell the micelle corona and cause the micelle core size to shrink. More work needs to be done to explore this possibility.

7.4 Modification of Theory to Include Free Energy Stored During Flow

The objective here was to determine an expression for the free energy stored during a stationary flow F_S in terms of ζ, p, and n, which, when the total free energy is minimized, reflect the effect of processing on these parameters. Marrucci (1972) developed an expression for the free energy stored by a dilute solution of elastic dumbbells; however, as Rangel-Nafaile et al. (1984) pointed out, this expression probably has a much wider range of applicability than for the conditions for which it was derived. In fact, Mazich and Carr (1983) showed that the expression developed by Marrucci is applicable to polymer blends. Following is the development of the term for free energy stored during flow for a polymer blend, and then the logic used here to convert this expression to an expression in terms of ϕ and ζ.

The excess free energy due to elongation of elastic dumbbell entities (two friction centers separated by a frictionless spring) in solution is given by Marrucci (1972)

$$f_{el} = \frac{3ckT}{2} \left[\frac{r^2 - r_o^2}{r_o^2}\right] \qquad 7.17$$

where c is the number density of dumbbell entities, r_o^2 is the mean square end-to-end distance of the dumbbells, and r^2 is the mean

square end-to-end distance of the dumbbells at thermodynamic equilibrium. Equation 7.17 gives the excess free energy for the deformation of the dumbbells away from their thermodynamic equilibrium dimensions.

For an elastic dumbbell, the contribution of the dumbbells to the stress tensor is given by

$$\underset{\cong}{\tau} = \frac{3ckT}{r_o^2} < \underset{\sim}{r}\,\underset{\sim}{r} > - ckT\,\underset{\cong}{I} \qquad 7.18$$

where $\underset{\sim}{r}$ is the end-to-end vector and the brackets denote an average value. Taking the trace of equation 7.18 yields

$$tr\,\underset{\cong}{\tau} = \frac{3\,ckT\,r^2}{r_o^2} - 3ckT \qquad 7.19$$

Combining equations 7.19 and 7.17 yields

$$f_{el} = \frac{3}{2}\,ckT\,\left(\frac{r^2 - r_o^2}{r_o^2}\right) = \frac{tr\,\underset{\cong}{\tau}}{2} \qquad 7.20$$

In the case of steady shear for the elastic dumbbell model, $tr\,\underset{\cong}{\tau} = N_1$, where N_1 is the first normal stress difference. Also, if one considers the case of a solution of many different types of dumbbell entities, the above analysis yields (Mazich & Carr, 1983)

$$f_{el} = \frac{3}{2}\,kt\,\sum_i \frac{c_i(r^2 - r_o^2)_i}{r_{oi}^2} = tr\,\underset{\cong}{\tau}/2 = N_1/2 \qquad 7.21$$

It can be seen from equation 7.21 that energy is stored during flow by stretching of the polymer chains. For the micelle system there are three different types of polymer chains being stretched during flow: the homopolymer chains, the diblock chains in the bulk, and the diblock chains in the micelles. It can also be seen from equation 7.21 that the free energy stored during shear will change with the total number of diblock chains in the system and the number of diblock chains that are in micelles relative to the number of diblock chains in the matrix.

Equation 7.21 implies that for blends of diblock in an excess of homopolymer most of the energy stored during flow is stored by stretching of matrix homopolymer, and the stretching of the diblock molecules gives a small contribution. Therefore, a semi-empirical expression for F_S is developed by assuming the free energy stored during flow of the micelle system can be determined from a perturbation expansion of the first normal stress difference of the blend in terms of the amount of diblock in micelles $\phi\zeta$, and the amount of diblock in the matrix $\phi(1-\zeta)$. This perturbation expansion is expressed as follows

$$F_S = \Omega a^3 N_{1,total}/2 = \Omega a^3 N_{1,H} [1 + b_1 \phi\zeta + b_2 \phi(1-\zeta)]/2$$

$$= \frac{\Omega a^3}{2} N_{1,H} [1 + \phi\zeta (b_1-b_2) + b_2 \phi] \qquad 7.22$$

where $N_{1,total}$ is the first normal stress difference for the blend. F_S is then added to F_M in equation 7.11, and the total free energy

is minimized as before. Assuming that F_S is directly additive to the expressions given in equation 7.13 is similar to the assumption of additivity of the expressions for free energy due to flow and the static free energy for different phases used by Rangel-Nafaile, Metzner, and Wissbrun (1984) and Wolf (1984) in their theories for the effect of flow on polymer solutions. This assumption implies that the expressions used for determining free energy of a static system are unaffected by flow, which is true if the effects of flow on the system are all incorporated in the expression for F_S.

7.5 Predictions From Theory for the Effect of Flow on Micelle Formation

Before considering the numerical results for the effect of flow on micelle formation, an asymptotic expression, which incorporates both the effect of energy stored during flow and χ_{AH}, for the fraction of diblock dissolved in the matrix will be considered. As illustrated by LOW and by ten Brinke and Hadziionnou, such an asymptotic relation can be obtained by taking the derivative of the total free energy with respect to ϕ_1 and setting this expression equal to zero, which yields

$$f + \frac{1}{p} \ln \left(\frac{\zeta(\phi-\phi_1)}{1-\zeta\phi}\right) - \ln \phi_1 - \frac{N}{N_H} (\zeta - 1) \ln (1 - \phi_1) + (\alpha - 1)$$

$$x(1 - \zeta\phi_1) - \chi_{AB} \left[N_B - 2\phi_1 \frac{N_B^2}{N} + \zeta \frac{N_B^2}{N} \phi_1^2\right] + \frac{N}{\phi kT} \frac{\partial F_S}{\partial \zeta} \qquad 7.23$$

where $\partial F_S/\partial\zeta = N_{1,H}a^3 (b_1 - b_2)/2kT$. For the case of $\phi_1 \ll 1$ and $p \gg 1$, ϕ_1 to a good approximation is given by

$$\phi_1 \cong \exp[f - \chi_{AB} N_B - \alpha - 1 + \frac{N_a^3}{2\phi kT} N_{1,H} (b_1 - b_2)] \qquad 7.24$$

where the value of f is determined from $\partial f/\partial p = 0$ and $\partial f/\partial n = 0$. A striking result of equation 7.24 is that for large $\chi_{AB}N_B$, ϕ_1 will be approximately zero unless the term with $N_{1,H}$ is on the same order as $\chi_{AB}N_B$. In other words, even for a high degree of incompatibility between the matrix polymer and the B-block of the diblock, for $b_1 - b_2 > 0$, if a high enough stress is imposed on the blend, the diblock will start to dissolve in the matrix. When the criteria for application of equation 7.24 are met, then equation 7.24 is a good approximation of the critical micelle concentration. For the case where $\phi_1 << 1$ no longer holds, as is the case for low χ_{AB} where $\chi_{AB}N_B$ no longer dominates the exponential in equation 7.24, then as ten Brinke and Hadziioannou pointed out, the term $2 N_B^2 \phi_1/N$ can no longer be omitted in the asymptotic development, and an improved approximation for the critical micelle concentration is given by

$$\phi_c(\chi_{AH}, N_{1,H}) \cong \frac{\exp[f-\chi_{AB}N_B+\alpha-1 + \frac{N_a^3 N_{1,H}(b_1-b_2)}{2\phi kT}]}{1 - \frac{2 N_B^2 \chi_{AB}}{} \exp[f-\chi_{AB}N_B+\alpha-1+\frac{N_a^3 N_{1,H}(b_1-b_2)}{2\phi kT}]} \qquad 7.25$$

for values of $\chi_{AB}N_B$ such that equation 7.24 is still a good approximately when $\chi_{AH} = 0$ and $N_{1,H} = 0$ then equation 7.25 can be rewritten as

$$\phi_c(\chi_{AH}, N_{1,H}) \cong \frac{\phi_c(0)\exp[\chi_{AH}\eta(1-\eta) + \frac{N_a^3 N_{1,H}(b_1 - b_2)}{2\phi kT}]}{1 - \frac{2\phi_c(0)N_B^2\chi_{AB}}{N}\exp[\chi_{AH}\eta(1-\eta) + \frac{N_a^3 N_{1,H}(b_1-b_2)}{2\phi kT}]} \quad 7.26$$

where $\phi_c(0)$ is given by equation 7.24 with $\chi_{AH} = 0$ and $N_{1,H} = 0$. The expression in equation 7.26 reveals that the critical micelle concentration will increase with increase in χ_{AH}, as was seen in Figure 7.3. The effect of stored free energy during flow depends on the sign of $b_1 - b_2$. If $b_1 - b_2$ is positive, then the critical micelle concentration increases due to flow; however, if $b_1 - b_2$ is negative, then the critical micelle concentration decreases due to flow.

As mentioned earlier, the objective here was to compare theoretical predictions for the effect of flow on AB/A blends containing micelles to the experimental results obtained for the blends in Chapter V. This requires an expression for F_S in equation 7.22 that pertains to these blends. The value of $N_{1,H}$ for use in equation 7.22 was obtained from steady shear testing with a Rheometrics Mechanical Spectrometer RMS-800 in the parallel plate mode, and the result was $N_{1,H} = 5.218 \times 10^{-8}(\sigma)^{2.52}$ where σ is the shear stress in dynes/cm^2. At present it is not possible to determine the morphology for AB/A blend during a stationary flow, so the constants b_1 and b_2 for a particular blend cannot be readily determined. In an alternative approach, by assuming that b_2 was

much smaller than b_1, b_1 was estimated by nondestructive dynamic mechanical testing of the blends at equilibrium, as detailed in Chapter VI. Using this approach, b_1 was approximately equal to 1.57, and the subsequent expression for $N_{1,total}$ seemed to be very good for representing the amount of energy stored by the blends at small concentrations of diblock.

Numerical calculations with the above expression for F_S predicted a decrease in the degree of micellization with increase in shear stress as illustrated in Figures 7.9 and 7.10. The decrease in micellization occurred gradually with stress at low diblock-homopolymer incompatibility, χ_{AB} = .015, but the dissolution of diblock occurred abruptly at a critical shear stress for high degree of diblock-homopolymer incompatibility χ_{AB} = .071. The decrease in degree of micellization due to flow is in line with the experimental results shown in Figure 7.8. The stresses in Figures 7.9 and 7.10 can be compared to the maximum stress in the twin screw extruder, which is estimated from the measured viscosity of the pure polystyrene of 3,260 poise and the maximum shear rate in the extruder of 809 sec^{-1} to be 2.36 x 10^6 dynes/cm^2. Actually, the average stress in the extruder will be less than this value, and is probably in a range that would include the values shown in Figures 7.9 and 7.10. The mixing in the extruder is a nonequilibrium process, so it would be fortuitous to achieve exact agreement between theory and experiment. Nevertheless, the theory accurately predicts the decrease in degree of micellization that was seen experimentally.

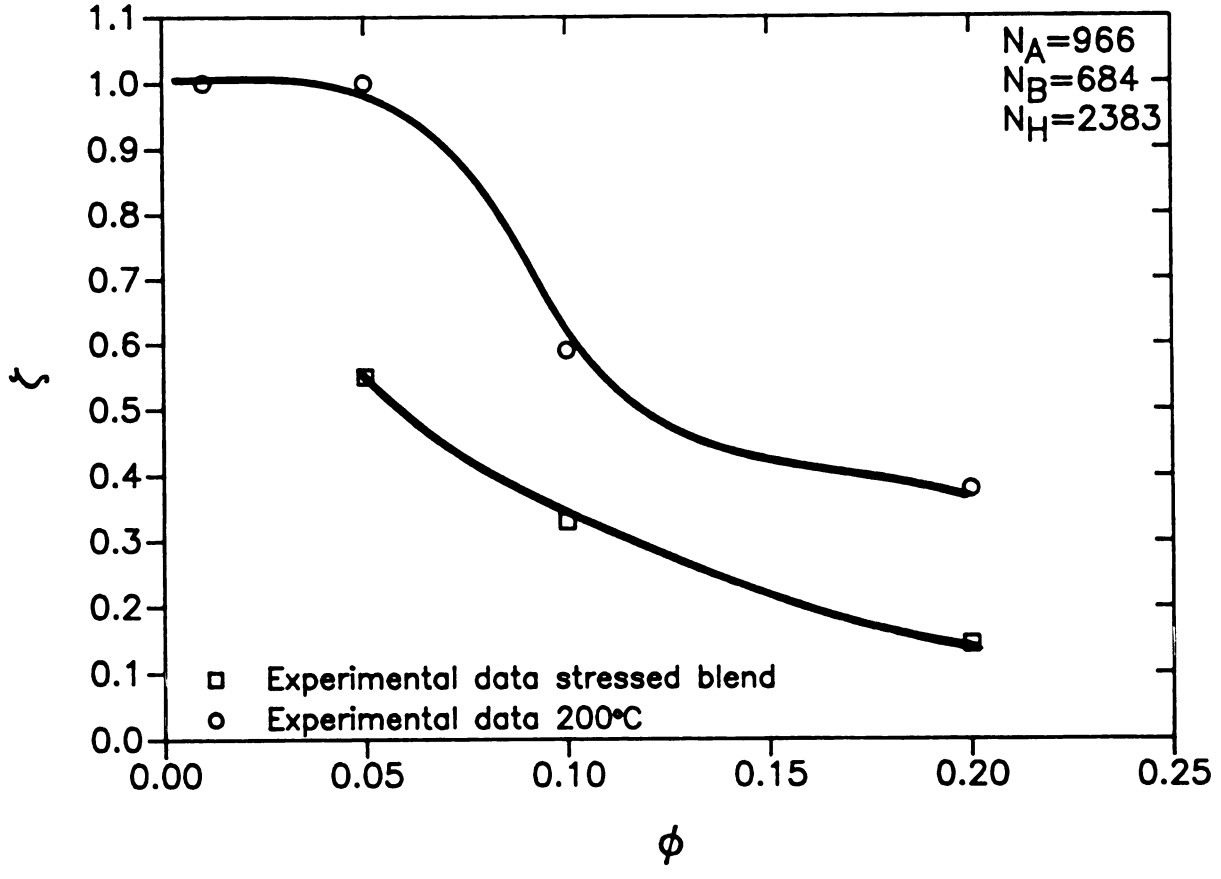

Figure 7.8 Degree of micellization versus volume fraction of AB diblock copolymer from experimental data.

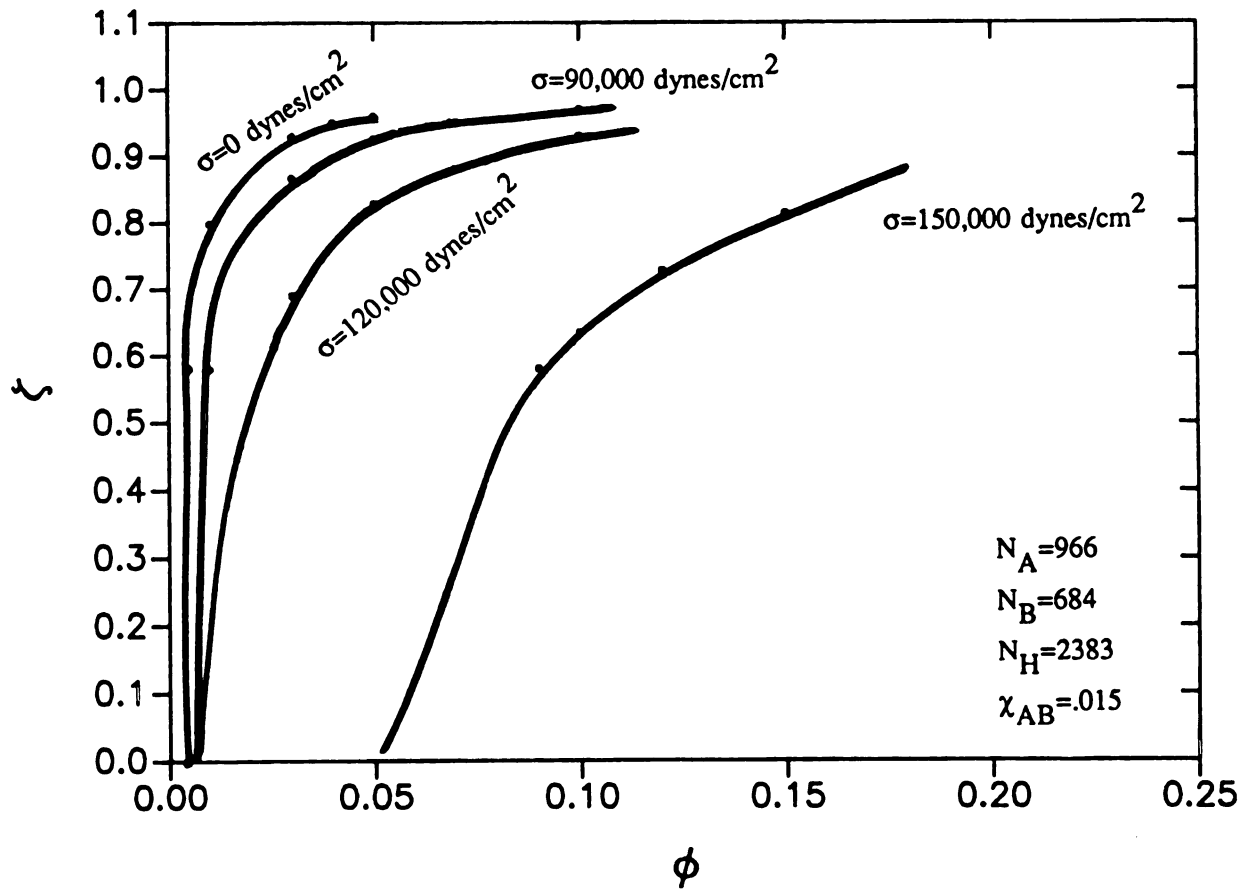

Figure 7.9 Degree of micellization versus volume fraction of AB diblock copolymer at different levels of shear stress with χ_{AB}=.015.

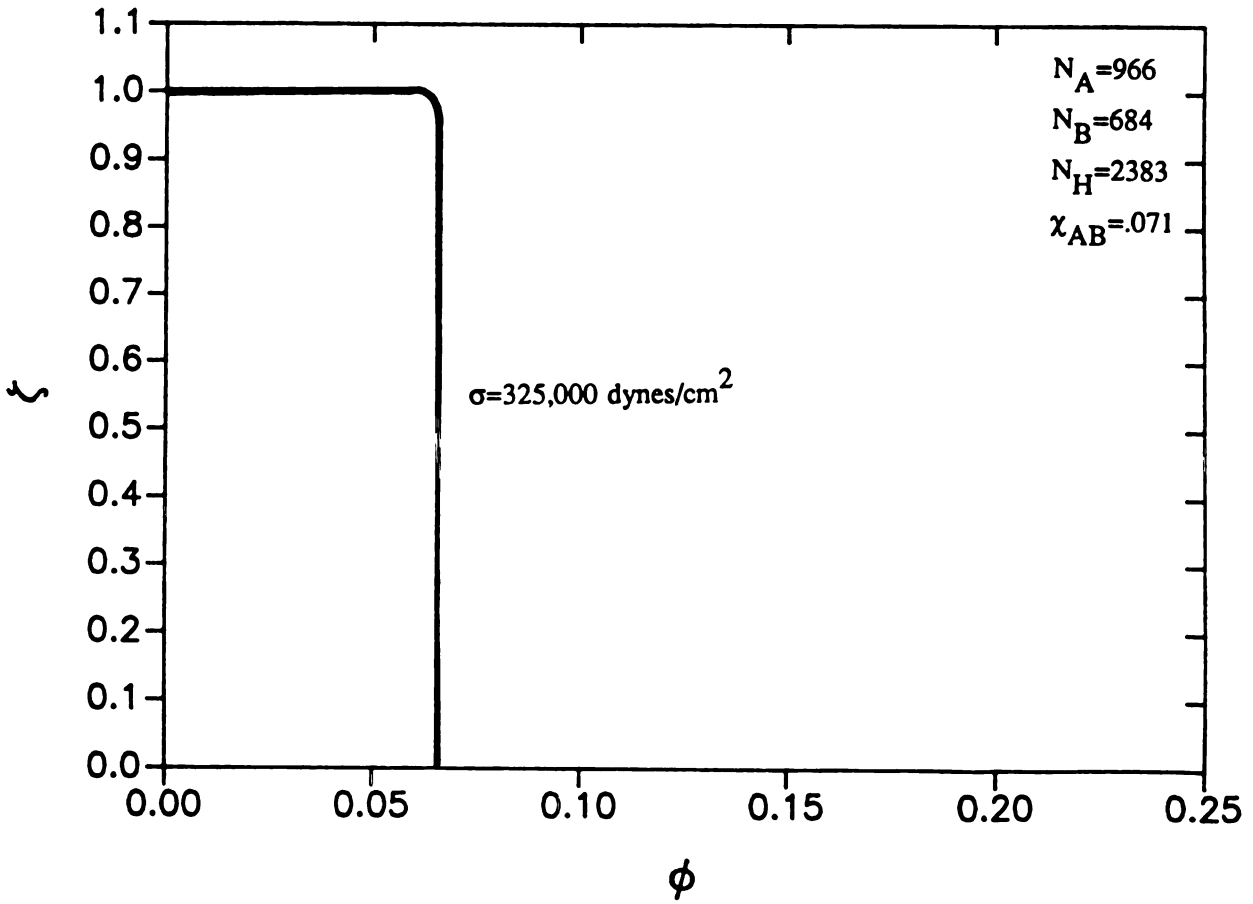

Figure 7.10 Degree of micellization versus volume fraction of AB diblock copolymer at a shear stress of 325,000 dynes/cm^2 with χ_{AB}=.071.

Figure 7.7 shows that experimentally the size of the micelle cores decreases due to flow. An explanation of this may be that due to flow the A-block in the corona stretches significantly, which, as described earlier (see Figure 7.5), would result in a decrease in the size of the micelle core. This would imply that stress leads to an additional free energy term in each micelle corona. A recommendation for future work is to explore this possibility.

7.6 Summary of Results From Modified Theory

The theory of Leibler et al. (1983) for micelle formation in AB diblock blends in A homopolymer was modified here to account for unfavorable interactions between the A-block in the corona and the matrix homopolymer and to account for the effect of energy stored by the blend during flow. The modified theory predicts that the fraction of diblock in the micelle corona and the number of diblock molecules aggregated into a single micelle increase with increase in incompatibility between the A-block in the corona and the matrix homopolymer. It was also revealed that an increase in incompatibility results in an increase in size of the micelle core, but the overall size of the micelle stays constant. It is suggested here that the apparent degree of incompatibility between A-block in the corona and matrix homopolymer may change with diblock content and due to flow, which would explain the experimental results. The modified theory also predicts a decrease in degree of micellization due to flow, which was seen experimentally.

A failure of the theory here is to explain the decrease in degree of micellization with increase in diblock content seen in Figure 7.8 for both the equilibrium blend and the stressed blend. In all of the existing theories for micelle formation in AB/A blends, a trend of ζ increasing with ϕ, as shown in Figures 7.2, 7.6, and 7.9, is predicted. It seems clear that there is an effect which opposes micelle formation beyond a certain point at each diblock concentration which has not been taken into account. At each concentration, as micelles are formed the space available for formation of more micelles becomes limited. It is possible that the effect of this space-filling constraint is more severe than that predicted by the term for the entropy of mixing for the micelles S_m.

CHAPTER VIII

CONCLUSIONS AND RECOMMENDATIONS

8.1 Conclusions

Morphological and rheological experiments have been performed on melt blends of a high molecular weight tapered styrene-butadiene diblock in an excess of high molecular weight polystyrene. The blends were created in a twin screw extruder, and it was found by annealing the blends at a high temperature and then rapidly quenching that equilibrium structures were obtained in the blends at high temperatures.

An analysis of the morphology after processing and at equilibrium revealed a number of trends. First, as the concentration of diblock in the blend increased, there was a transition from a spherical to cylindrical micelle structure for the blends. This transition occurred at a lower diblock concentration during processing than it did at equilibrium. Second, as the blend diblock content increased, the size of the micelle core went through a maximum at a concentration of approximately 5% diblock both at equilibrium and during processing. Third, above 5% diblock as the diblock content increased, the total number of diblock molecules participating in micelles stayed approximately constant, and the added diblock was dissolved either in the corona of the micelle or

in the matrix polystyrene. This conclusion is based on the plausible assumption that the micelle core consisted totally of polybutadiene. Fourth, processing caused the micelles to have a smaller core size than at equilibrium, and processing caused the total number of diblock molecules participating in micelles to decrease. Fifth, there was a tendency for micelles to cluster at equilibrium, but this tendency did not exist during melt processing. A hypothesis was introduced, based on results from the literature, that in AB/A blends where the matrix homopolymer has a larger molecular weight than the A-block, such as in the blends studied here, there are unfavorable interactions between the A-block in the corona and the matrix polymer. The result of this unfavorable interaction would be to exclude matrix homopolymer from the corona.

The above experimental results prompted two modifications of the existing theories on micelle formation in AB/A blends. First, the theory was modified to include the effect of unfavorable interactions between the A-block in the corona and A homopolymer when the homopolymer had a larger molecular weight than the A-block. Second, the theory was modified to analyze the effect of added energy during flow which arises from stretching of the polymer molecules. The modified theory predicted that as incompatibility between A-block in the corona and matrix homopolymer increases, the micelle corona thickness decreases at the same rate as the micelle core radius increases, with the overall result that the micelle stays approximately the same size. The total number of diblock molecules participating in micelles decreases and the number of

diblock molecules participating in a single micelle increases with an increase in A-block/A homopolymer incompatibility. Since the theory predicts a change in micelle core size with change in incompatibility between A-block and A homopolymer, it is hypothesized that the changes seen experimentally in core size may be related to an apparent change in incompatibility between A-block matrix polymer in the micelle corona. The modified theory predicts the effect of stress is to decrease the total number of diblock chains participating in micelles, which was in line with the experimental results. It was found that if the degree of incompatibility between B-block and homopolymer was high, there was a critical stress above which the micelles totally dissolved. However, if the B-block/homopolymer incompatibility was low, the dissolution of micelles occurred more slowly as stress was increased.

Dynamic mechanical tests were performed on the blends at temperatures ranging from 130^{o}C to 200^{o}C. Although the morphology studies revealed that there was a change in structure with temperature for the blends, it was possible to create a single master curve of G' and G" for each blend. This is contrary to other studies with pure diblocks, where a change in structure results in master curves with branches. A more sensitive measure of changes in structure with temperature seemed to be obtained with plots of G' versus G" here. Plots of G' versus G" resulted in a single curve for the 160^{o}C and 200^{o}C data for each blend, but the 130^{o}C data did

not superimpose onto this curve. This is taken to indicate the structure at 160°C is more like the structure seen in the micrographs at 200°C than it is like the structure seen in the 130°C micrographs. An average relaxation time was calculated from Cole-Cole plots for each blend, and this relaxation time was found to go through a minimum with diblock concentration; also, at a given frequency, G', G", and hence η', all went through a minimum with concentration. The initial decrease in these values was associated with the micelle structure causing the average distance between entanglements for the matrix polymer to increase, and hence the reptation time to decrease. The subsequent increase in G', G", and mean relaxation time after a diblock content of 5% is associated with the long relaxation mechanism of formation and dissociation of agglomerates of micelles. It was found that $\tan(\delta)$ decreased monotonically with diblock concentration at constant G*, and this was taken to indicate an increase in the amount of energy stored with increase in diblock concentration at a constant stress. Based on a comparison of rheological results and morphological results, a linear relation between the amount of energy stored during flow and diblock concentration times amount of diblock dissolved in matrix polymer was derived for low diblock concentrations. This expression was then used in the modified theory for micelle formation in AB/A blends mentioned earlier.

8.2 Recommendations

The results of the experimental and theoretical study done here suggest some future work that would increase understanding of the mechanism of micelle formation in AB/A blends and would better explain the effect of micelle structures on rheology. Some suggestions follow.

It was found for the AB/A blends studied here that above a certain concentration of diblock the number of diblock micelles participating in micelles remained constant. It has been suggested here that the remainder of the diblock is either dissolved in the micelle corona (a possibility that has not been explored theoretically) or the matrix homopolymer. If one could determine the composition of the micelle corona and the micelle core, one could answer this question. This might be accomplished with analytical electron microscopy, which allows chemical analysis of samples with size of 2 nm or greater.

An interesting study would be to monitor the morphology of AB/A blends in a stationary flow. In other words, if one could impose different steady-state stresses on the blends and monitor the equilibrium morphology at this stress, then such information about the effect of energy added during flow could be obtained.

Another study, which would have industrial impact, would be to compare the equilibrium and processing morphology obtained for melt blends of AB diblock copolymer with A homopolymer and B homopolymer where micelle structures still exist. This would have implications

in forming impact-modified blends with a desired morphology by using materials that are cheaper than pure diblock copolymers.

In the rheological tests it was difficult to separate the effect of polydispersity and the effects of micelle structure on the dynamic mechanical properties of the blends studied here. It would be interesting to establish if the minimum in G' and G" with diblock concentration seen here occurs for monodisperse samples. A rheological study of monodisperse samples would also allow one to determine exactly how the micelle structure affects the reptation and tube modification of the matrix polymer.

There seem to be two experimental phenomena, seen in the study here and by other workers, that existing theories on micelle formation in AB/A blends fail to predict. One is the tendency for diblock molecules to dissolve in the corona or the matrix polystyrene rather than form micelles as diblock is added to the blend. The other is the tendency for micelles to agglomerate rather than repel at equilibrium. A new theoretical approach that explains these tendencies, especially the first tendency, would be informative.

A modification of the micelle formation theory for AB/A blends to include blends of AB diblock with A homopolymer and B homopolymer may not be that difficult. This theory could then be compared to the experiments suggested for these blends earlier.

APPENDIX

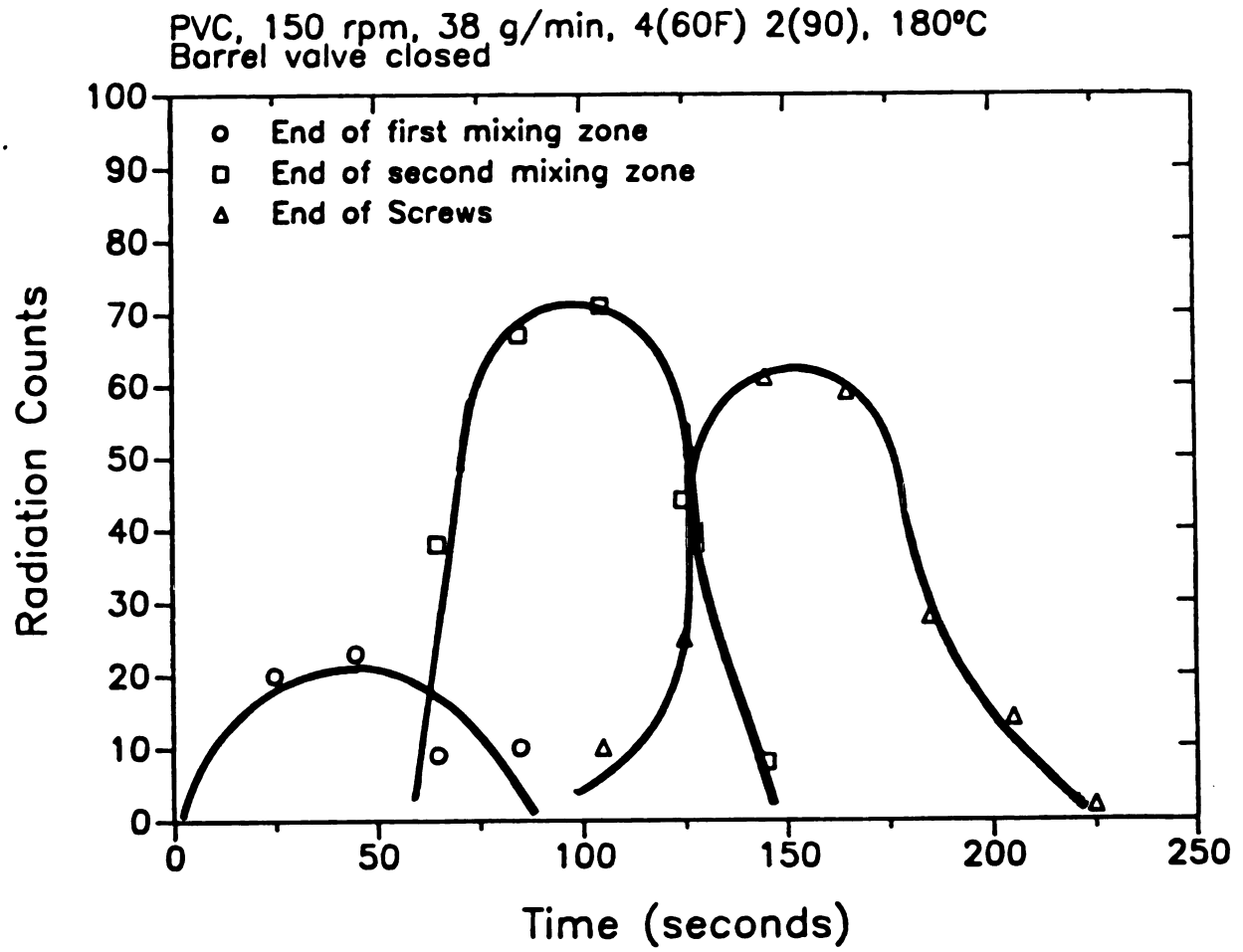

Figure 2.A Experimental residence time distributions for PVC.

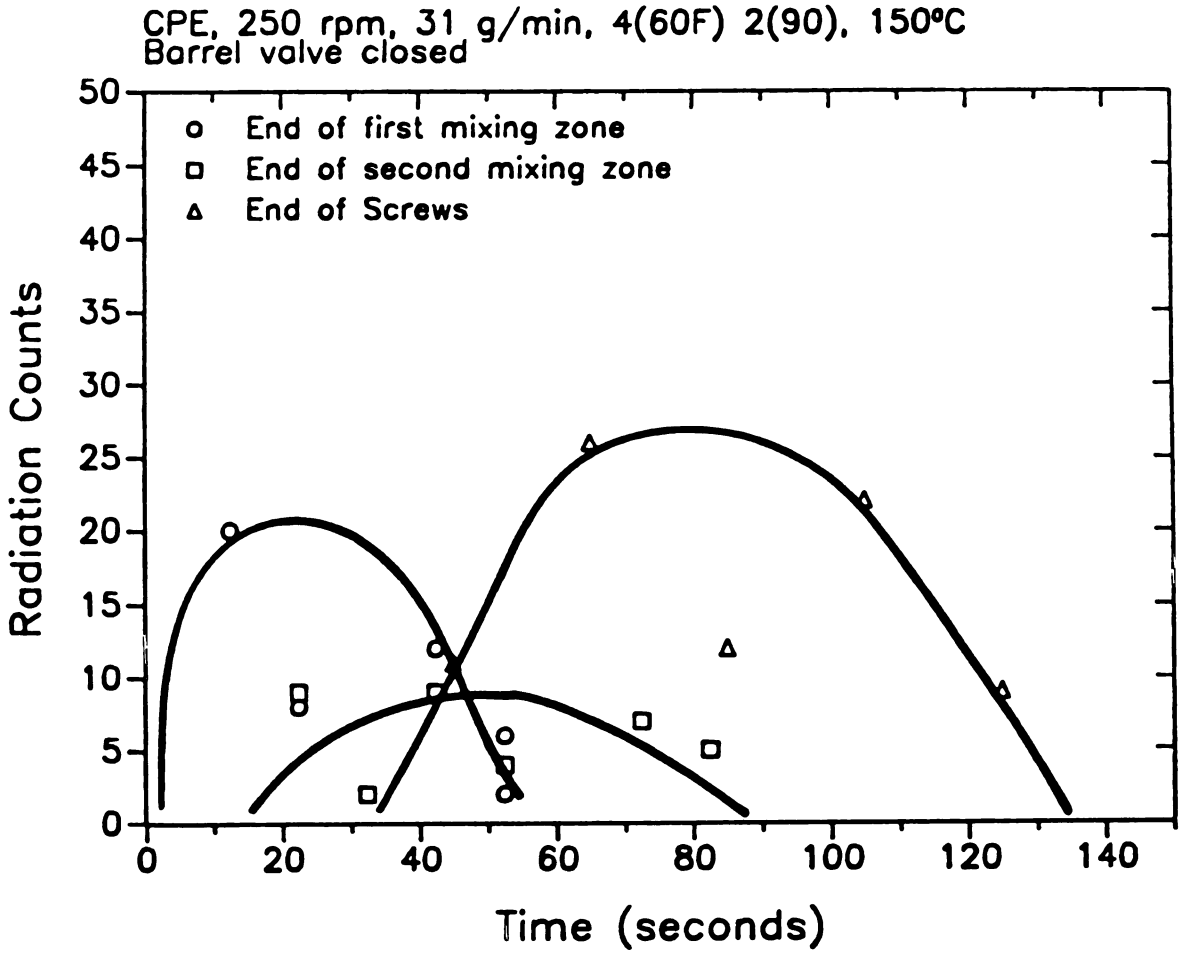

Figure 2.B Experimental residence time distributions for CPE.

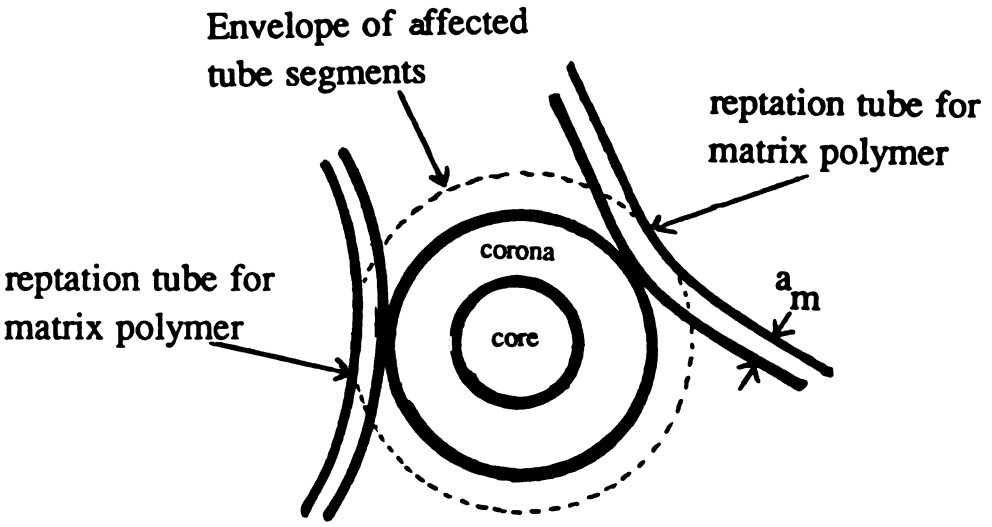

Figure 6.A Schematic of tubes through which matrix polymer reptates when matrix polymer does not penetrate the micelle corona. Entanglement density is equal to zero at the interface between the micelle corona and the matrix.

Table A1.--Verification of calculations; comparison to Leibler, Orland, and Wheeler (1983).

xN	ϕ	p	ϕ_1	η	ζ
15	.11	76.8	.101	.198	.110
	.12	77.3	.103	.198	.202
	.13	77.6	.105	.199	.286
	.14	77.8	.105	.200	.363
	.15	78.1	.106	.200	.430
	.17	78.3	.107	.200	.544
	.20	78.6	.109	.200	.676
xN	ϕ	p	ϕ_1	η	ζ
20	.009	77.0	7.98×10^{-3}	.190	.116
	.01	79.2	8.05×10^{-3}	.195	.199
	.03	78.8	8.30×10^{-3}	.192	.742
	.05	79.2	8.40×10^{-3}	.193	.854
	.10	79.2	8.52×10^{-3}	.193	.940

Table A2.--Results with joint localization energy, and χ_{AH} and flow energy modifications.

N_A = 100, N_B = 100, N_H = 40.

χ_{AB}	χ_{AH}	ϕ	p	ϕ_1	η	ζ	R_B	R_A
.100	0	.05	66.6	.0429	.180	.165	8.1	7.1
		.07	67.5	.044	.181	.430	8.2	7.1
		.10	67.9	.045	.182	.643	8.2	7.1
		.13	68.2	.047	.182	.762	8.2	7.1
		.15	68.4	.046	.182	.815	8.2	7.1
		.17	68.5	.046	.183	.857	8.2	7.7

N_A = 966 N_B = 684 N_H = 2383

χ_{AB}	χ_{AH}	ϕ	p	ϕ	η	ζ	R_A	R_B	σ
.071	0	.05	326	~0	.27	~1	21.9	26.1	0
		.10	324	~0	.27	~1	21.9	26.1	
		.15	326	~0	.27	~1	21.9	26.1	
		.20	326	~0	.27	~1	21.9	26.1	
.015	0	.005	168	.002	.17	.58	22.1	21.7	
		.01	195	.002	.21	.798	22.1	21.7	
		.02	196	.002	.21	.90	22.1	21.7	
		.03	196	.002	.21	.93	22.1	21.7	
		.04	196	.002	.21	.95	22.1	21.7	
		.06	196	.002	.21	.96	20.1	22.7	
.071	0	.06	326	~0	.271	~1	21.9	26.2	0
	.001	.05	349	~0	.306	~1	21.0	26.7	
	.002	.05	377	~0	.337	~1	20.1	27.5	
	.003	.05	412	~0	.382	~1	19.1	28.2	
	.004	.05	466	~0	.453	~1	17.8	29.4	
	.005	.05	539	~0	.550	~1	16.3	30.9	
	.006	.05	667	~0	.720	~1	14.4	33.2	
	.007	.05	808	~0	.916	~1	12.9	35.3	

x_{AB}	x_{AH}	ϕ	p	ϕ_1	η	ζ	R_A	R_B	σ
.015	.003	.01	--	--	--	--	--	--	0
		.03	255	.024	.291	.21	19.3	24.1	
		.05	255	.023	.291	.554	19.3	24.1	
		.07	247	.024	.283	.699	19.5	23.8	
		.10	251	.024	.287	.805	19.5	23.8	
		.12	253	.024	.289	.849	19.5	23.8	
		.15	252	.024	.287	.891	19.4	24.0	
.015	.0037	.08	275	.052	.322	.398	18.6	24.7	0
		.11	275	.052	.322	.596	18.6	24.7	
		.13	275	.052	.322	.679	18.6	24.7	
		.14	275	.052	.322	.708	18.6	24.7	
		.15	276	.058	.395	.734	18.6	24.7	
		.20	276	.052	.322	.836	18.6	24.7	
.015	0	.01	194	.0043	.208	.579	21.7	22.0	90,000
		.03	196	.0043	.208	.867	21.7	22.0	
		.05	196	.0044	.207	.926	21.7	22.0	
		.07	196	.044	.208	.751	21.7	22.0	
		.10	197	.044	.208	.970	21.7	22.0	
.015	0	.01	196	.005	.208	.466	21.7	22.0	100,000
		.03	194	.005	.206	.833	21.7	22.0	
		.05	196	.005	.208	.906	21.7	22.0	
		.07	197	.005	.208	.938	21.7	22.0	
.015	0	.01	--	--	--	--	--	--	120,000
		.02	196	.010	.208	.52	21.8	22.0	
		.03	193	.010	.204	.69	21.8	22.0	
		.05	196	.010	.209	.828	21.7	22.0	
		.07	197	.010	.209	.880	21.7	22.0	
		.10	197	.010	.209	.930	21.7	22.0	
.015	0	.08	--	--	--	--	--	--	150,000
		.09	200	.046	.214	.580	21.5	22.2	
		.10	201	.046	.215	.634	21.5	22.2	
		.12	201	.046	.215	.728	21.5	22.2	
		.11	202	.047	.215	.813	21.5	22.2	

x_{AB}	x_{AH}	ϕ	p	ϕ_1	η	ζ	R_A	R_B	σ
.071	0	.05	--	--	--	--	--	--	335,000
		.10	326	-0	.27	-1	21.9	26.2	
		.20	326	-0	.27	-1	21.9	26.2	
.071	0	.05	--	--	--	--	--	--	350,000
		.10	--	--	--	--	--	--	
		.20	--	--	--	--	--	--	
.071	0	.05	326	-0	.27	-1	21.9	26.2	325,000
		.10	326	-0	.27	-1	21.9	26.2	
		.20	326	-0	.27	-1	21.9	26.2	

REFERENCES

REFERENCES

Ahuja, S., H. Chang, and R. Schreiber, Poly. Eng. Sci. 22(11), 692 (1982).

Bates, F. S., C. V. Berney, and R. E. Cohen, Macromolecules, 16, 1101 (1983).

Berney, C. V., R. E. Cohen, and F. S. Bates, Polymer, 23, 1222 (1982).

Bird, R. B., W. E. Stewart, and E. N. Lightfoot, Transport Phenomena, John Wiley & Sons, New York (1960).

Booy, M. L., Poly. Eng. Sci., 20(18), 1220 (1980).

Bywater, S., Poly. Eng. Sci., 24(2), 104 (1984).

Chapiro, A., Radiation Chemistry of Polymer Systems, High Polymers XV, Interscience Pub., Great Britain (1962).

Cohen, R. E., and A. R. Ramos, Macromolecules, 12, 131 (1979).

de Gennes, P. G., J. Chem. Phys., 55, 572 (1971).

Diogo, A. C., G. Marin, and P. Monge, J. Non-Newtonian Fluid Mech. 23 435 (1987).

Doi, M., and S. F. Edwards, J. Chem. Soc. Faraday. Trans. 74, 1789, 74, 1802, 74, 1818 (1978; 75, 38 (1979).

Dumoulin, M. M., C. Farha, and L. A. Utracki, Poly. Eng. Sci., 24, 1319 (1984).

Eastmond, G. C., and D. G. Phillips, Polymer, 20, 1501 (1979).

Eise, K., J. Curry, and J. F. Nangeroni, Poly. Eng. Sci., 23, 642 (1983).

Elmendorp, J. J., and A. K. Van Der Vegt, Poly. Eng. Sci., 26(19), 1332 (1986).

Favis, B. D., and Chalifoux, J. P., Proceedings Fourth Annual Meeting Polymer Processing Society, 9/5, 1988).

Fayt, R., R. Jerome, and P. Teyssie, J. Poly. Sci.; Poly. Let., 24, 25 (1986).

Fayt, R., R. Jerome, and P. Teyssie, J. Poly. Sci.; Physics, 29, 2209 (1982).

Fayt, R., R. Jerome, P. Teyssie, J. Poly. Sci.; Poly. Let., 19, 19 (1981).

Ferry, J. D. Viscoelastic Properties of Polymers, 3rd ed., Wiley, New York (1980).

Gebizlioglu, O. S., A. S. Argon, and R. E. Cohen, Polymer, 26, 519 (1985).

Gouinlock, E. V., and R. S. Porter, Poly. Eng. Sci., 17, 535 (1977).

Graessley, W. W., Adv. Poly. Sci., 47, 67 (1982).

Graessley, W. W., and M. J. Struglinski, Macromolecules, 19, 1754 (1986).

Grassie, N., and G. Scott, Polymer Degradation and Stabilization, Cambridge Univ. Press (1985).

Hadziioannou, G., and A. Skoulios, Macromolecules, 15, 271 (1982).

Han, C. D., and M. S. Jhon, J. Appl. Poly. Sci., 32, 3809 (1986).

Heikens, D., N. Hoen, W. Barentsen, P. Piet, and H. Ladau, J. Poly. Sci.: Poly. Symp., 62, 309 (1978).

Heydman, P. H., and H. D. Guicking. Koll. Z. Poly., 193(1), 16 (1966).

Inoue, T., T. Soen, T. Hashimoto, and H. Kawai, in Block Copolymers, ed. S. Aggarwal, Plenum Press (1970).

Janssen, L. P. B. M., R. W. Hollander, M. W. Spoor, and J. M. Smith, AIChE J., 26(9), 640 (1979).

Karian, H. G., J. Vinyl Tech., 7(4), 154 (1985).

Kato, K., Poly. Eng. Sci., 7, 38 (1967).

Katsoros, J. D., M. F. Malone, and H. H. Winter, Proceedings Fourth Annual Meeting of the Polymer Processing Society, 9/2 (1988).

Kim, J., C. D. Han, and S. G. Chu, J. Poly. Sci.: Poly. Phys., 26, 677 (1988).

Kim, W. S., W. W. Skatschkow, and S. D. Jewmenow, Plaste und Kantschuk, 20(9), 696 (1973).

Kinning, D. J., and E. L. Thomas. Preprints of Structural Studies of Micelles in Block Copolymer/Homopolymer Blends to appear in J. Chem. Phys.

Kinning, D. J., and E. L. Thomas, Macromolecules, 17, 1712 (1984).

Leibler, L., H. Orland, and J. C. Wheeler, J. Chem. Phys. 79, 3550 (1983).

Leibler, L., and P. A. Pincus, Macromolecules, 17, 2922 (1984).

Lyngaae-Jorgensen, J., N. Alle, and F. L. Marten, Ch. 28 in Multiphase Polymers, Adv. Chem. Ser., American Chemical Society (1979).

Lyngaae-Jorgensen, J., and K. Sondergaard, Poly. Eng. Sci., 27(5), 344 (1987).

Lyngaae-Jorgensen, J., and K. Sondergaard, Poly. Eng. Sci., 27(5), 351 (1987).

Maheshri, J. C., and C. E. Wyman, Poly. Eng. Sci., 20(9), 601 (1980).

Marrucci, G., Trans. Soc. Rheol., 16, 321 (1972).

Martinez, E. B., and M. C. Williams, Journal of Rheology, 24(4), 421 (1980).

Mayes, A. M., and M. Olvera de la Cruz, Macromolecules, 21, 2543 (1988).

Mazich, K. A., and S. H. Carr, J. Appl. Phys., 54, 551 (1983).

Meier, D. J., J. Poly. Sci.: Part 6, 26, 81 (1969).

Min, K., J. L. White, and J. F. Fellers, Poly. Eng. Sci., 24, 1327 (1984).

Monfort, J. P., J. J. Labaig, and P. Monge, Polymer, 17, 1054 (1976).

Monfort, J. P., G. Marin, and P. Monge, Macromolecules, 17, 1551 (1984).

Modern Plastics Encyclopedia, 59(10A), McGraw-Hill (1982).

Molau, G. E., in Block Copolymers, ed. S. Aggarwal, Plenum Press (1970).

Noolandi, J., and M. K. Hong, Macromolecules, 15, 482 (1982).

Onogi, S., T. Masuda, and K. Kitagawa, Macromolecules, 3, 109 (1970).

Owen, E. D., Degradation and Stabilization of PVC, Elsevier Applied Science Pub., New York (1984).

Paul, D. R., and S. Newman, Polymer Blends, Vol. I and II, Acad. Press (1978).

Plochocki, A. P., Poly. Eng. Sci., 26(1), 82 (1986).

Prausnitz, J. M., Molecular Thermodynamics of Fluid-Phase Equilibria, Prentice-Hall, Englewood Cliffs (1960).

Rangel-Nafaile, C., A. B. Metzner, and K. F. Wissbrun, Macromolecules, 17, 1187 (1984).

Rauwendaal, C., Polymer Extrusion, Hanser Pub., New York (1986).

Riess, G., and Y. Jolivet, Ch. 22 in Copolymers, Polyblends, and Composites, ed. N. A. J. Platzer, Adv. Chem. Ser. (1975).

Rigby, D., and R. J. Roe, Macromolecules, 19, 721 (1986).

Rigby, D., and R. J. Roe, Adv. Poly. Sci., 82, 1 (1988).

Robensen, L. M., Poly. Eng. Sci., 24(8), 587 (1984).

Roe, R.-J., Macromolecules, 19, 728 (1986).

Roe, R.-J., M. Fishkis, and J. C. Chang, Macromolecules, 14, 1091 (1981).

Roe, R.-J., and W. C. Zin, Macromolecules, 13, 189 (1980).

Roovers, J., Macromolecules, 20, 148 (1987).

Rostami, S., and D. J. Walsh, Poly. Eng. Sci., 27, 315 (1987).

Rumscheidt, F. D., and S. G. Mason, J. Coll. Sci., 16, 238 (1961).

Sakai, T., N. Hashimoto, and N. Kobayashi, SPE ANTEC Tech. Papers, 46, 146 (1987).

Selb, J., P. Marie, A. Rameau, R. Duplessix, and Y. Gallot, Polymer Bulletin, 10, 444 (1983).

Shen, M., and H. Kawai, AIChE J., 24(1), 1 (1978).

Silberg, A., and W. Kuhn, Nature, 170, 450 (1952).

Smith, W. M., Manufacture of Plastics, Reinhold Pub., New York (1964).

Szydlowski, W., R. Brzoskowski, and J. L. White, Int. Poly. Proc., 1, 207 (1987).

Ten-Brink, G., and G. Hadziioannou, Macromolecules, 20, 486 (1987).

Todd, D. B., Poly. Eng. Sci., 15(6), 437 (1975).

Todd, D. B., SPE ANTEC Tech. Papers, 37, 220 (1979).

Todd, D. B., and H. F. Irving, Chem. Eng. Prog., 65(9), 84 (1969).

Tyrin 2552 Technical Data Sheet provided by Dow Chemical Company (1987).

Van Oene, H., J. Coll. Interf. Sci., 40, 448 (1972).

Walsh, P. J., J. S. Higgins, and A. Maconnachie, eds., Polymer Blends and Mixtures, Martinus Nijhoff Pub., NATO ASI Series (1985).

Watanabe, H., T. Kotaka, T. Hashimoto, M. Shibayama, and H. Kawai, J. of Rheology, 26(2), 153 (1982).

Watanabe, H., and T. Kotaka, Macromolecules, 16, 769 (1983).

Whitmore, M. D., and J. Noolandi, Macromolecules, 18, 657 (1985).

Widmaier, J. M., and G. C. Meyer, J. Poly. Sci.: Poly. Phys., 18, 2217 (1980).

Wolf, B. A., Makromol. Chem. Rapid Commun., 1, 231 (1980).

Wolf, B. A., Macromolecules, 17, 615 (1984).

Wolf, B. A., and H. Kremer, J. Poly. Sci.: Poly. Let., 18, 789 (1980).

Wolf, D., N. Holin, and D. H. White, Poly. Eng. Sci., 26(9), 640 (1986).

Wu, S., Poly. Eng. Sci., 27, 335 (1987).